Università degli Studi di Torino
Doctoral School of Sciences and Innovative Technologies
PhD Programme in Chemical and Materials Sciences XXXII Cycle

Surface functionalization of aluminas for adsorption and biocatalysis

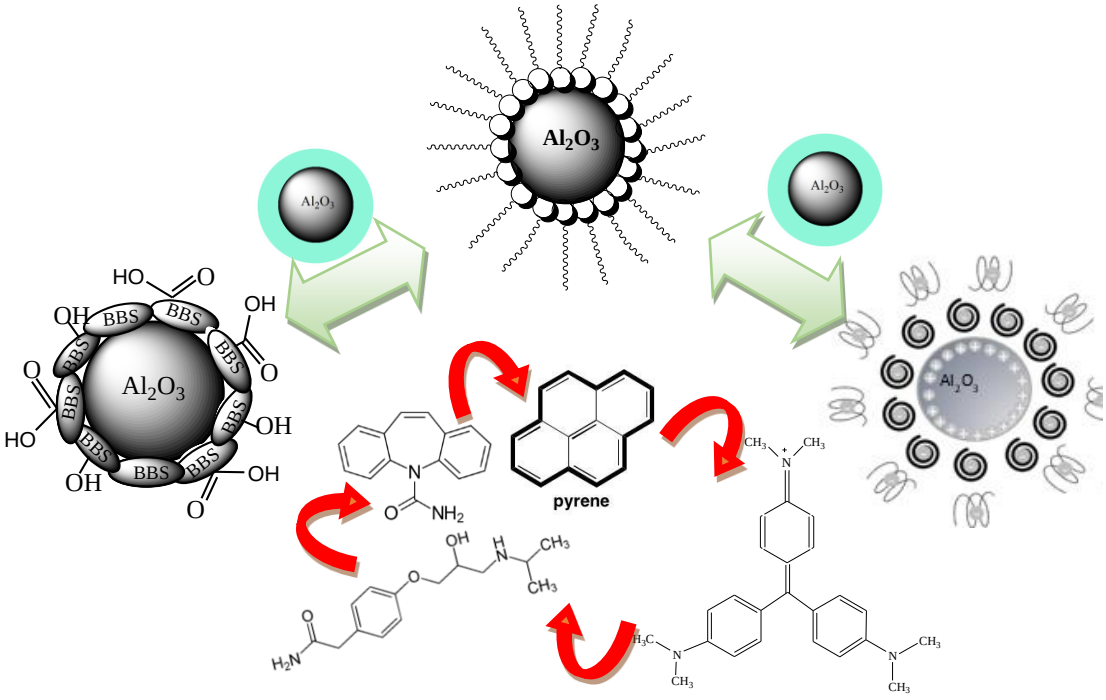

Razieh Sadraei

Supervisor:
Prof. Giuliana Magnacca

Università degli Studi di Torino

Doctoral School of Sciences and Innovative Technologies

PhD Programme in Chemical and Materials Sciences XXXII cycle

Surface functionalization of aluminas for adsorption and biocatalysis

Candidate: **Razieh Sadraei**

Supervisor: Prof. **Giuliana Magnacca**

Jury Members: Prof. **Enzo Laurenti**
Università di Torino

Prof. **Barbara Bonelli**
Politecnico di Torino

Prof. **Vittorio Boffa**
University of Alborg

Head of the Doctoral School: Prof. Massimo Maffei
PhD Programme Coordinator: Prof. Mario Chiesa

Torino, 2020

Acknowledgements

I would first like to acknowledge Prof. Giuliana Magnacca, for her kind support and guidance for the duration of my PhD. The training I received in critical thinking, scientific writing and the numerous conferences I was able to attend has greatly enhanced my communication skills and made me a better scientist. It has been a great pleasure learning from her and I will carry these skills with me in the future.

Thanks to my committee members Prof. Barbara Bonelli, Prof. Vittorio Boffa and Prof. Enzo Laurenti for their helpful discussions. To Prof. Enzo Laurenti for his support and advice with my enzyme work and for allowing me access to his laboratory and for his insightful discussions throughout my PhD project. To Prof. R. Scott Murphy, of the Chemistry and Biochemistry department of University of Regina in Canada, for supporting my visiting program two times during my PhD degree, and for helping me out in writing scientific reports as well as practical work like preparation and characterizations related to Fluorescence spectroscopy of this study. In the period I spent in Canada, I had the pleasure of working with many talented faculty, students and staff during my time at Canada. I would also like to express my appreciation for the HPLC training I received from Prof. Paola Calza in the Centre of Analytical Chemistry. I would like to thank Prof. Maria Cristina Paganini for her advice and help in one of my sub-project. Notable mentions are extended to my lab colleagues Dr. Roberto Nisticò and Dr. Pavlo Ivanchenko. I express my gratitude to Dr. Yadollah Ganjkhanlou for his friendship and motivation that were filled with scientific brainstorming. He has given me a lot of support and encouragement over these last two years and for that I am grateful.

I am grateful to the undergraduate trainees who worked on my projects (Alexandr Sasha Popov, Flavio Neves Dos Santos and Fabio Cucchiara). Special mention to my lab-mate

Jordan Rothwell who made significant contributions to the lab's research and will be remembered forever.

I would like to thank the Department of Chemistry of the University of Turin, Italy, for providing such a professional and friendly place to conduct my research. Special thanks go to the graduate program coordinator: Prof. Mario Chiesa, for always improving the quality of education provided in the Chemistry Department. Many thanks to all the staff and students from the NIS (Nanostructured Interfaces and Surfaces) centre for their help and support. Special thanks to all the members of the SURFIN research group for helping me with my experiments.

I would like to especially acknowledge Mat4treat project for funding most of my graduate studies. Mat4treat is a project funded by the European Union under the Marie Skłodowska-Curie Actions (MSCA) – Research and Innovation Staff Exchange (**Project number:** 645551, Coordinator: Prof. Giuliana Magnacca)

A huge thank goes out to my parents Khadijeh Sadraei and Morteza Sadraei and my sisters Raheleh and Maryam Sadraei for always being there and supporting the decisions I made. This degree would not have been possible without their love and support. Special thanks to my best friend Masa who listened my numerous presentations, even if she did not understand everything I was talking about, and encouraged me to keep moving forward. To all the undergraduate and graduate professors who taught me chemistry have contributed indirectly to the research. I gratefully acknowledge their efforts, teachings, and guidance.

Last but not the least, thank you to my husband and true love, Dr. Vahid Jafari Sadeghi for his unwavering belief in my abilities, patience, and constant encouragement throughout my degree. He has been my biggest cheerleader and inspired me to think about my projects from different perspectives. His intelligence, kindness and love have in large part shaped me into the scientist I am today. He constantly challenged me to push beyond my comfort

level, and his passion for science has surrounded me in a wonderfully positive environment for the last 3 years. I am grateful for his support and continued love.

Razieh Sadraei

January 2020

Table of Contents

Content of Figures

Content of Tables

Content of Schemes

Chapter One

1. General Introduction

1.1. Mesoporous Alumina

Aluminium oxide, commonly called alumina, is a compound of aluminium and oxygen with chemical formula Al2O3. Nowadays more than 90 million tons of alumina are produced per year for several purposes (1). Mesoporous alumina has attracted scientific interest since the 1940s. Aluminum metal naturally develops a passivating layer of aluminum oxide approximately 3-4 nm thick under ambient conditions (1)(2).

Mesoporous γ–alumina (MA) with pore diameters between 2 and 50 nm is a common catalyst support in heterogeneous reactions. The main advantages of mesoporous aluminas are as follows (3):

1) High surface area leads to increased density of active sites and high loadings of organic moieties while maintaining a high dispersion of the active phase.

2) MA contains a relatively high density of basic sites compared to conventional non-porous aluminas. Basic sites, increasing the interaction between opposite charged compounds and alumina supports, typically enhance catalytic activity of catalysts.

3) Surface area and pore properties of MA are tunable.

4) MA is thermally stable.

Pore size, surface area, thermal stability, and site acidity can be optimized by varying the preparation conditions. Therefore, the synthesis and characterization

of MA are required to determine structures and properties, which lead to find appropriate applications in various fields (1).

MAs have various applications, for instance for producing ceramic membranes, for paint and cosmetic formulations, for pollution control, for refinery and chemical catalysis in particular as support (4)(5).

The oxides of aluminium are widely used in ceramics, refractories and abrasives due to their hardness, chemical inertness, high melting point, non-volatility and resistance to oxidation and corrosion. The transparency of alumina film extend its application in optics as well. Al_2O_3 is an electrical insulator having high thermal conductivity.

Aluminas are generally synthesized in nano size(6). Among the seven polymorphs of transition alumina identified so far, namely γ, η, δ, θ, χ and ρ phases, the γ form is one of the most extensively used in industrial catalysis owing to its comparatively large surface area, unique surface characteristics, and exceptional structural stability. Conventional γ-alumina can form through the thermal dehydration of a crystalline aluminum oxyhydroxide (boehmite) at a temperature above 450 °C. The property of such alumina particles depends on size, morphology, surface and phase homogeneity and these properties can be controlled by selecting a proper synthetic route. γ-alumina with high surface area and mesoporous properties is commonly used as a well-known support.

Alumina is the protagonist of this work, focused at the development of different hybrid materials for the treatment of polluted water. To this aim alumina precursors as boehmite and ammonium dawsonite were considered. Ammonium dawsonite was prepared by the conventional hydrothermal route. Both precursors

yield, after a thermal treatment in the range 500-1000 °C, gamma delta and theta phases of alumina which are applied as supports for immobilization of different molecules such as bio-based substances, soybean peroxidase as a representative protein and arachidic acid as an example of lipid.

Zeta potential measurements allow to define the surface charge of the supports in order to choose the best conditions to achieve an efficient interaction between alumina surface and immobilized molecules and also to reach the optimal conditions for achieving an efficient adsorption of different substrates, i.e. pollutants or model pollutants.

In the following, I provide an overview of aluminas including gamma and delta-theta phases, together with their synthesis procedures, presentation of their structures and properties.

Aluminas are mainly prepared by calcination of precursors, which can be both crystalline or amorphous. (4).

Aluminium monohydroxide, also known as aluminium oxyhydroxide (boehmite – AlO[OH]), is water insoluble but crystallizes into micro or nanocrystals of various shapes. In general, boehmite represents one of the most important raw material for the production of aluminium oxide. Thermal treatment of AlO(OH) leads to phase transitions and loss of hydroxide groups. Thermal treatment of AlO(OH) results in transformation of AlO(OH) into different crystalline structures of aluminas (γ, η, χ, δ, θ) dependently on the treatment temperature. Also, the sequence of transition aluminas achievable by thermal treatment depends strongly on the starting

materials and the obtained phase definitively affects the resulting properties (particle size, surface area, pore size distribution and so on) (7).

The other precursor considered in this thesis is the ammonium dawsonite. Ammonium Aluminum Carbonate Hydroxide (AACH with formula $NH_4Al(OH)_2CO_3$) can be a promising alternative precursor for preparation of γ-Al_2O_3 with high purity, high specific surface area and new textural properties. The remarkable difference between these two precursors and the resulting gamma-alumina is their shape which can become really important for choosing the applications: alumina from boehmite is almost spherically shaped whereas alumina from dawsonite is acicular (8)(9)(10)(11). The question, therefore, is: why is necessary to know the shape of the particles or precursor uses of a material? The answer is given by Allen "Particle shape is a fundamental powder property, affecting powder packing and thus bulk density, porosity, permeability, cohesion, flowability, caking behavior, attrition, interaction with fluids and the covering power of pigments". Thus, one of the purposes of this dissertation is to investigate the behaviors of each precursor, when they are involved in the preparation of hybrid materials.

1.1.2. Synthesis

Powders of MA can be synthesized by several well-established synthesis methods, such as Bayer, sol-gel, precipitation and hydrothermal processes (3).

Among others, hydrothermal synthesis is an attractive environmental friendly alternative to the above mentioned approaches (12) , with the advantage of being a single-step, low energy consumption process with no need of subsequent high-

temperature calcination and/or extensive milling. Further advantages include the quality of the product, which presents high chemical and phase purity, low aggregation level and narrow crystallite size distribution, in addition to an excellent control of the particle morphology. It is possible to produce a wide range of particle shapes, both equiaxed, such as cubes, spheres, diamonds and bipyramids, and elongated morphologies, such as fibers, whiskers, nanorods, nanotubes and also platelets, nanoribbons, nanobelts, etc. The particle size can also range from a few nanometers to large crystals.

Although various synthesis method are possible for AACH, including gas–liquid, gas–solid, solid–solid, and liquid–liquid reactions, AACH is mostly produced by liquid phase. Typically an aluminum salt, ammonium (bi)carbonate, ($Al(NO_3)_3$, $(NH_4)Al(SO_4)_2$, or $AlCl_3$) is solved in water in the presence of a precipitating agents such as $(NH_4)_2CO_3$ or NH_4HCO_3 (13)(14).

Xu et al. have reported the preparation of gamma-alumina obtained from AACH with a specific surface area of 1029 m^2/g, for water purification application. They obtained an adsorption capacity up to 52.1 mg/g for Cr(VI) removal, demonstrating AACH is a very promising adsorbent for water purification due to its high surface area, thermal stability and presence of surface functional groups (15).

1.2. Surface charge and functionalization

The knowledge of the surface charge and its measurement is fundamental in all the applications dealing with surface properties of materials. As a consequence, a modification of the surface charge of a material becomes important to optimize the

applicability of the material in a specific process. Several methods for the modification and control of surface charges have been developed to date. Control over charges can be achieved by binding different functional groups to the material surface, for instance. In the case of alumina, several studies suggest that most of the applications are due to the presence of charged functional groups such as hydroxyl, carboxyl, amino, and nitro present at the surface of materials. These studies have laid the basis for researches aimed at altering the properties of alumina surfaces by adding proper functional groups through different methods (16).

Sergio Bertazzo and his colleagues have studied the surface charge of alumina functionalized with carboxylic acid with different carbon chain length. They could successfully control the surface charge as well as the Isoelectric Point (IEP) of alumina using different concentration of carboxylic acids or changing the size of the carbon chain of the acid without changing the hydrophobicity of alumina surface. They defined that the IEP correlates with the number of carbons in the chain of the functionalizing acid (17)(18).

In conclusion, particle surface functionalization is a tool influencing adsorption phenomena. Charged functional groups exposed at the particle surface drive the adsorption of oppositely charged components, and hydrophilic/hydrophobic groups guide the adsorption by interacting with water molecules. Therefore, the surface functionalization can definitely change the adsorption of any substrate onto alumina surface. Subsequently, it is possible to employ a specific surface modification with different functional groups through which it is possible to establish specific interaction with the substrates. The nature of functionalizing groups can also affect the hydrophobicity of a surface that can be modified from

hydrophilic to hydrophobic leading to hybrid materials with application in adsorption of non-polar contaminants.

Nanoalumina (Al_2O_3) is an excellent material to investigate how surface chemistry can change the adsorption properties. In fact, it can be easily surface-functionalized without being structurally modified given its high stability and inertness(18).

In this work soybean peroxidase protein was supported on alumina in order to obtain a heterogeneous biocatalyst, and in similar way, through electrostatic interactions, the same aluminas were functionalized with bio-based substances. In both cases the procedures take advantage from the presence of OH surface groups of alumina establishing good interaction with carbonylic (-CO)/carboxylic (−COOH) or, in general, polar groups (19).

On the other hand, hydrophobicity of solid surfaces is a term related to the behavior of solid surfaces when placed in contact with liquid water. Most hydrophobic surfaces, even those that are strongly hydrophobic, contain surface sites that are hydrophilic, but it is not known to what extent such sites influence the water wetting behavior of the surfaces, or what concentrations or disposition of these polar sites is required to render a surface macroscopically hydrophobic rather than hydrophilic. Powders of hydrophobic solids tend to have surfaces that are even more heterogeneous than those of flat solid surfaces, as exemplified by the surfaces of coal, carbon blacks, active carbons and graphites (20).

Literature studies (21)(22)(23)(24)(25)(26)(27) showed that the surface of oxide powders can be efficiently hydrophobized. The objective of the functionalization was to change the native hydrophilic character of the support. As it is mentioned

above, alumina possesses an intrinsic hydrophilic character, as a result of the presence of hydroxyl groups on the surface. The surface modification process can be used to increase the hydrophobicity of the surface by introducing a hydrophobic chain on the surface. Hydrophobization of alumina surface can be done using various methods, however always compounds with a reactive grouping should be used (e.g. methoxy, ethoxy or active chlorine) (27).

Joanna Kujawa successfully modified the surface of alumina particles using two types of perfluoroalkylsilane (PFAS) molecules chemically grafted to have the surface of alumina more hydrophobic for drug delivery application (28).

In another study the functionalization of alumina surface was carried out using carboxylic acids having highly branched hydrocarbon chains. Shirin Alexander is one of the scientists preparing superhydrophobic mesoporous nanoalumina by functionalization with short highly branched hydrocarbon chains through chemical interaction established between hydrocarbon carboxylic groups and OH groups of alumina (22).

In all cases, the surface of alumina was functionalized considering the assumption that strong interactions can establish between polar group of substrates or surfactants and the alumina surface.

1.3. Adsorption

Global warming and climate change cause environmental pollution that poses severe health risks to people all around the world (30). Adsorption using hybrid materials has been demonstrated to be an effective technique to remove hazardous

materials from water due to its easy operation, low cost, and high efficiency. In general, adsorption is defined as the enrichment of molecules, atoms or ions in the vicinity of an interface. Adsorption can be classified into two categories: physical (physisorption) and chemical (chemisorption) Both are efficient methods to uptake pollutants from decontaminated air and water (31)(32)(33)(15)(20)(34).

In general terms, pollution should be considered as a global concern, and so the adoption of environmental friendly measures to achieve the efficient use of natural resources and the management of industrial waste is becoming one of the main strategies for a sustainable development all over the world (35).

Pollution of water bodies due to discharge of effluents from different industries is of major concern worldwide. Tanneries, refineries, textile manufacturing units, and chemical manufacturing plants are the major culprits in this respect. Apart from these, one of the major actor to such water pollution is the industry directly dealing with dyes. Units involved in paper manufacturing, cloth dyeing, treatment of leather, and printing produce effluents containing dyes. These dyes are either non-biodegradable and can produce toxic degradation products. When the dyes are discharged with no control, their removal from effluents is of outmost importance from the point of view of environmental pollution. The decontamination of toxic dyes via reliable and environmental friendly techniques has attracted huge interest recently. Currently, among various treatment procedures of wastewater containing dyes, the adsorption process has become one of the most useful techniques (36)(37)(38).

Several efforts have been dedicated to the development of advanced technologies for water remediation, particularly for the removal of contaminants of emerging

concern (CECs) including pharmaceuticals and personal care products (PPCPs), pesticides, pesticide metabolites, endocrine disrupting compounds (EDCs), and algal toxins. Most of those organic contaminants are neither biodegradable nor easy to remove completely from water through conventional water treatment plants because of their physical or chemical properties (e.g., high polarity and solubility in water). An array of methods, such as ultrasonic irradiation, electrochemical degradation, solid-phase extraction, photodegradation, ozonation and advanced oxidation processes (AOPs) have been developed and applied to trap or degrade those organics from water. Considering the drawbacks of the mentioned methods (for example, toxic byproducts can be left behind after AOP or ozonation processes), adsorption might be a suitable alternative because of its simplicity, reliability, and cost effectiveness in trapping efficiently CECs including PPCPs from water. Therefore, adsorption technology has come into the focus of researchers, environmentalists, as well as industrialists over the last decade. Adsorbents, upon proper functionalization, can efficiently handle trace levels of CECs with high selectivity, and fixed beds made of these adsorbents can be used sequentially coupled to other advanced treatment processes (39)(35)(40)(41)(42).

Despite these advantages and the progress reported in the literature for the development of new adsorbents, there is a tremendous need for more studies based on CEC adsorption to help identifying variables or information that could bridge the gap between lab scale testing and large-scale implementation (43).

Development of new and/or highly efficient adsorbents is still the most demanding factor for effective removal of organics from water via adsorption. Several types of adsorbents, especially porous ones, have already been developed and shown their

efficiency in water purification. Various adsorbents like mesoporous materials, silica, alumina and activated carbons have been used for such treatment. Alumina is widely used as adsorbent owing large specific surface area, open porosity, surface acidity/basicity and high thermal stability (44)(45).

In the last decade, the application of biowaste, as green and low-cost reactant, has received great attention. Bio-based substances (BBS) have attractive properties, which make them valuable materials to be used in a wide range of fields, especially in separation and purification technologies. In recent years, it was shown that solid supports functionalized with BBS are efficient adsorbents for depollution processes. They can effectively enhance the adsorption capacity of more traditional sorbents for treating both organic and inorganic pollutants (43).

In 2015, Yunhui Wang discovered that the surface modification of alumina particles enhanced the adsorption performance of alumina surface toward alkaline methyl orange. His results demonstrated that the surface acidity-alkalinity of alumina determined its adsorption performance and selectivity for organic compounds (44).

1.4. Development of alumina monolith

Many researchers begin to pay attention to the fabrication of new type of adsorbent materials that can be easily recovered by simple separation processes after adsorption of organic pollutants without wasting money and time (46)(47)(48)(49)(50). In fact, powdery adsorbents face many difficulties in recovery and reusability, in particular working in a big scale whereas massive adsorbent materials can be used more easily (51)(52).

To be effective, these massive materials need to expose high surface area and therefore to be porous (53). In 2012, Prof. G. Magnacca and her colleagues discovered a new method to prepare siliceous monoliths. The same method was applied to the preparation of alumina monoliths. The description of the results obtained is reported in the third chapter of this dissertation (55).

1.5. Overview of dissertation

I prepared several hybrid materials by modifying the surface of alumina with different molecules like Bio Based Substances (BBS), a protein and a lipid. Alumina shows numerous advantages like presence of defective active surface sites, positive surface charge to achieve effective functionalization of the surface also following green chemistry procedures for capturing polar molecules (organic dyes and CECs) as well as non-polar substrates (for the treatment of oil field produced-water). The behavior of the materials was tested with proper substrates in order to assess the adsorption capacity and the reversibility of the adsorption.

The first hybrid materials presented in the second chapter of this dissertation deal with the surface functionalization of alumina with BBS. These materials were tested in the presence of an organic dye and emerging contaminants in aqueous media demonstrating to be very fast in the adsorption.

Chapter three describes the method for fabricating alumina porous monoliths. They were characterized and tested before and after the functionalization with BBS and compared with the parent powders. The characterization was done by means of X-Ray Diffraction (XRD) to evidence the crystal structure, Fourier Transform Infrared

spectroscopy (FT-IR) for evaluating the presence of BBS on the monoliths, thermogravimetric analysis (TGA) to measure the thermal stability of the monoliths and quantify of the BBS amount immobilized on them, N_2 adsorption at 77K for the investigation on the surface area and porosity of the systems, zeta potential measurements to carry out the effect of BBS immobilization on the surface charge of the particles. The tests were done using the positively charged crystal violet (CV) as well as the negatively charged methylene blue (MB) dyes.

In chapter four, different phases of alumina were applied as supports for immobilization of Soybean Peroxidase (SBP) for biocatalytic applications and the resulting materials were compared with a previously examined heterogeneous biocatalyst containing SBP covalently immobilized on silica monoliths. The hybrid systems were investigated to obtain structural information regarding their activity. The amount of SBP immobilized, the stability and activity of the hybrid systems were tested. The joint use of infrared and fluorescence spectroscopy, using the adsorption of NO as a probe molecule, provided insights into the structure-activity relationship of free and supported SBP and to define a general strategy to predict the activity of supported enzymes.

Chapter five explains the functionalization of alumina and silica surface by arachidic acid. The lipid immobilization allows decreasing the intrinsic hydrophilicity of alumina producing hydrophobic materials able in capturing apolar pyrene molecules and, in principle, similar apolar substrates. The preparation methods considered were very simple to apply, as they base on the formation of electrostatic interactions between the oxide surface and the polar head of the functionalizing agent allowing to expose the hydrophobic tails able in establishing dispersive

interactions with apolar molecules. The lipid was prepared in form of film using chloroform but also simply dispersed as powder avoiding the use of organic solvents in order to test a green preparation method. The pyrene adsorption occurs very fast on all the samples, in particular in the presence of the highest amount of lipid, indicating that the hybrid materials could conveniently apply to the treatment of real PW samples.

In conclusions, a summary of the obtained results and some future perspectives are presented in chapter 6 and 7.

1.6. References

1. Cardoso CS, Licea YE, Huang X, Willinger M, Louis B, Pereira MM. Microporous and Mesoporous Materials Improving textural properties of g - alumina by using second generation biomass in conventional hydrothermal method. Microporous Mesoporous Mater. 2015;207:134–41. Available from: http://dx.doi.org/10.1016/j.micromeso.2015.01.015

2. Rowthu S, Hoffmann P. Perfluoropolyether-Impregnated Mesoporous Alumina Composites Overcome the Dewetting-Tribological Properties Trade-Off. ACS Appl Mater Interfaces. 2018;10(12):10560–70.

3. Shaghayegh Ghanizadeh, Xujin Bao, Bala Vaidhyanathan JB. Synthesis of nano [alpha] -alumina powders using hydrothermal and precipitation routes : a comparative study. Ceram Int. 2014;40:1311–9.

4. Padilla I, Lopez-Delgado A, Lopez-Andres S, Alvarez M, Galindo R, Vazquez-Vaamonde AJ. The application of thermal solar energy to high temperature processes: case study of the synthesis of alumina from boehmite. Sci World J. 2014;2014(January):825745. Available from: http://www.ncbi.nlm.nih.gov/pubmed/24523648

5. Souza P De, Carlos A, Coelho V, São U De, Usp P, Prof A, et al. Hydrothermal Synthesis of Well-Crystallised Boehmite Crystals of Various Shapes. 2009;12(4):437–45.

6. Fulvio PF, Brosey RI, Jaroniec M. Synthesis of mesoporous alumina from boehmite in the presence of triblock copolymer. ACS Appl Mater Interfaces. 2010;2(2):588–93.

7. Demichelis R, Noël Y, Ugliengo P, Zicovich-Wilson CM, Dovesi R. Physico-chemical features of aluminum hydroxides as modeled with the hybrid B3LYP functional and localized basis functions. J Phys Chem C. 2011;115(27):13107–34.

8. Stoica G, Pérez-Ramírez J. Reforming dawsonite by memory effect of AACH-derived aluminas. Chem Mater. 2007;19(19):4783–90.

9. Zhang L, Wu Y, Zhang L, Wang Y, Li M. Synthesis and characterization of mesoporous alumina with high specific area via coprecipitation method. Vacuum. 2016;133:1–6. Available from: http://dx.doi.org/10.1016/j.vacuum.2016.08.005

10. Lafficher R, Digne M, Salvatori F, Boualleg M, Colson D, Puel F. Ammonium aluminium carbonate hydroxide NH4Al(OH)2CO3 as an alternative route for alumina preparation: Comparison with the classical boehmite precursor. Powder Technol. 2017;320:565–73.

11. Mehboob S, Mehmood M, Ahmed M, Ahmad J, Tanvir MT, Ahmad I. Terahertz time domain spectroscopy of hydrothermally synthesized boehmite and ammonium dawsonite nanostructures. Infrared Phys Technol. 2016;78:200–8. Available from: http://dx.doi.org/10.1016/j.infrared.2016.08.007

12. Stoica G, Groen JC, Abelló S, Manchanda R, Pérez-Ramírez J. Reconstruction of dawsonite by alumina carbonation in (NH4)2CO3: Requisites and mechanism. Chem Mater. 2008;20(12):3973–82.

13. Sadraei R, Murphy RS, Laurenti E, Magnacca G. Characterization Methodology to Evaluate the Activity of Supported Soybean Peroxidase. Ind Eng Chem Res. 2019;58(41).

14. Li GC, Liu YQ, Guan LL, Hu XF, Liu CG. Meso/macroporous γ-Al $_2$O $_3$ fabricated by thermal decomposition of nanorods ammonium aluminium carbonate hydroxide. Mater Res Bull. 2012;47(4):1073–9.

15. Alzate-Sánchez DM, Smith BJ, Alsbaiee A, Hinestroza JP, Dichtel WR. Cotton fabric functionalized with a β-cyclodextrin polymer captures organic pollutants from contaminated air and water. Chem Mater. 2016;28(22):8340–6.

16. Bertazzo S, Rezwan K. Control of α-alumina surface charge with carboxylic acids. Langmuir. 2010;26(5):3364–71.

17. Zhivkov AM, Hristov RP. Adsorption of carboxymethyl cellulose on alumina particles. J Colloid Interface Sci. 2014;447:159–66. Available from: http://dx.doi.org/10.1016/j.jcis.2014.11.051

18. Meder F, Kaur S, Treccani L, Rezwan K. Controlling mixed-protein adsorption layers on colloidal alumina particles by tailoring carboxyl and hydroxyl surface group densities. Langmuir. 2013;29(40):12502–10.

19. Nagarjuna R, Sharma S, Rajesh N, Ganesan R. Effective Adsorption of Precious Metal Palladium over Polyethyleneimine-Functionalized Alumina Nanopowder and Its Reusability as a Catalyst for Energy and Environmental Applications. ACS Omega. 2017;2(8):4494–504.

20. Radian A, Mishael Y. Effect of humic acid on pyrene removal from water by polycation-clay mineral composites and activated carbon. Environ Sci Technol. 2012;46(11):6228–35.

21. Kujawa J, Cerneaux S, Kujawski W. Colloids and Surfaces A : Physicochemical and Engineering Aspects Characterization of the surface modification process of Al 2 O 3 , TiO 2 and ZrO 2 powders by PFAS molecules. Colloids Surfaces A Physicochem Eng Asp. 2014;447:14–22.

22. Alexander S, Eastoe J, Lord AM, Guittard F, Barron AR. Branched Hydrocarbon Low Surface Energy Materials for Superhydrophobic Nanoparticle Derived Surfaces. ACS Appl Mater Interfaces. 2016;8(1):660–6.

23. Kujawa J, Kujawski W. Functionalization of Ceramic Metal Oxide Powders and Ceramic Membranes by Perfluoroalkylsilanes and Alkylsilanes Possessing Different Reactive Groups: Physicochemical and Tribological Properties. ACS Appl Mater Interfaces. 2016;8(11):7509–21.

24. Crouse CA, Pierce CJ, Spowart JE. Influencing solvent miscibility and aqueous stability of aluminum nanoparticles through surface functionalization with acrylic monomers. ACS Appl Mater Interfaces. 2010;2(9):2560–9.

25. Portilla L, Halik M. Smoothly tunable surface properties of aluminum oxide core-shell nanoparticles by a mixed-ligand approach. ACS Appl Mater Interfaces. 2014;6(8):5977–82.

26. Vlassiouk I, Rios F, Vail SA, Gust D, Smirnov S. Electrical conductance of hydrophobic membranes or what happens below the surface. Langmuir. 2007;23(14):7784–92.

27. Al-Shatty W, Lord AM, Alexander S, Barron AR. Tunable Surface Properties of Aluminum Oxide Nanoparticles from Highly Hydrophobic to Highly Hydrophilic. ACS Omega. 2017;2(6):2507–14.

28. Turov V V., Gun'ko VM, Pakhlov EM, Krupska T V., Tsapko MD, Charmas B, et al. Influence of hydrophobic nanosilica and hydrophobic medium on water bound in hydrophilic components of complex systems. Colloids Surfaces A Physicochem Eng Asp. 2018;552(May):39–47. Available from: https://doi.org/10.1016/j.colsurfa.2018.05.017

29. Li SY, Xiang XG, Ma BH, Meng XD. Facile preparation of diverse alumina surface structures by anodization and superhydrophobic surfaces with tunable water droplet adhesion. J Alloys Compd. 2019;779:219–28. Available from: https://doi.org/10.1016/j.jallcom.2018.11.222

30. Cho SY, Cho KM, Chong S, Park K, Kim S, Kang H, et al. Rational Design of Aminopolymer for Selective Discrimination of Acidic Air Pollutants. ACS Sensors. 2018;3(7):1329–37.

31. Thommes M, Kaneko K, Neimark A V., Olivier JP, Rodriguez-Reinoso F, Rouquerol J, et al. Physisorption of gases, with special reference to the evaluation of surface area and pore size distribution (IUPAC Technical Report). Pure Appl Chem. 2015;87(9–10):1051–69.

32. Shi Q, Yan L, Chan T, Jing C. Arsenic Adsorption on Lanthanum-Impregnated Activated Alumina: Spectroscopic and DFT Study. ACS Appl Mater Interfaces. 2015;7(48):26735–41.

33. Oh HT, Lim SJ, Kim JH, Lee CH. Adsorption Equilibria of Water Vapor on an Alumina/Zeolite 13X Composite and Silica Gel. J Chem Eng Data. 2017;62(2):804–11.

34. Wang Y, Dang Q, Liu C, Yu D, Pu X, Wang Q, et al. Selective Adsorption toward Hg(II) and Inhibitory Effect on Bacterial Growth Occurring on Thiosemicarbazide-Functionalized Chitosan Microsphere Surface. ACS Appl Mater Interfaces. 2018;10(46):40302–16.

35. Hamza RA, Iorhemen OT, Tay JH. Occurrence, impacts and removal of emerging substances of concern from wastewater. Environ Technol Innov. 2016;5:161–75. Available from: http://dx.doi.org/10.1016/j.eti.2016.02.003

36. Ortiz-Martínez K, Vargas-Valentín DA, Hernandez-Maldonado AJ. Adsorption of contaminants of emerging concern from aqueous solutions using Cu2+ amino

grafted SBA-15 mesoporous silica: Multicomponent and metabolites adsorption. Ind Eng Chem Res. 2018;57(18):6426–39.

37. Richardson SD, Ternes TA. Water Analysis: Emerging Contaminants and Current Issues. 2014;

38. Wasti A, Ali Awan M. Adsorption of textile dye onto modified immobilized activated alumina. J Assoc Arab Univ Basic Appl Sci. 2016;20:26–31. Available from: http://dx.doi.org/10.1016/j.jaubas.2014.10.001

39. Bhadra BN, Jhung SH. A remarkable adsorbent for removal of contaminants of emerging concern from water: Porous carbon derived from metal azolate framework-6. J Hazard Mater. 2017;340:179–88. Available from: http://dx.doi.org/10.1016/j.jhazmat.2017.07.011

40. Martín-Pozo L, de Alarcón-Gómez B, Rodríguez-Gómez R, García-Córcoles MT, Çipa M, Zafra-Gómez A. Analytical methods for the determination of emerging contaminants in sewage sludge samples. A review. Talanta. 2019;192(September 2018):508–33. Available from: https://doi.org/10.1016/j.talanta.2018.09.056

41. Núñez M, Borrull F, Pocurull E, Fontanals N. Sample treatment for the determination of emerging organic contaminants in aquatic organisms. TrAC - Trends Anal Chem. 2017;97:136–45.

42. Bilal M, Rasheed T, Nabeel F, Iqbal HMN, Zhao Y. Hazardous contaminants in the environment and their laccase-assisted degradation – A review. J Environ Manage. 2019;234(January):253–64.

43. Ayati A, Ranjbari S, Tanhaei B, Sillanpää M. Ionic liquid-modified composites for the adsorptive removal of emerging water contaminants: A review. J Mol Liq. 2019;275:71–83. Available from: https://doi.org/10.1016/j.molliq.2018.11.016

44. Wang Y, Wei Q, Huang Y. Preparation and adsorption properties of the biomimetic gama-alumina. Mater Lett. 2015;157:67–9. Available from: http://dx.doi.org/10.1016/j.matlet.2015.05.119

45. Aazza M, Ahlafi H, Moussout H, Maghat H. Ortho-Nitro-Phenol adsorption onto alumina and surfactant modified alumina: Kinetic, isotherm and mechanism. J Environ Chem Eng. 2017;5(4):3418–28.

46. Unuabonah EI, Günter C, Weber J, Lubahn S, Taubert A. Hybrid clay: A new highly efficient adsorbent for water treatment. ACS Sustain Chem Eng. 2013;1(8):966–73.

47. Ye S, Liu Y, Feng J. Low-Density, Mechanical Compressible, Water-Induced Self-Recoverable Graphene Aerogels for Water Treatment. ACS Appl Mater Interfaces. 2017;9(27):22456–64.

48. Sadraei R, Paganini MC, Calza P, Magnacca G. An Easy Synthesis for Preparing Bio-Based Hybrid Adsorbent Useful for Fast Adsorption of Polar Pollutants. Nanomaterials. 2019;9(5):731.

49. Ko YG, Lee HJ, Kim JY, Choi US. Hierarchically porous aminosilica monolith as a CO2 adsorbent. ACS Appl Mater Interfaces. 2014;6(15):12988–96.

50. Alauzun JG, Ungureanu S, Brun N, Bernard S, Miele P, Backov R, et al. Novel monolith-type boron nitride hierarchical foams obtained through integrative chemistry. J Mater Chem. 2011;21(36):14025–30.

51. Magnacca G, Laurenti E, Vigna E, Franzoso F, Tomasso L, Montoneri E, et al. Refuse derived bio-organics and immobilized soybean peroxidase for green chemical technology. Process Biochem. 2012;47:2025–31.

52. Darunte LA, Terada Y, Murdock CR, Walton KS, Sholl DS, Jones CW. Monolith-Supported Amine-Functionalized Mg2(dobpdc) Adsorbents for CO2 Capture. ACS Appl Mater Interfaces. 2017;9(20):17042–50.

53. Lee HY, An CJ, Piao SJ, Ahn DY, Kim MT, Min YS. Shrinking core model for Knudsen diffusion-limited atomic layer deposition on a nanoporous monolith with an ultrahigh aspect ratio. J Phys Chem C. 2010;114(43):18601–6.

54. Broekhuis RR, Budhlall BM, Nordquist AF. Monolith catalytic process for producing sorbitol: Catalyst development and evaluation. Ind Eng Chem Res. 2004;43(17):5146–55.

Chapter Two

An easy synthesis for preparing bio-based hybrid adsorbent useful for fast adsorption of polar pollutants

Abstract

For the first time, γ-Al_2O_3 and Bio-Based Substances (BBS) hybrids (**A**-BBS) were prepared through a simple electrostatic interaction occurring between alumina, used as a support, and BBS (Bio-Based Substance from composted biowastes) carrying positive and negative charges, respectively. We evaluated the optimal amount of BBS to be immobilized on the support and the stability of the resulting **A**-BBS in order to use this novel hybrid material as an adsorbent for the removal of polar pollutants. Characterization was carried out by X-Ray Diffraction (XRD) for evaluating the crystal structure of the support, Fourier transform infrared spectroscopy (FT-IR) to evidence the presence of BBS on the hybrid material, thermogravimetric analysis (TGA) to measure the thermal stability of the hybrid materials and quantify the BBS amount immobilized on the support, N_2 adsorption at 77K for the evaluation of the surface area and porosity of the systems, Zeta potential measurements to evaluate the effect of BBS immobilization on the surface charge of the particles and chose the substrates possibly interacting with them. Firstly, we tested the adsorption capability of three samples differently coated with BBS toward cationic species considering various adsorbate/adsorbent ratio. Crystal Violet (CV) was chosen as model pollutant to compare the performance of the hybrid materials with those of other materials described in the literature. The adsorption data were modeled by Langmuir and Freundlich adsorption

isotherms. Then, we studied the adsorption capability of the developed material towards molecules with different structures; for such purpose, two contaminants of emerging concerns (carbamazepine and atenolol) were tested. The results indicate that **A**-BBS could be applied in wastewater treatment for the removal of significant amount of polar species. In addition, a comparison with literature data concerning CV adsorption was carried out in order to evaluate the environmental impact of synthetic routes used to prepare different adsorbents.

Keywords: adsorption; crystal violet; hybrid materials; electrostatic interaction; alumina support; Contaminant of Emerging Concern removal

2.1. Introduction

The removal of pollutants from urban and industrial wastewaters is one of the most important issues to be solved by modern research. In fact, water pollution has increased in the last decades by the virtue of the disposal of industrial effluents enriched with toxic species (1) which has hazardous effects on flora, fauna and humans. Moreover, the growth of the world population results in a limitation of water supplies and scarcity of water resources, therefore the necessity of clean water has become fundamental for our society (1)(2).

In the last decades, new chemicals were detected in wastewaters as a result of new industrial processes and increased consumption of pharmaceuticals and personal care products (3,4).

Among other pollutants, synthetic dyes (5) can be found in the effluent of many industries, including textile, plastic, printing and dye manufacturing companies. In this group of contaminants, the cationic organic aromatic dyes are ones of the most present pollutants, released from industries, causing various harmful influences on aquatic bodies as well as organisms. Therefore their removal has been deeply studied in recent years (6)-(8).

Crystal violet (CV) belongs to this group of contaminants. It has been widely used as a dermatological agent and biological stain as well as a coloring agent for dyeing leather, silk, wool, paper, and cotton (6)-(9).

Several techniques have been used to remove organic pollutants and synthetic dyes from urban and industrial wastewaters such as membrane separation (2), biological (10) and electrochemical treatments (11), flocculation, liquid-liquid extraction (12), advanced

oxidation processes (AOP) (13) and coagulation. Out of methods listed above, the adsorption technique(14) has attracted considerable attention because of the simple procedures needed, because no toxic substances are produced, because of ability to treat concentrated forms of the pollutants, and to reuse the spent adsorbent via regeneration. Moreover, it plays a central role in drinking water purification and wastewater treatment (3),(7),(15),(16).

Mesoporous material, thanks to their large and tunable porosity find potential applications as catalysis, encapsulation of proteins, filtration and separation of large molecules, membrane technology, drug delivery, dosing, sensing, among many others (17),(18) Furthermore, their large specific surface area and huge number of adsorbing active sites suggest their possible application as adsorption materials (19).

In particular, alumina found various technological applications, i.e. as electrical insulator, presenting exceptional high resistance to chemical agents, as well as giving an excellent performance as catalyst or support for many applications(20),(21).

Mesoporous γ-Al_2O_3 has been not only widely applied in all the field mentioned above (17),(22) but in the recent years the chance to synthesize hybrid materials to enhance the useful properties of an oxide opens the way to very interesting opportunities. The literature reports that many oxides have been modified using organic moieties able in enhancing the adsorption capacity of the original material. Among others, bio-based substances (BBS), extracted from composted green wastes, are very interesting macromolecules with a complex lignin-derived structure and characterized by several functional groups (they contain long aliphatic chains, aromatic rings and several acid and basic functional groups such as carboxyl, primary and substituted amine and amide, carbonyl, hydroxyl, phenol,

ether or ester (23),(24), appealing for their importance in the valorization of the organic refuses. BBS have been found to exhibit typical properties of anionic surfactants and polyelectrolytes (25),(26) and have been used in the formulation of detergents, textile dyeing baths, emulsifiers, auxiliaries for soil/water remediation, flocculants, and dispersants, as binding agents and templates for ceramics manufacture, as well as for application in agriculture and animal husbandry (27). BBS have been reported to bear chemical similarities with humic substances, and to exhibit enhanced adsorption capacity towards polar pollutants given the presence of several carboxylate and phenolic groups carrying negative charges at neutral pH, as well as photosensitizing properties (27) promoting significant mineralization of the organic carbon (24).

Hence, the aim of this study is to prepare new hybrid materials by surface immobilization of negatively charged BBS molecules on the positively charged surface of γ-Al_2O_3 taking advantage of electrostatic interactions occurring between them. After characterization and stability test, the materials were used as adsorbents and compared with other systems cited in the literature (reported in Table 2.1) to evaluate their adsorption capacity towards the cationic dye Crystal Violet (CV). Once identified the best adsorbing material for CV removal, two Contaminants of Emerging Concern (CECs) (28), namely Atenolol and Carbamazepine, were tested.

Table2. 1. Removal of CV from aqueous solutions by several adsorbents reported in the literature.

adsorbents	qm (max capacity) (mg/g)	Ref.	Temperature °C	pH
Zeolite from fly ash	19.6	(29)	25	5
Acid treated zeolite	17.7	(29)	25	5
Magnetic nanocomposite	158.73	(6)	50	6.5
Soil silver nanocomposite	1.923	(30)	30	4.68
Jute fiber carbon	27.99	(31)	30	9
Semi-IPN hydrogels	35.09	(7)	25	7.4
Coniferous pinus bark powder (CPBP)	32.78	(32)	30	8
Chitosan hydrogels beads	76.9	(33)	30	7
Phosphoric acid activation carbon (PAAC)	60.42	(34)	28	6
Sulphuric acid activated carbon (SAAC)	85.84	(34)	28	6.04
Magnetically modified activated carbon	67.1	(35)	20	9
Nanomagnetic iron oxide	16.5	(35)	20-40	9

Magnetic nanocomposite	81.7	(36)	(10-50)	8.5
Unye bentonite	131	(37)	22	6.5
MCM-41	236.64	(38)	25	4
Saw dust	341	(39)	(15-50)	neutral pH
Modified sphagnum peat moss	121.95	(40)	20	6.5
Polyacrylic Acid-bound magnetic nano particles	116	(41)	25	6
Acid-treated montmorillonite	400.0	(42)	30	5.9
Treated ginger waste	277.7	(43)	(30-50)	6.2
Carboxylate-functionalized cellulose nanocrystals	243.9	(44)	30	6
Mango stone biocomposite	352.79	(45)	33	8
Multi-walled carbon nanotubes	90.52	(46)	25	6-8
Carbon nanotubes supported nanocables	228.30	(47)	(25-45)	9
Polyacrylamide-bentonite composite	144.60	(48)	30	6
γ-zirconium phosphate	320.20*	(49)	25	9

Modified Cellulose	169.9-218.8	(50)	50	9
Surfactant-modified nano-alumina	254.3	(51)	25	4
CaCO3–LTN Hybrids	6.34*	(52)	25	6
CaCO3 bare	3.35	(52)	25	6
De-oiled soya	5	(16)	30	8

* The related amounts are not q_m but refer to the following experimental conditions: In Ref. 49: 500 mg of adsorbent in 523.3 ml of 1.5×10^{-2} M dye in water for a contact time of 48 h, Ref. 52: 30 mg of adsorbent was poured in 5 ml of 0.1mM of dye under stirring for 420 min.

2.2. Experimental

2.2.1. Materials

γ- alumina was kindly supplied by Centro Ricerche FIAT, the X-ray diffraction pattern confirms the expected crystalline structure of the material consistent with the reference card 01-075-0921 related to γ-Al_2O_3. As a simple electrostatic interaction of the support with the BBS molecules is not expected to modify the crystalline structure of the support, the hybrid sample diffractograms are not shown.

BBS were extracted from composted organic refuses (from urban public park trimming and home gardening residues) aged for more than 180 days supplied by ACEA Pinerolese Industriale (23). The extraction procedure was described elsewhere(53).

Crystal violet (CV) was purchased from Merck and used without any further treatment to prepare solution in ultrapure MilliQ water for adsorption tests.

Carbamazepine and Atenolol were provided by Sigma-Aldrich (Steinheim, Germany) in analytical purity ≥ 99.0% and used in adsorption experiments.

All aqueous solutions for HPLC analysis were prepared using ultrapure water Millipore Milli-QTM (resistivity > 18 MΩ). All chemicals were used without further purification.

2.2.2. Preparation of hybrid materials

The γ-Al_2O_3 particles were used as support for different amounts of BBS immobilized at their surface by simple electrostatic interaction occurring between the two components carrying opposite surface charges.

Hybrid materials were prepared by mixing 1 g of γ-Al_2O_3 in 20 ml of distilled water containing 0.1, 0.2 and 0.4 g of BBS under stirring for 24 h at 25°C. The pH of solution was about 6.5 during the preparation. The samples were washed with 10 mL of distilled water for 10 minutes and every time centrifuged at 4000 rpm for 10 min. The washing solution was tested using UV-Vis spectrophotometer to evidence the presence of leached BBS molecules. The procedure was carried out several times, till the washing solution did not evidence the presence of BBS in the UV-Vis spectra. Drying process was performed in the oven at 40 °C for 24 h. Hybrid samples were named **A**-BBS0.1, **A**-BBS0.2 and **A**-BBS0.4, the reference pure alumina sample was indicated as **A**.

2.2.3. Characterization methods

X-ray diffraction (XRD) analyses of alumina support was obtained using a X'Pert PRO MPD diffractometer from PANalytical, equipped with Cu anode and working at 45 kV and 40 mA in a Bragg-Brentano geometry. In this study, the flat sample-holder configuration was used.

Fourier transform infrared (FTIR) spectra were recorded in transmission mode by means of a Bruker Vector 22 spectrophotometer equipped with Globar source, DTGS detector, and working with 128 scans at 4 cm^{-1} resolution in the 4000–400 cm^{-1} range. Samples were dispersed in KBr (approximatively, sample : KBr weight ratio was 0.045).

Nitrogen adsorption-desorption experiments were carried out using an ASAP 2010 Micromeritics volumetric apparatus. Before the measurements, the samples were outgassed at 40 °C for 24 h. Specific surface areas (SSA) were calculated using the Brunauer, Emmett and Teller (BET) method. Pore volumes (PV) and Pore Size Distribution (PSD) were determined by the Barrett, Joyner and Halenda method (54) applied to the isotherm desorption branch.

Zeta potential measurements were performed on the instrument Zetasizer by Malvern. 10 mg of BBS and hybrid materials were suspended in 20 ml of deionized water under constant stirring (400 rpm) for 15 min. The zeta potential measurements were performed starting from the natural pH of the suspension then decreasing it point by point by addition of 0.1 M HCl and successively increasing it with 0.1 M NaOH. A digital pH meter (Metrohm, model 827 pH lab, swiss mode) was used to measure the pH of the solution.

Thermo-gravimetric analysis (TGA) was carried out using a TA Q600 (TA Instruments). Thermal analyses were performed with a heating ramp of 10 °C/min from RT to 600°C under air in order to quantify the amount of BBS immobilized on γ-Al_2O_3 particles.

2.2.4. Adsorption procedures

2.2.4.1. Analytical instruments

UV-Vis spectrophotometer (Varian Cary 300 Scans) was used to determine the adsorption of CV (maximum absorbance at 584 nm).

A Merck-Hitachi liquid chromatographer equipped with Rheodyne injector L-6200 and L-6200A pumps for high-pressure gradients, L-4200 UV-Vis detector and a LiChrocart RP-C18 column (Merck, 12.5 cm x 0.4 cm) was used to determine the concentration of atenolol and carbamazepine during the experiments. The detection wavelength was set at 224 nm for atenolol and 284 nm for carbamazepine). Isocratic elution (1 mL min^{-1} flow rate) was carried out with 60% of phosphate buffer $1x10^{-2}$ M at pH 2.8 and 40% acetonitrile and retention times were 5 min.

2.2.4.2. Kinetic of CV adsorption

The kinetic of the adsorption was followed contacting 10 ppm of CV with 20 mg of adsorbing hybrid materials (total volume 10 mL) at pH 6.5 (therefore, a CV : adsorbent ratio of 1:2 wt. was applied to all the preliminary measurements). The mixture was stirred vigorously under isolated orbital mixing plate (rotation at 1000 rpm) keeping the temperature at 15°C. The

adsorption phenomenon was followed measuring every 10 minutes the absorbance of the dye in the supernatant after centrifugation (at 4000 rpm for 10 min) by means of a UV-Vis spectrophotometer. Although an equilibrium time of less than or equal to 10 minutes was evidenced, all the experiments were carried out leaving adsorbent and adsorptive in contact for 30 minutes. All the measurements (data not showed) were carried out in duplicate.

2.2.4.3. CV adsorption study and model application

The adsorption experiments performed on the hybrid absorbents were carried out at 15°C and pH=6.5 (natural value of the suspensions in CV) modifying the relative amount of CV and adsorbent in order to explore a wide Ce range (10 to 100 mg of dye were mixed with 20 mg of adsorbents in 10 mL).

Adsorption studies were carried out using 20 mg of adsorbents in contact with 10 batches containing 10 mL of different concentration of CV aquatic solution (from 10 to 100 ppm). The batches were sealed and placed in a shaker for 30 minutes at 15°C and pH=6.5 to obtain the measurement of the adsorption capacity. The experiments were performed in duplicate and average values were reported.

The adsorption capacity was calculated by using Eq. (1):

$$q_e = \frac{(C_0 - C_e) \times V}{W}, \quad (1)$$

Where C_0 (mg/L) is the initial dye concentration and Ce (mg/L) is the concentration of dye at equilibrium, V (L) is the volume of dye concentration, W (g) is the mass of the adsorbent

and q_e (mg/g) is the amount of dye CV adsorbed. The percentage removal of CV was calculated from the formulae given below:

$$R\% = \frac{(C_0 - C_e)}{C_0} \times 100 \quad (2)$$

Freundlich and Langmuir models were applied to the experimental data.

2.2.4.3.a. Freundlich model

The Freundlich model considers an adsorption taking place on a heterogeneous surface. The isotherm model can be represented by the following equation:

$$ln\, q_e = ln\, K_F + \left(\frac{1}{n}\right) lnC_e \quad (3)$$

where Ce is the adsorbate equilibrium concentration expressed in mg/L, qe is the amount of adsorbate in the adsorbent at equilibrium expressed in mg/g, KF is the Freundlich constant representing the affinity of the adsorptive towards the adsorbing material, 1/n is the Freundlich constant, representing the degree of affinity adsorptive/adsorbing material and indicating how much the adsorption process is favored (n<1 indicates a poor adsorption and the desorption as the favored process, 1<n<2 indicates a good equilibrium between adsorption/desorption, 2<n<10 represents a very good adsorption going towards an irreversible phenomenon (55)).

KF and n can be determined from the linearized plot ln qe vs. Ce (not reported for the sake of brevity).

2.2.4.3.b. Langmuir model

The Langmuir model assumes the adsorption reaches a monolayer of coverage. (56)

The general equation is:

$$q_e = \frac{q_o b C_e}{1+bC_e}, \quad (4)$$

where C_e is the adsorbate equilibrium concentration expressed in mg/L, C_e is the adsorbate initial concentration expressed in mg/L, q_e is the amount of adsorbate in the adsorbent at equilibrium expressed in mg/g, q_o is the monolayer coverage capacities expressed in mg/g, K_L is the Langmuir constant indicating the ratio of reagents and products at the equilibrium.

In the linearized form Eq. (4) becomes:

$$\frac{C_e}{q_e} = \frac{1}{K_L q_o} + \frac{C_e}{q_o},$$

or:

$$\frac{1}{q_e} = \frac{1}{q_o} + \frac{1}{K_L q_o C_e},$$

The plot reporting $\frac{1}{q_e}$ vs $\frac{1}{C_e}$ allows to obtain q_0 and K_L.

The value:

$$R_L = \frac{1}{1+K_L C_0}, \quad (5)$$

indicates if the adsorption is unfavored (if $R_L > 1$), if shows a linear trend (if $R_L = 1$) or if the adsorption is favored (if $0 < R_L < 1$). $R_L = 0$ indicates that the reaction is irreversible.

2.2.4.4. Contaminants of Emerging Concern (CECs) adsorption study

Kinetic studies were performed using 10 ppm of Atenolol and Carbamazepine in contact with 20 mg of **A**-BBS0.4 in a volume of 10 mL, at 20°C and pH 6.5. Adsorption studies were performed using different amounts of Atenolol and Carbamazepine in contact with 20 mg of **A**-BBS0.4 in duplicate. The mixtures were kept under stirring at 20°C, pH 6.5 and the residual amount of contaminants was measured at 30 minute-contact time in order to obtain the adsorption isotherms.

2.3. Results and discussion

2.3.1. Materials characterization

2.3.1.1. FTIR spectroscopy

The IR spectra of alumina before and after BBS immobilization were collected in order to assure BBS presence on hybrid alumina systems. The recorded spectra, together with the reference BBS spectrum, are reported in Figure 2.1. The pure alumina sample shows the presence of atmospheric water molecules interacting with the surface and producing a signal

at 1630 cm^{-1} (δ_{HOH} vibration) and a large absorption around 3500 cm^{-1} (ν_{OH} vibrations), whereas the intense signal at low wavenumbers (< 1000 cm^{-1}) is due to alumina framework vibrations. Pure BBS shows again an intense signal at around 3500 cm-1 due to OH groups and atmospheric moisture interacting with the surface (ν_{OH} vibrations), a large signal at 1600 cm^{-1} due to both carbonyl (C=O) stretching and vibration of water molecules adsorbed at the surface (δ_{HOH} signal), and other two signals at 1400 and 1000 cm^{-1} due to carboxylic acid/ C–H bending and OCO vibrations, respectively. Another very weak signals can be observed at around 3000 cm^{-1} due to ν_{CH} stretching vibrations.

Specific signals due to BBS (evidenced in the Figure by vertical lines) are visible in the spectra of the hybrid materials at around 1600, 1400 and 1000 cm^{-1}, whereas the less intense signals at around 3000 are not visible due to the small amount of BBS immobilized on the support. In any case, the presence of these absorptions confirms that alumina functionalization was carried out and, moreover, their increasing intensity suggests an increase of the amount of the functionalizing phase on the **A** support increasing the amount of BBS used during the material preparation. No modification of the signal positions was observed with respect to pure BBS (see curve A in the figure), as expected for a simple electrostatic interaction occurring between alumina surface and BBS molecules. Moreover, it is possible to evidence an important contribute of the hydration layer on the hybrid samples surface, as witnessed by the growth of the signal at 1600 (δ_{HOH} vibration) and 3500 cm^{-1} (ν_{OH}), given the polar nature of BBS molecules leading to a stronger interaction with atmospheric moisture.

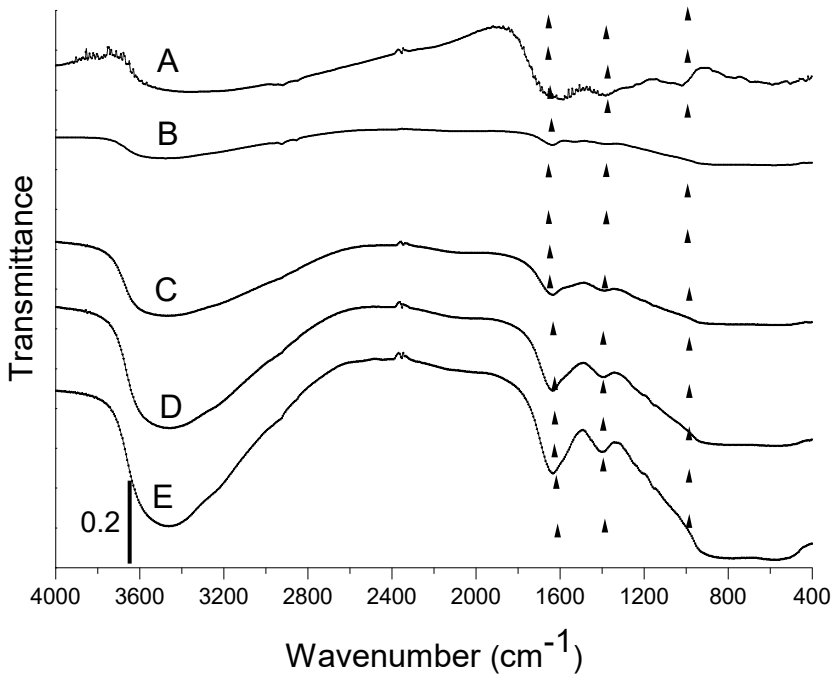

Figure 2. 1. FTIR spectra of BBS (curve A) pure gamma alumina (B), A-BBS0.1 (C), A-BBS0.2 (D) and A-BBS0.4 (E). The spectra were shifted for the sake of clarity, the vertical lines represent the most intense signals due to BBS.

2.3.1.2. Gas-volumetric N_2 adsorption at 77K

The adsorption/desorption isotherms of all hybrid materials and reference non-modified sample are of the IV type (IUPAC classification) indicating that all materials are mesoporous (Figure 2.2. A).

As it can be seen, the hysteresis loops of all the samples are very similar, although the height of the step decreases by increasing the amount of BBS indicating a minor amount of

mesopores after functionalization of the support. Nevertheless, the amount of BBS immobilized seems to be not enough to modify the featuring morphology of the material. The value of BET specific surface area of the materials are reported in Table 2.2 together with the total amount of mesopores, evaluated by BJH model on the desorption branch of the isotherms, whereas the pore size distribution curves are reported in Figure 2.2. B. The specific surface area of the samples decreases increasing the amount of BBS, although to a very limited extent. This suggests that BBS is not immobilized at the external surface of the particles, since they do not act as aggregating agent between the single alumina particles, as the loss of specific surface area of the material after functionalization should be much higher. This indicates that BBS are allocated essentially into the mesopore empty space, probably because in that space the electrostatic interaction of the support with the molecule can be stronger. The pore size distribution curves allow to obtain other important details concerning the interaction BBS-solid. All samples show two families of mesopores, the first one quite narrow centered at 37 Å of width and another one very wide covering the values 20-180 Å of width. Both families of pores are affected by support functionalization because the large mesopores decrease in amount and width, the relative maximum shifting from 80 to 60 Å of width, whereas the smaller ones increases in intensity after functionalization. This feature suggests that the smallest pores are not involved in the functionalization, probably because of the limited dimensions, whereas BBS are placed into the largest pores, which are those decreasing in amount and size after functionalization causing the increase of the amount of the smallest ones. Also the fact that the hystheresis loops of the isotherms do not change shape after functionalization confirms again that BBS molecules enter into the pores

sticking at the internal walls of the solid (causing a decrease of their size) rather than fixing at their entrance (causing the modification of the pore shape which is not observed indeed).

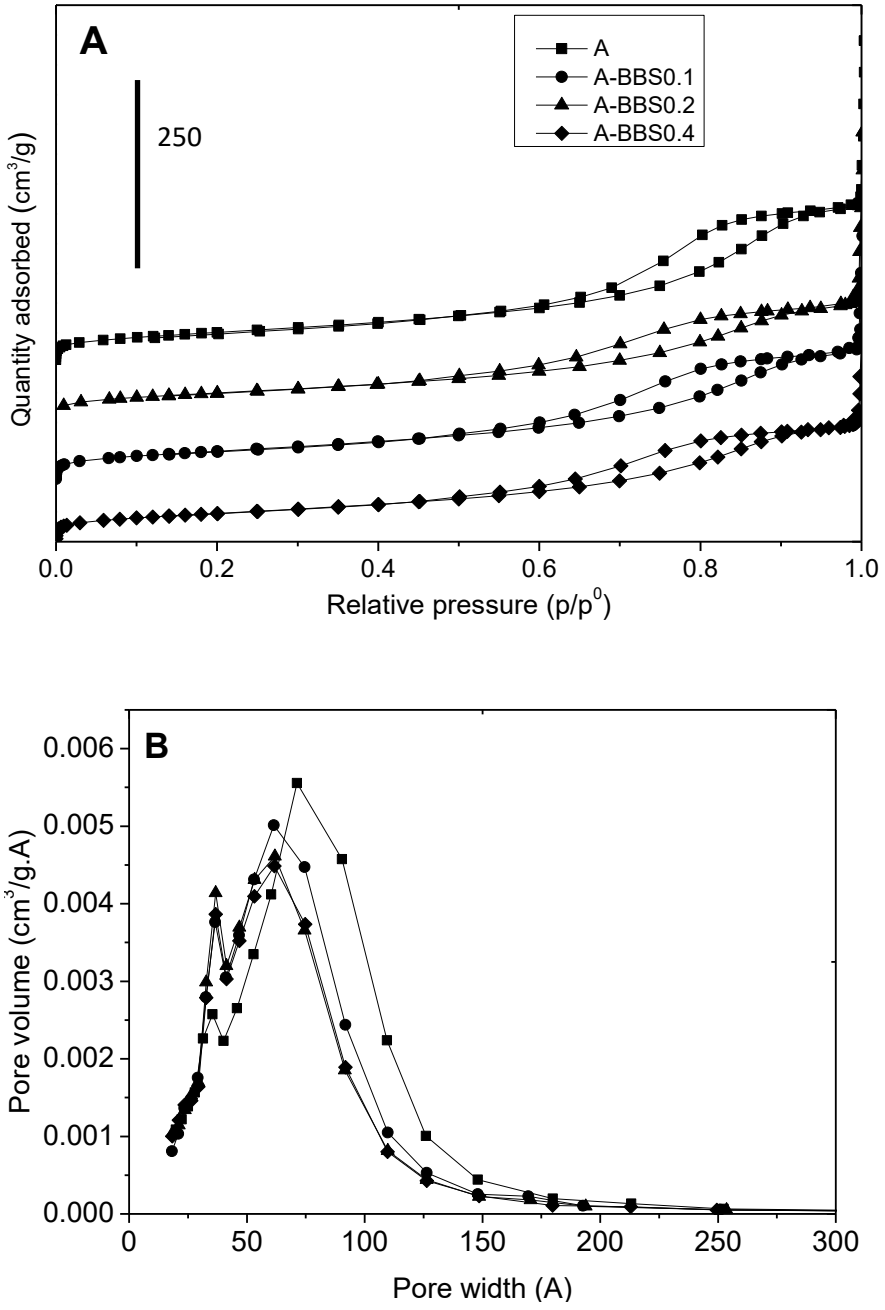

Figure 2. 2. Nitrogen adsorption-desorption isotherms (section A) and BJH desorption pore size distribution (section B) of reference alumina (squares) and hybrid materials: A-BBS0.1 (circles), A-BBS0.2 (triangles) and A-BBS0.4 (diamond). In section A the curves were shifted for the sake of clarity.

Table2. 2 Texture features for reference and hybrid materials.

Materials	BET Specific surface area (m2/g)	BJH Pore volume (cm3/g)
A	186	0.42
A-BBS0.1	181	0.33
A-BBS0.2	172	0.30
A-BBS0.4	165	0.29

2.3.1.3. TGA

Figure 2.3, upper section, shows the results of TGA analysis on sample **A** before and after immobilization of BBS in the temperature range 40-650°C under air, Figure 2.3, lower section, reports the curve related to BBS weight loss registered in the same conditions. BBS evidences two main regions of weight loss, the first in the range 40-220°C related to physisorbed and chemisorbed water elimination, the second, occurring in two steps, in the range 220-650°C related to the oxidation of BBS. Analogously, all the curves of **A** and hybrid materials present two important weight losses. The foster falls in the range 40-220°C and is due to the removal of adsorbed water molecules: this contribution increases increasing the amount of BBS on the hybrid samples as a consequence of the increased interaction with

atmospheric moisture given by the increased polarity of the materials. The latter falls in the range 220-650°C and deserves some comments. Alumina sample possesses surface OH groups that can be partially eliminated via condensation reaction in form of water molecules at high temperature: the weight loss observed in the range 220-650°C (1.1 %) can be assigned to this phenomenon. Otherwise, the hybrid materials treated at high temperature can experience both the OH elimination via condensation reaction and the elimination of organic moieties through an oxidation reaction which forms CO_2 and H_2O. From the comparison of the four curves, it is possible to quantify the amount of the three contributions, namely adsorbed water molecules, amount of OH eliminated via condensation reaction and organic content, for the four samples as reported in Table 2.3.

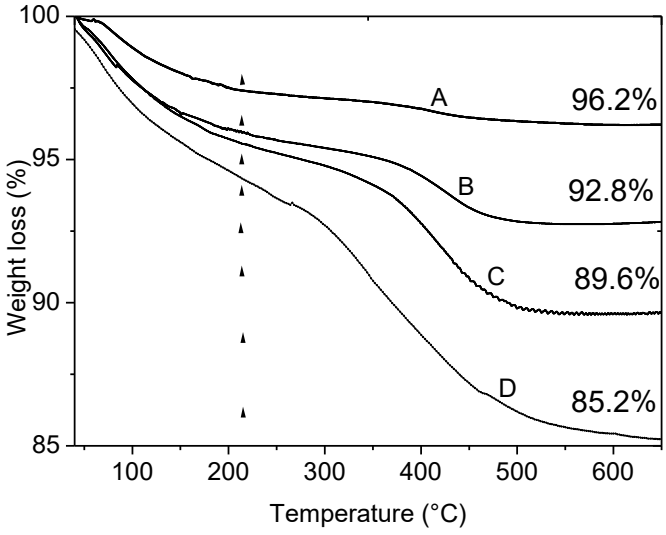

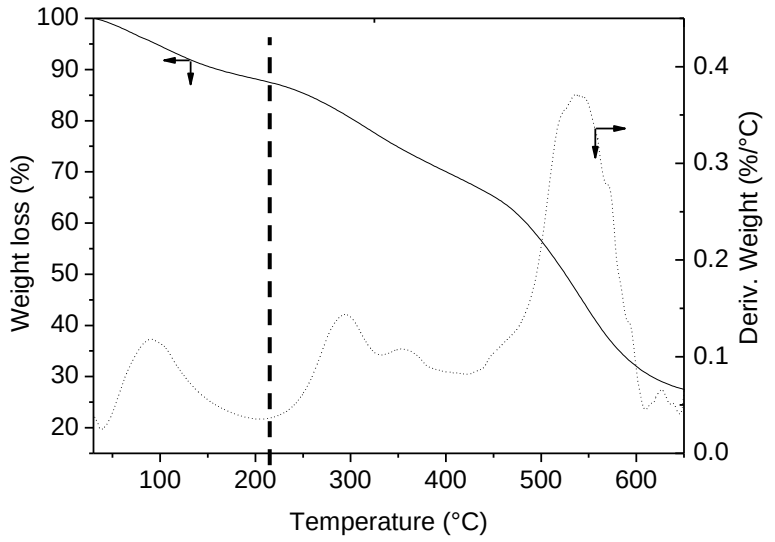

Figure 2. 3. TGA curves obtained in air. Upper section: A (curve A), A-BBS0.1 (B), A-BBS0.2 (C) and A-BBS0.4 (D); lower section: the weight loss (solid line) and derivative weight loss (dotted line) of BBS. The values indicated in the upper picture indicate the total weight loss measured for the materials, the vertical dotted lines indicate the temperature of 220°C used for the quantification of water and organics loss.

Table2. 3. Weight losses observed for reference and hybrid materials.

Materials	40-220°C (Adsorbed water %)	220-650°C (Organic content and OH groups eliminated %)	OH groups eliminated (%)	Measured organic content (%) ± 0.1
A	2.8	-	1.1	-
A-BBS0.1	4.4	2.7	1.1	1.6

A-BBS0.2	4.9	5.4	1.1	4.3
A-BBS0.4	6.5	8.2	1.1	7.1

The amount of BBS actually loaded onto the support is obtained by calculating the percentage of weight loss for **A**-BBS0.1, **A**-BBS0.2 and **A**-BBS0.4 in the range of 220 to 650 °C and subtracting that observed for **A** support in the same range. The amount of organic matter actually immobilized on hybrid samples depends on the concentration of the BBS solution used for the functionalization: in these experiments the maximum loading has been reached by **A**-BBS0.4 with 7.2 % of organic matter immobilized.

2.3.1.4. Zeta potential

The zeta potential measurements have been used in order to evaluate the surface charge of the support and its modification after BBS functionalization. This is a very important indication, dealing with adsorption, in order to forecast the type of substrate that can be subjected to efficient interaction with the materials.

Figure 2.4 shows the trend of zeta potential in the pH range 3-11. From the measured trends it is possible to conclude the reference **A** material possesses a positive surface charge in the range 4-7.9 and this makes easy an interaction of the solid with negatively charged substrates. At neutral pH, in particular, BBS molecules bring a negative charge given essentially by dissociated COOH and phenolic Ph-OH groups, therefore the interaction with the alumina positive solid surface occurs very easily. Consequently, the isoelectric point (IEP) of hybrid materials shifts to lower pH increasing the BBS loading.

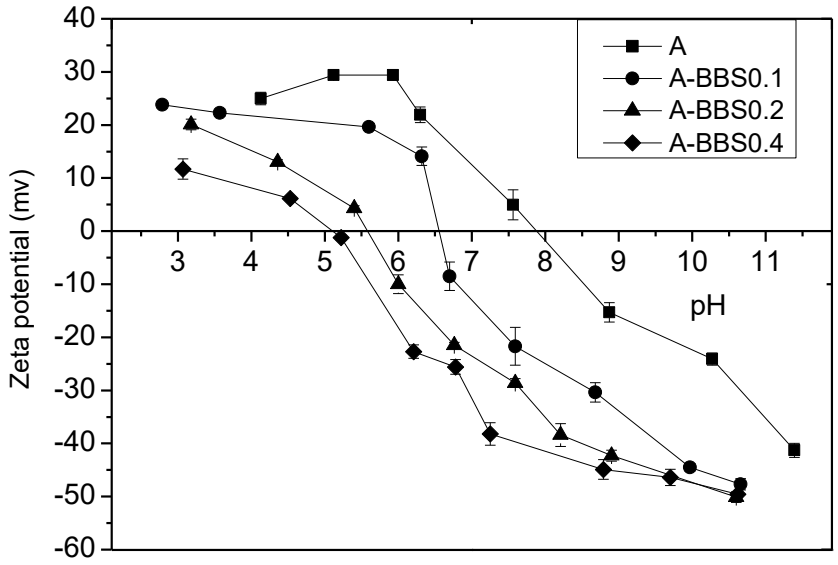

Figure 2. 4. Zeta potential trends of A (squares), A-BBS0.1 (circles), A-BBS0.2 (triangles) and A-BBS0.4 (diamonds) as a function of pH.

2.3.2 Removal of crystal violet

2.3.2.1. Effect of CV concentration

The chemical structure of CV is reported in Scheme 2.1.

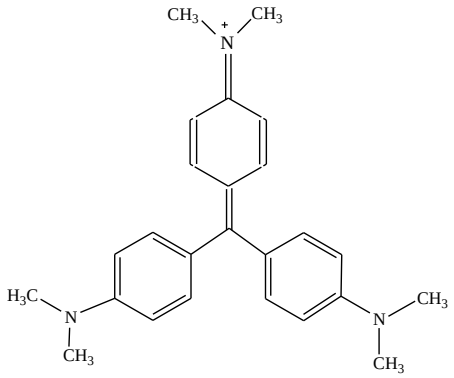

Scheme 2. 1. Structure of Crystal Violet

Different concentrations of dye from 10 to 100 ppm have been used for adsorption experiment keeping constant the amount of hybrid absorbents. Results reported in Figure 2.5 indicate that an increase of the dye concentration leads to a decrease in the amount of dye adsorbed from 43% to 17% for **A**-BBS0.1, from 80% to 37% for **A**-BBS0.2 and from 91% to 67% for **A**-BBS0.4. Although the removal decreases increasing CV concentration because of the adsorbing materials saturation, the amount of dye removed by **A**-BBS0.4 remains at the value of about 70%, indicating a very good performance. On this material the adsorption of atenolol and carbamazepine was performed.

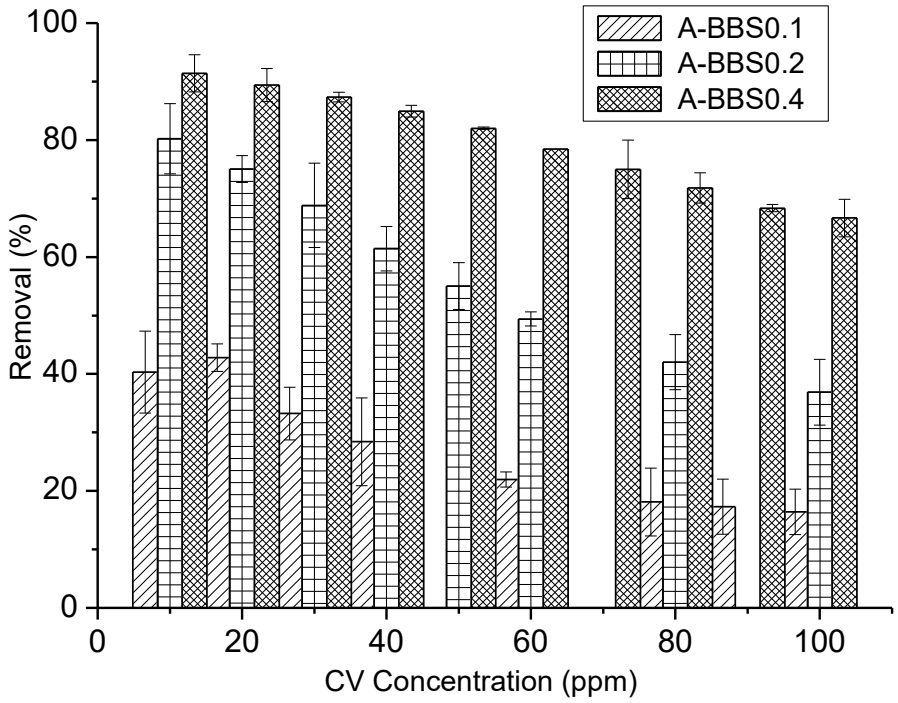

Figure 2. 5. Adsorption % of dye CV by different hybrid adsorbents A-BBS0.4, A-BBS0.2 and A-BBS0.1, versus initial dye concentration at 15 °C.

2.3.2.2. Adsorption isotherms and model application

In Figure 2.6 the removal of CV by the hybrid adsorbents was reported in form of adsorption isotherms. Clearly **A**-BBS0.1 reached the saturation in our experimental conditions, whereas **A**-BBS0.2 and, even more, **A**-BBS0.4 are still far from the saturation.

Langmuir and Freundlich models were applied to the experimental data and the most significant results are reported in Table 2.4. A very good fitting was obtained applying Langmuir model, as indicated by very high values of r^2. q_m obtained by this model defines the amount of CV saturating the samples (monolayer amount): the value obtained for the best

adsorbent **A**-BBS0.4 corresponds to a maximum adsorption of about 35 mg/g. The RL values (always $0<R_L<1$) obtained for all the samples indicate a favored adsorption, as also suggested by Freundlich n values always higher than 2.

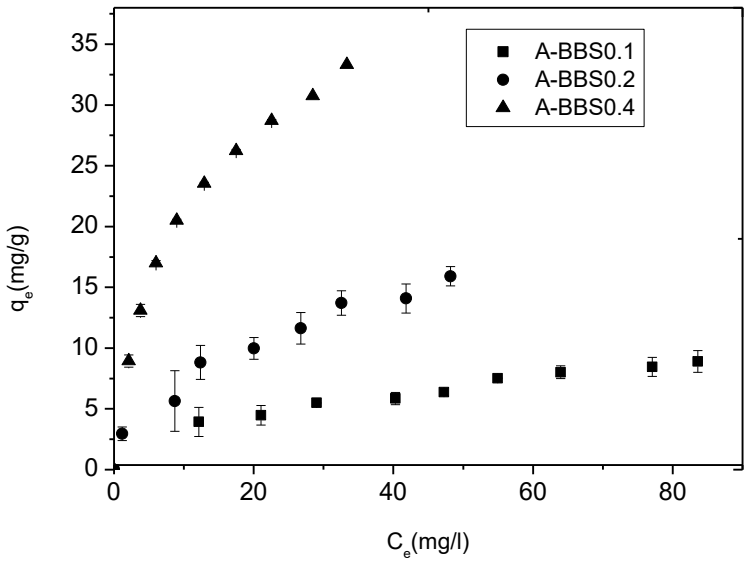

Figure 2. 6. Equilibrium isotherms for the adsorption of CV by different hybrid adsorbents in MilliQ water at 15 °C.

Table2. 4. Langmuir and Freundlich model parameters calculated by linear fitting of the adsorption data.

Model		**A**-BBS0.1		**A**-BBS0.2		**A**-BBS0.4	
		Value	S.E.	Value	S.E.	Value	S.E
Langmuir	q_m (mg/g)	8.92	0.59	21.38	2.50	35.09	0.61
	K_L (mg/L)	0.065	0.020	0.087	0.048	0.09	0.090
	r^2	0.975	-	0.977	-	0.992	-

	RL	0.898		0.861		0.763	
Freundlich	KF (mg/g)(L/mg)	14.08	5.58	28.547	6.75	67.54	8.455
	n	2.52	0.65	2.170	0.203	2.084	0.164
	r^2	0.995	-	0.94	-	0.978	-

2.4. Removal of CECs

Figure 2.7 reports the kinetic of adsorption relative to two different CECs, Carbamazepine and Atenolol, whose structures are shown in Scheme 2.2. These CECs were chosen on the basis of their chemical structure: both molecules show positively charged structure at pH 6.5 (57), but while Atenolol possessed a branched aliphatic chain, Carbamazepine is a polyaromatic and more compact molecule.

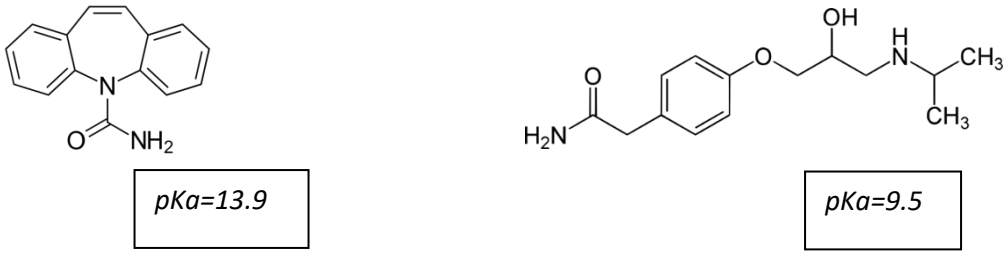

Scheme 2. 2. Structure of Carbamazepine (left side) and Atenolol (right side) and related pKa (58)-(59).

The efficiency of the material remained acceptable with the larger polar molecule atenolol which is more easily adsorbed with 51% of removal in 30 minutes thanks to its polar

structure and consequently stronger interaction with adsorbent, whereas in the case of carbamazepine only 32% of removal was reached in 30 min suggesting a worse affinity between the material and the polyaromatic substrate.

Langmuir and Freundlich models were also applied to CEC adsorption and the most significant results are reported in Table 2.5. Good fittings were observed applying both Langmuir and Freundlich models as indicated by very good values of r^2. q_m obtained by these models defines the amount of Carbamazepine and Atenolol saturating the samples (monolayer amount): the values obtained for the Carbamazepine and Atenolol correspond to maximum adsorption of about 3.06 and 3.26 mg/g respectively. A comparison study of capacity of adsorption for different adsorbents was performed and the results are reported in Table 2.6. Considering the literature we have reached promising results in particular in the adsorption of Carbamazepine.

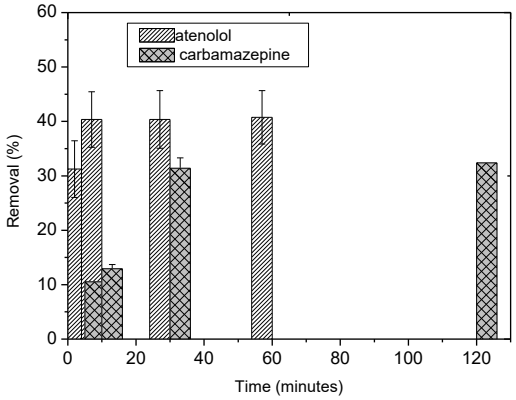

Figure 2. 7. Kinetic of removal of 10 ppm of Carbamazepine and Atenolol at 20°C by 20 mg of A-BBS0.4 in 10 mL of solution expressed in removal percentage.

Table2. 5. q_m of adsorption of CECs by A-BBS0.4

Model		Carbamazepine		Atenolol	
		Value	S.E.	Value	S.E.
Langmuir	q_m (mg/g)	3.0628	0.06	3.26	0. 145
	KL (mg/L)	0.119	0.057	0.11	0.008
	r^2	0.917	-	0.904	-
Freundlich	KF (mg/g)(L/mg)	0.405	0.07	4.43	0.13
	n	1.526	0.35	0.77	0.006
	r^2	0.905	-	0.906	-

Table2. 6. Removal of organic pollutants from wastewater

adsorbents	q_m (mg/g)	Ref.	CEC	Temperature (°C)	pH
A-BBS0.4	3.26 3.06	This study	Atenolol Carbamazepine	20	6.5

Agricultural soils	0.01	(60)	Carbamazepine	25	9.2
Functionalized silica	0.04	(61)	Carbamazepine	25	7
Granulated cork	1.84	(62)	Carbamazepine	20±2	4.6
Activated carbon	18.8	(63)	Atenolol	25	6
Graphene oxide	95	(64)	Atenolol	25	2

2.5. Conclusions

New hybrid absorbents were prepared following a very easy procedure and characterized via TGA, XRD, Zeta potential, FTIR spectroscopy and nitrogen adsorption then, they were tested towards the removal of selected pollutants. BBS can functionalize the alumina surface given the electrostatic attraction of opposite charges carried by the two components. In this way, cationic pollutants can be captured by the negatively charged surface of the adsorbent. The electrostatic interaction is, therefore, the major driving force for the adsorption process, but the polarity of the pollutant molecules affects both kinetics and adsorbed amounts as less polar molecules interact at lower extent and in longer time.

The strength of these new hybrid materials is not so much in photocatalytic efficiency, (the comparison in CV removal is reported in Figure 2.8), as in the simplicity of preparation and in its definitely "green" way. In fact not only the efficiency of the materials should be taken

in account but also other aspects deserve to be considered, i.e. the easiness and the green aspects related to the materials preparation procedure and the energy and economic savings. In fact, several materials with very good performances reported in Table 2.1 are prepared following complex procedures and use of non-green processes. In order to perform this comparison, we considered only the materials with better performance in CV adsorption with respect to the **A**-BBS hybrid system and we classified them on the basis of the following aspects: energy consumption (calcination and/or thermal treatment at temperature higher than 200°C), multistep/complex synthesis, use of non-green compounds (acids, bases, solvents and so on). In the classification we assigned a color code from green to orange to red considering the absence of these negative aspects or their simultaneous presence during the preparation. As evidenced in Figure 2.8, several materials possessing much better adsorption capacity with respect to the **A**-BBS system show orange or red color, whereas only few, as **A**-BBS0.4, show the green color.

From this perspective, the **A**-BBS materials can be developed further and their performance optimized in view of their use in in-field applications.

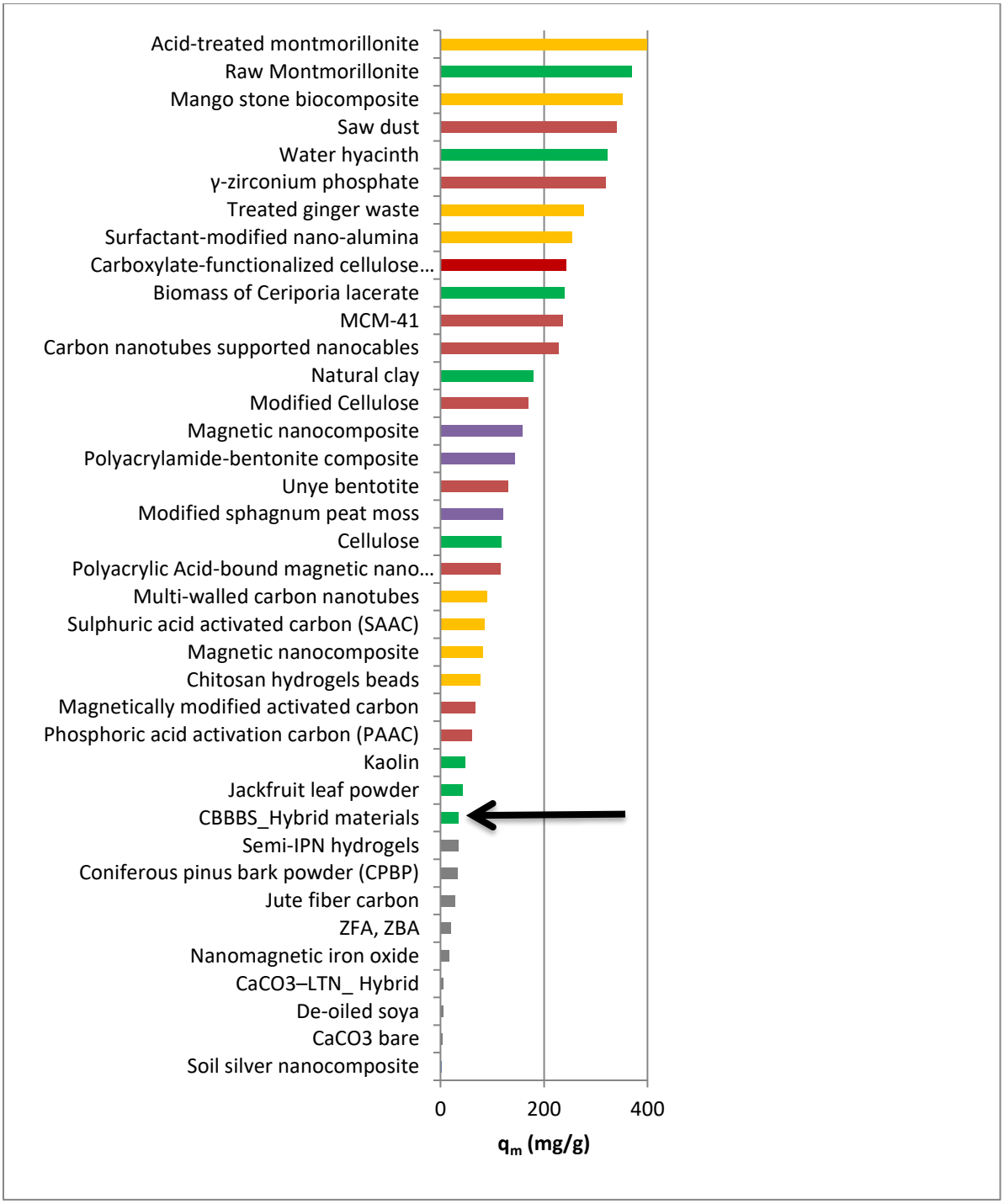

Figure 2. 8. Removal of CV from aqueous solution by A-BBS and adsorbents materials reported in the literature and listed in this work (Table 2.1). The colors have been assigned on the base of aspects related to possible upscaling of the processes involving the materials: energy consumption, multistep/complex synthesis, use of non-green compounds, as described in the text.

Funding: This project has received funding from the European Union's Horizon 2020 research and innovative programme under the Marie Sklodowska-Curie grant agreement No 645551.

2.6. References

1. Zhang R, Shen B, Li C, Zheng C, Hou X. Integrating photochemical vapor generation with photo-oxidation trapping for effective mercury removal from polluted water and its on-line monitoring. Microchem J. 2016;129(6):98–103. Available from: http://dx.doi.org/10.1016/j.microc.2016.06.014

2. Farsi A, Malvache C, De Bartolis O, Magnacca G, Kristensen PK, Christensen ML, et al. Design and fabrication of silica-based nanofiltration membranes for water desalination and detoxification. Microporous Mesoporous Mater. 2017 Jan;237:117–26. Available from: http://linkinghub.elsevier.com/retrieve/pii/S1387181116304048

3. Calza P, Zacchigna D, Laurenti E. Degradation of orange dyes and carbamazepine by soybean peroxidase immobilized on silica monoliths and titanium dioxide. Environ Sci Pollut Res. 2016;5(2):1–8. Available from: http://link.springer.com/10.1007/s11356-016-7399-1

4. Richardson SD, Ternes TA. Water Analysis: Emerging Contaminants and Current Issues. Anal Chem. 2018;90(1):398–428.

5. Zhu C, Jiang C, Chen S, Mei R, Wang X, Cao J, et al. Chemosphere Ultrasound enhanced electrochemical oxidation of Alizarin Red S on boron doped diamond (BDD) anode : Effect of degradation process parameters. 2018;209(4):685–95.

6. Rai P, Gautam RK, Banerjee S, Rawat V, Chattopadhyaya MC. Synthesis and characterization of a novel SnFe2O4@activated carbon magnetic nanocomposite and its effectiveness in the removal of crystal violet from aqueous solution. J Environ Chem Eng. 2015;3(4):2281–91.

7. Li S. Removal of crystal violet from aqueous solution by sorption into semi-interpenetrated networks hydrogels constituted of poly(acrylic acid-acrylamide-methacrylate) and amylose. Bioresour Technol. 2010;101(7):2197–202.

8. Hassanzadeh-Tabrizi SA, Motlagh MM, Salahshour S. Synthesis of ZnO/CuO nanocomposite immobilized on ??-Al2O3 and application for removal of methyl orange. Appl Surf Sci. 2016;3(5):231–9.

9. Brião G V., Jahn SL, Foletto EL, Dotto GL. Adsorption of crystal violet dye onto a mesoporous ZSM-5 zeolite synthetized using chitin as template. J Colloid Interface Sci. 2017;508:313–22.

10. Rasool K, Lee DS. Effect of ZnO nanoparticles on biodegradation and biotransformation of co-substrate and sulphonated azo dye in anaerobic biological sulfate reduction processes. Int Biodeterior Biodegrad. 2016;109:150–6. Available from: http://dx.doi.org/10.1016/j.ibiod.2016.01.015

11. Wang C, Wang F, Xu M, Zhu C, Fang W, Wei Y. Electrocatalytic degradation of methylene blue on Co doped Ti/TiO2 nanotube/PbO2 anodes prepared by pulse electrodeposition. J Electroanal Chem. 2015;759:158–66.

12. Muthuraman G, Teng TT, Leh CP, Norli I. Extraction and recovery of methylene blue from industrial wastewater using benzoic acid as an extractant. J Hazard Mater. 2009;163(1):363–9.

13. Aguilar ZG, Brillas E, Salazar M, Nava JL, Sirés I. Evidence of Fenton-like reaction with active chlorine during the electrocatalytic oxidation of Acid Yellow 36 azo dye with Ir-Sn-Sb oxide anode in the presence of iron ion. Appl Catal B Environ. 2017;206:44–52. Available from: http://dx.doi.org/10.1016/j.apcatb.2017.01.006

14. Erto A, Chianese S, Lancia A, Musmarra D. On the mechanism of benzene and toluene adsorption in single-compound and binary systems : energetic interactions and competitive effects. Desalin Water Treat. 2017;86(July 2016):259–65.

15. Marković DD, Lekić BM, Rajaković-Ognjanović VN, Onjia AE, Rajaković L V. A new approach in regression analysis for modeling adsorption isotherms. Sci World J. 2014;2014(152):257–61.

16. Mittal A, Mittal J, Malviya A, Kaur D, Gupta VK. Adsorption of hazardous dye crystal violet from wastewater by waste materials. J Colloid Interface Sci. 2010;343(2):463–73.

17. Nisticò R, Magnacca G, Jadhav SA, Scalarone D. Polystyrene- block -poly(ethylene oxide) copolymers as templates for stacked, spherical large-mesopore silica coatings:

dependence of silica pore size on the PS/PEO ratio. Beilstein J Nanotechnol. 2016;7:1454–60. Available from: http://www.beilstein-journals.org/bjnano/content/7/1/137

18. Molinari A, Magnacca G, Papazzoni G, Maldotti A. HydrophobicW10O324-/silica photocatalyst for toluene oxidation in water system. Appl Catal B Environ. 2013;138–139(4):446–52. Available from: http://dx.doi.org/10.1016/j.apcatb.2013.03.025

19. Ghaemi N, Daraei P. Enhancement in copper ion removal by PPy@Al2O3 polymeric nanocomposite membrane. J Ind Eng Chem. 2016;40:26–33. Available from: http://linkinghub.elsevier.com/retrieve/pii/S1226086X1630140X

20. Ghanizadeh S, Bao XJ, Vaidhyanathan B, Binner J. Synthesis of nano alpha-alumina powders using hydrothermal and precipitation routes: a comparative study. Ceram Int. 2014;40(1):1311–9.

21. Deravanesiyan M, Beheshti M, Malekpour A. Alumina nanoparticles immobilization onto the NaX zeolite and the removal of Cr (III) and Co (II) ions from aqueous solutions. J Ind Eng Chem. 2015;21:580–6.

22. Morterra C, Magnacca G. A case study: surface chemistry and surface structure of catalytic aluminas, as studied by vibrational spectroscopy of adsorbed species. Catal Today. 1996;27(3–4):497–532.

23. Nisticò R, Barrasso M, CarrilloLeRoux GA, Seckler MM, Sousa W, Malandrino M, et al. Biopolymers from Composted Biowaste as Stabilizers for the Synthesis of Spherical and Homogeneously Sized Silver Nanoparticles for Textile Applications on Natural Fibers. ChemPhysChem. 2015;7:3902–9.

24. Testa ML, Tummino ML, Agostini S, Avetta P, Deganello F, Montoneri E, et al. Synthesis, characterization and environmental application of silica grafted photoactive substances isolated from urban biowaste. RSC Adv. 2015;5(59):47920–7. Available from: http://dx.doi.org/10.1039/C5RA03164H

25. Schramm LL, Stasiuk EN, Marangoni DG. 2 Surfactants and their applications. Annu Rep Prog Chem, Sect C Phys Chem. 2003;99(2):3–48. Available from: http://xlink.rsc.org/?DOI=B208499F

26. Magnacca G, Laurenti E, Vigna E, Franzoso F, Tomasso L, Montoneri E, et al. Refuse derived bio-organics and immobilized soybean peroxidase for green chemical technology. Process Biochem. 2012;47(12):2025–31. Available from: http://dx.doi.org/10.1016/j.procbio.2012.07.021

27. Avetta P, Bella F, Bianco Prevot A, Laurenti E, Montoneri E, Arques A, et al. Waste cleaning waste: Photodegradation of monochlorophenols in the presence of waste-derived photosensitizer. ACS Sustain Chem Eng. 2013;1(12):1545–50.

28. Musmarra D, Prisciandaro M, Capocelli M, Karatza D, Iovino P, Canzano S, et al. Ultrasonics Sonochemistry Degradation of ibuprofen by hydrodynamic cavitation : Reaction pathways and effect of operational parameters. Ultrason Sonochem. 2016;29:76–83. Available from: http://dx.doi.org/10.1016/j.ultsonch.2015.09.002

29. Bertolini T, Bertolini TCR, Izidoro JC, Magdalena CP, Fungaro DA. Adsorption of Crystal Violet Dye from Aqueous Solution onto Zeolites from Coal Fly and Bottom Ashes.

Orbital - Electron J Chem. 2013;5(3):179–91. Available from: http://www.orbital.ufms.br/index.php/Chemistry/article/view/488

30. Satapathy MK, Das P. Optimization of crystal violet dye removal using novel soil-silver nanocomposite as nanoadsorbent using response surface methodology. J Environ Chem Eng. 2014;2(1):708–14. Available from: http://dx.doi.org/10.1016/j.jece.2013.11.012

31. Porkodi K, Vasanth Kumar K. Equilibrium, kinetics and mechanism modeling and simulation of basic and acid dyes sorption onto jute fiber carbon: Eosin yellow, malachite green and crystal violet single component systems. J Hazard Mater. 2007;143(1–2):311–27.

32. Ahmad R. Studies on adsorption of crystal violet dye from aqueous solution onto coniferous pinus bark powder (CPBP). Vol. 171, Journal of Hazardous Materials. 2009. p. 767–73.

33. Pal A, Pan S, Saha S. Synergistically improved adsorption of anionic surfactant and crystal violet on chitosan hydrogel beads. Chem Eng J. 2013;217:426–34.

34. Senthilkumaar S, Kalaamani P, Subburaam C V. Liquid phase adsorption of Crystal violet onto activated carbons derived from male flowers of coconut tree. J Hazard Mater. 2006;136(3):800–8.

35. Hamidzadeh S, Torabbeigi M, Shahtaheri SJ. Removal of crystal violet from water by magnetically modified activated carbon and nanomagnetic iron oxide. J Environ Heal Sci Eng. 2015;13(1):1–7.

36. Singh KP, Gupta S, Singh AK, Sinha S. Optimizing adsorption of crystal violet dye from water by magnetic nanocomposite using response surface modeling approach. J Hazard Mater. 2011;186(2–3):1462–73.

37. Eren E. Investigation of a basic dye removal from aqueous solution onto chemically modified Unye bentonite. J Hazard Mater. 2009;166(1):88–93.

38. Lee CK, Liu SS, Juang LC, Wang CC, Lin KS, Lyu M Du. Application of MCM-41 for dyes removal from wastewater. J Hazard Mater. 2007;147(3):997–1005.

39. Chakraborty S, De S, DasGupta S, Basu JK. Adsorption study for the removal of a basic dye: Experimental and modeling. Chemosphere. 2005;58(8):1079–86.

40. Hemmati F, Norouzbeigi R, Sarbisheh F, Shayesteh H. Malachite green removal using modified sphagnum peat moss as a low-cost biosorbent: Kinetic, equilibrium and thermodynamic studies. J Taiwan Inst Chem Eng. 2016;58:482–9. Available from: http://linkinghub.elsevier.com/retrieve/pii/S1876107015003302

41. Liao MH, Wu KY, Chen DH. Fast adsorption of crystal violet on polyacrylic acid-bound magnetic nanoparticles. Sep Sci Technol. 2004;39(7):1563–75.

42. Sarma GK, Sen Gupta S, Bhattacharyya KG. Adsorption of Crystal violet on raw and acid-treated montmorillonite, K10, in aqueous suspension. J Environ Manage. 2016;171:1–10. Available from: http://dx.doi.org/10.1016/j.jenvman.2016.01.038

43. Kumar R, Ahmad R. Biosorption of hazardous crystal violet dye from aqueous solution onto treated ginger waste (TGW). Desalination. 2011;265(1–3):112–8.

44. Qiao H, Zhou Y, Yu F, Wang E, Min Y, Huang Q, et al. Effective removal of cationic dyes using carboxylate-functionalized cellulose nanocrystals. Chemosphere. 2015;141:297–303.

45. Shoukat S, Bhatti HN, Iqbal M, Noreen S. Mango stone biocomposite preparation and application for crystal violet adsorption: A mechanistic study. Microporous Mesoporous Mater. 2017;239:180–9. Available from: http://dx.doi.org/10.1016/j.micromeso.2016.10.004

46. Sabna V, Thampi SG, Chandrakaran S. Adsorption of crystal violet onto functionalised multi-walled carbon nanotubes: Equilibrium and kinetic studies. Ecotoxicol Environ Saf. 2016;134:390–7. Available from: http://dx.doi.org/10.1016/j.ecoenv.2015.09.018

47. Liu W, Jiang X, Chen X. Synthesis and utilization of a novel carbon nanotubes supported nanocables for the adsorption of dyes from aqueous solutions. J Solid State Chem. 2015;229:342–9.

48. Anirudhan TS, Suchithra PS, Radhakrishnan PG. Synthesis and characterization of humic acid immobilized-polymer/bentonite composites and their ability to adsorb basic dyes from aqueous solutions. Appl Clay Sci. 2009;43(3–4):336–42.

49. Alhendawi HMH, Brunet E, Payán ER, Juanes O, Ubis JCR, Al-Asqalany M. Surfactant-assisted intercalation of crystal violet in layered γ-zirconium phosphate. Dye uptake from aqueous solutions. J Incl Phenom Macrocycl Chem. 2012;73(1–4):387–96.

50. Zhou Y, Zhang M, Wang X, Huang Q, Min Y, Ma T, et al. Removal of crystal violet by a novel cellulose-based adsorbent: Comparison with native cellulose. Ind Eng Chem Res. 2014;53(13):5498–506.

51. Zolgharnein J, Bagtash M, Shariatmanesh T. Simultaneous removal of binary mixture of Brilliant Green and Crystal Violet using derivative spectrophotometric determination, multivariate optimization and adsorption characterization of dyes on surfactant modified nano-γ-alumina. Spectrochim Acta - Part A Mol Biomol Spectrosc. 2015;137:1016–28.

52. Liu Y, Jiang Y, Hu M, Li S, Zhai Q. Removal of triphenylmethane dyes by calcium carbonate-lentinan hierarchical mesoporous hybrid materials. Chem Eng J. 2015;273:371–80.

53. Montoneri E, Boffa V, Savarino P, Perrone DG, Musso G, Mendichi R, et al. Biosurfactants from urban green waste. ChemSusChem. 2009;2(3):239–47.

54. Thommes M, Kaneko K, Neimark A V., Olivier JP, Rodriguez-Reinoso F, Rouquerol J, et al. Physisorption of gases, with special reference to the evaluation of surface area and pore size distribution (IUPAC Technical Report). Pure Appl Chem. 2015;87(9–10):1051–69.

55. García E, Medina R, Lozano M, Hernández Pérez I, Valero M, Franco A. Adsorption of Azo-Dye Orange II from Aqueous Solutions Using a Metal-Organic Framework Material: Iron-Benzenetricarboxylate. Materials (Basel). 2014;7(12):8037–57. Available from: http://www.mdpi.com/1996-1944/7/12/8037/

56. Esfandian H, Samadi-Maybodi A, Parvini M, Khoshandam B. Development of a novel method for the removal of diazinon pesticide from aqueous solution and modeling by artificial neural networks (ANN). J Ind Eng Chem. 2015;35:295–308. Available from: http://dx.doi.org/10.1016/j.jiec.2016.01.011

57. Calza P, Medana C, Padovano E, Giancotti V, Baiocchi C. Identi fi cation of the unknown transformation products derived from clarithromycin and carbamazepine using liquid chromatography / high-resolution mass spectrometry. Rapid Commun Mass Spectrom. 2012;26(April):1687–704.

58. Akpinar I, Yazaydin AO. Rapid and Efficient Removal of Carbamazepine from Water by UiO-67. Indusrial Eng Chem Res Res. 2017;56:15122–30.

59. Park J, Hwa K, Lee E, Lee S, Cho J. Science of the Total Environment Sorption of pharmaceuticals to soil organic matter in a constructed wetland by electrostatic interaction. Sci Total Environ. 2018;635:1345–50. Available from: https://doi.org/10.1016/j.scitotenv.2018.04.212

60. Calisto V, Esteves VI. Adsorption of the antiepileptic carbamazepine onto agricultural soils. 2012;1597–603.

61. Suriyanon N, Punyapalakul P, Ngamcharussrivichai C. Mechanistic study of diclofenac and carbamazepine adsorption on functionalized silica-based porous materials. Chem Eng J. 2013;214:208–18. Available from: http://dx.doi.org/10.1016/j.cej.2012.10.052

62. Mallek M, Chtourou M, Portillo M, Monclús H, Walha K, Salvadó V. Granulated cork as biosorbent for the removal of phenol derivatives and emerging contaminants. J Environ Manage. 2018;223(June):576–85. Available from: https://doi.org/10.1016/j.jenvman.2018.06.069

63. Haro NK, Vecchio P Del, Marcilio NR, F LA. Removal of atenolol by adsorption e Study of kinetics and equilibrium ris. 2017;154:214–9.

64. Kyzas GZ, Koltsakidou A, Nanaki SG, Bikiaris DN, Lambropoulou DA. Science of the Total Environment Removal of beta-blockers from aqueous media by adsorption onto graphene oxide. Sci Total Environ. 2015;537:411–20. Available from: http://dx.doi.org/10.1016/j.scitotenv.2015.07.144

Chapter Three

Easy recoverable hybrid alumina-based adsorbents for selective capture of cationic pollutants from wastewater

Abstract

Alumina porous monoliths were successfully fabricated using a simple and reproducible synthesis dispersing gamma alumina phase from commercial boehmite (GAB) in water containing water soluble Bio-Based Substances (BBS) obtained from composted biowaste. The wet mixture obtained was shaped in form of small spheres, then dried and calcined at 500°C in order to burn the organic matter and obtain mesoporous monoliths. They were successively functionalized with BBS in order to introduce BBS functional groups and obtain an efficient adsorbing system. Therefore, in this work, BBS acted as template/binder for the production of monoliths and as functionalizing agent of the produced monoliths. The reference powders, whose behaviors were described in a published paper (1), and the monoliths of GAB before and after functionalization were characterized by means of X-Ray Diffraction (XRD) to evidence their crystal structure, Fourier transform infrared spectroscopy (FT-IR) for evaluating the presence of BBS on the functionalized monoliths, thermogravimetric analysis (TGA) to measure the thermal stability of the supports and quantify the functionalizing BBS amount immobilized on them, N_2 adsorption at 77K for the investigation of the surface area and porosity of the systems, zeta potential measurements to analyze the effect of BBS immobilization on the surface charge of the supports

and to predict the type of interaction which can be established with substrates. Finally, the systems were applied in removal of pollutants with different charge, polarity and molecular structure, such as dyes (Crystal Violet and Acid Orange 7) and Contaminants of Emerging Concern (Carbamazepine and Atenolol).

Keywords: alumina, monolith, porous materials, functionalized monolith, electrostatic interaction, removal of pollutant, cationic molecules

3.1. Introduction

Water contamination has become a serious worldwide concern that can cause many health problems, particularly in industrial countries. The water pollution is going to be a big challenge because of the complex environmental conditions and enormous scale. Therefore, the scientists should develop simple, fast and more friendly methods for the determination, decomposition or removal, in general, of the organic pollutants (2),(3),(4),(5).

Among the possible techniques for wastewater treatment, the adsorption process by solid adsorbents demonstrates a high potential as one of the most efficient method for capturing organic contaminants from wastewaters avoiding the risk of secondary pollution brought by decomposition methods. Several adsorbents, like activated carbon (6), silica gel (7), organic clay (8), alumina (9),(10), iron powders (11),(12) and mesoporous silica (13),(14) have been successfully applied for the removal of dyes from water, but the development of new materials, more easily recoverable for a possible upscaling of the processes, is still needed. Many researchers have begun, therefore, to pay attention to the shape of the adsorbing materials as handleable forms can operate much more easily, in particular in terms of recovery and reusability. As the open-framework nature and large pore size (2–50 nm) are the key factors for a good diffusion of the molecules inside the adsorbing materials and a consequent fast adsorption process (15),(16), the research focuses on the production of massive materials possessing these features, for instance, in 2012, a new method to prepare mesoporous silica monoliths by employing Bio based substances (BBS) isolated from composted urban wastes has proposed (17). In addition to this aspect, the adsorption capacity of materials can be enhanced introducing functional groups with high affinity for different substrates by manes of

functionalization processes. The choice of the functional groups allows defining a specific activity of the adsorbing material towards a specific substrate. Oxides carrying OH groups at the surface are very good candidates for being surface modified as they can be easily functionalized exploiting several strategies reported in the literature, some of them basing on physical methods, others basing on chemical ones (18),(19),(1),(20). As in a previous paper we reported the performances of BBS-functionalized alumina powders(1), in this work, we are considering the upscaling of the previous study producing mesoporous gamma alumina-based monoliths (GAB-M) functionalized with BBS (GAB-M-BBS).

Summarizing, the current research comprehends the following points: (1) the fabrication of new alumina monoliths, (2) their functionalization with BBS, (3) their physico-chemical characterization compared with the parent alumina powder, and (4) the adsorption study.

3.2. Experimental

3.2.1. Materials for synthesis

Commercial boehmite (CB) was kindly supplied by Centro Ricerche FIAT and used to prepare gamma-Al_2O_3 (GAB) after calcination in a furnace at 500°C for 3 h, as reported in the literature(1).

Bio Based Substance (BBS) were extracted from composted organic refuses aged for more than 180 days supplied by ACEA Pinerolese Industriale. The extraction procedure was described by E. Montoneri, et al(21),(22),(23).

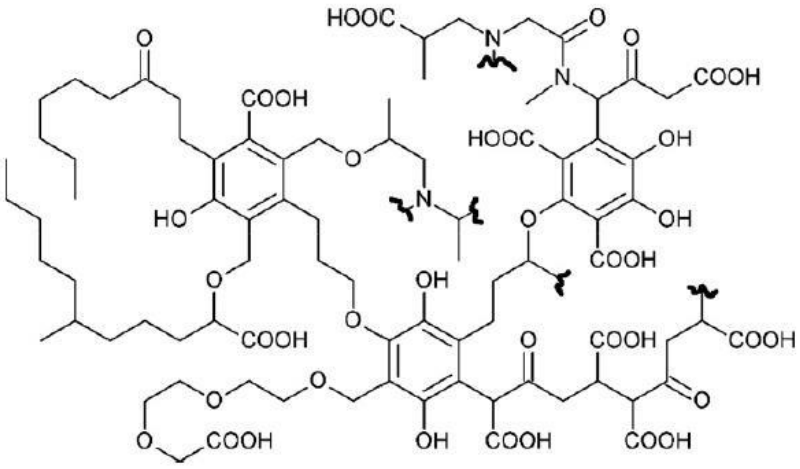

Scheme 3. 1. Virtual molecular fragments of BBS.

3.2.2 Materials and methods for characterization study

X-ray diffraction (XRD) analysis was used to investigate the morphology and crystal structure of powders and monoliths. The measurements were performed by using a X'Pert PRO MPD diffractometer from PANalytical, equipped with Cu anode worked at 45 kV and 40 mA in a Bragg-Brentano geometry. In this work, the flat sample-holder configuration was employed.

Fourier transform infrared (FTIR) spectroscopy was applied in a transmission mode by using Bruker Vector 22 spectrophotometer equipped with Globar source, DTGS detector and working in the transmission mode in the range of 4000 to 400 cm^{-1} at 4 cm^{-1} resolution. Before investigation all the samples were mixed with KBr powder (1:20 ratio) and pressed to form pellets.

Nitrogen adsorption-desorption measurements at 77 K were carried out by means of ASAP 2020 Micromeritics gas-volumetric apparatus. Prior to the experiments, the samples before and after functionalization were activated at 300 °C and 40 °C respectively for 24 h. Specific surface areas (SSA) were calculated by applying the Brunauer, Emmett and Teller (BET) method(24). Pore volumes and Pore Size Distribution were determined by using the Barrett, Joyner and Halenda method (24) applied to the isotherm adsorption branch.

Thermo-gravimetric analysis (TGA) was performed by means of TA Q600 (TA Instruments). Materials before and after functionalization were heated at a rate of 10 °C/min from 40 to 650°C under air.

Zeta potential measurements have been used in order to determine the surface charge of the particles in water at different pH and the point of zero charge of the dispersions (1). They have performed using the instrument Zetasizer by Malvern (model ZS90). The suspensions were prepared by mixing 10 mg of sample (after finely crushing in an agate mortar in the case of monoliths) in 20 ml of deionized water under constant stirring (400 rpm) for 15 min. The pH of the suspensions was adjusted in different pH in the range of 3-11 by addition of 0.1M HCl and 0.1 M NaOH solutions. The suspensions were shaken at 25 °C temperature for 15 min until the pH had stabilized. A digital pH meter (Metrohm, model 827 pH lab, swiss mode) was used to measure the pH. In all batch experiments the refractive index value of alumina was selected.

3.2.3. Materials and methods for adsorption study

UV-Vis spectrophotometer (Varian Cary 300 Scans) was applied to study the adsorption of the dyes Crystal Violet (CV, positively charged, maximum absorbance at 584 nm) and Acid Orange 7

(AO, negatively charged, maximum absorbance at 480 nm) and of the contaminants Atenolol (polar, maximum absorbance at 224 nm) and Carbamazepine (apolar, maximum absorbance at 284 nm).

The kinetics of the adsorption was carried out following the experimental procedure described in(1), i.e. contacting 20 mg of adsorbents materials with 10 ppm of contaminant solutions in the total volume of 10 ml at pH 6.5 and keeping under shaking at the temperature of 22±2 °C. The removal was evaluated considering the residual contaminant concentrations after separation of the supernatant and measurement of contaminant absorption using a calibration curve.

3.3. Results and discussion

3.3.1. Preparation of materials

3.3.1.1. Preparation of monoliths as support

Following the procedure previously applied for preparation of silica monolith(17), 0.5 g of BBS were stored under stirring in 7.5 mL water at room temperature for 2 h. GAB (2 g) was added to the BBS solution. 5 ml water was then added and the mixture was stirred for 2h. The mixture was left at ambient condition for relaxing and dried at ambient temperature for the time needed to obtain a mud in order to model small spheres of about 0.5 cm of diameter. These spheres were dried overnight at Room Temperature (RT) and then calcined in furnace at 500°C for 4 h in order to remove all organics and yield a mechanically stable, porous monolith named GAB-M. The image of the spheres after calcination is presented in the inset of Figure 3.1.

3.3.1.2. BBS-Functionalization of monoliths

As alumina powders were successfully BBS-functionalized thanks to a simple electrostatic interaction occurring in water at circumneutral pH (1), we tried the same procedure to functionalize the surface of GAB-M. The functionalized monoliths were prepared using 1 g of GAB-M dispersed in water at natural pH (about 6.5) containing 20 g/l of water soluble BBS and two different procedures:

The mixture container was sealed and gently shaken (in order to avoid the monolith breakage) using an orbital mixing plate with rotation at 1000 rpm for 24h at 25±2°C.

The mixture contained was sealed and, after shaking at RT, was placed in an oven at 60°C overnight, then cooled down and again placed in an oven at 80°C overnight.

At the end of both procedures, the samples were washed with 10 ml of water several times till no signal of leached BBS molecules from GAB-M-BBS samples was evidenced in the UV-Vis spectra of the washing medium. The following drying process was carried out in the oven at 40 °C for 24h.

The first procedure did not allow a complete functionalization of the monolith as the BBS brown color was present only in the outermost layer of the spheres, whereas the second treatment allowed a complete functionalization. The image of the functionalized porous monoliths, named GAB-M-BBS, is reported in Figure 3.1. These samples were used for the subsequent

characterization and the powders obtaining in the previous work (1), GAB and GAB-BBS, were used as reference materials for comparison.

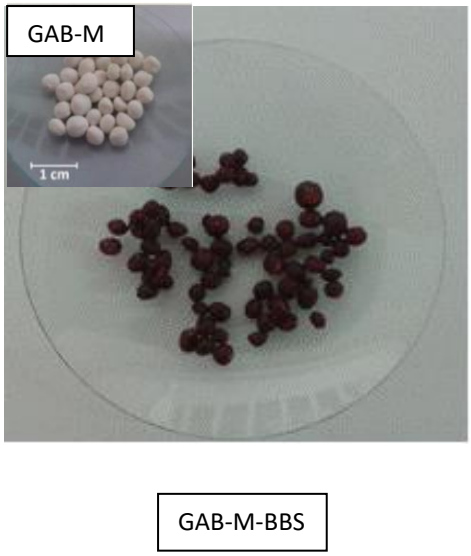

Figure 3. 1. GAB-M before (in the inset) and after functionalization with BBS.

The preparation route of the non-functionalized monoliths and the following functionalization methods were carried out several times in order to define the reproducibility of the procedures. In all the attempts the samples presented very similar behaviors, as witnessed by FTIR spectra, XRD, TGA and N_2 adsorption/desorption analyses.

3.3.2 Material characterization.

3.3.2.1. XRD measurements

X-Ray diffraction analysis was performed to investigate the effect of monolith fabrication process on the crystal structure of GAB powder. Figure 3.2 shows the diffraction patterns for both GAB and GAB-M samples. As it can be seen, the crystallographic patterns of the monoliths GAB-M are not different from GAB one. The typical reflections of gamma-Al_2O_3 (reference pattern 01-075-0921) can be evidenced in both diffractograms.

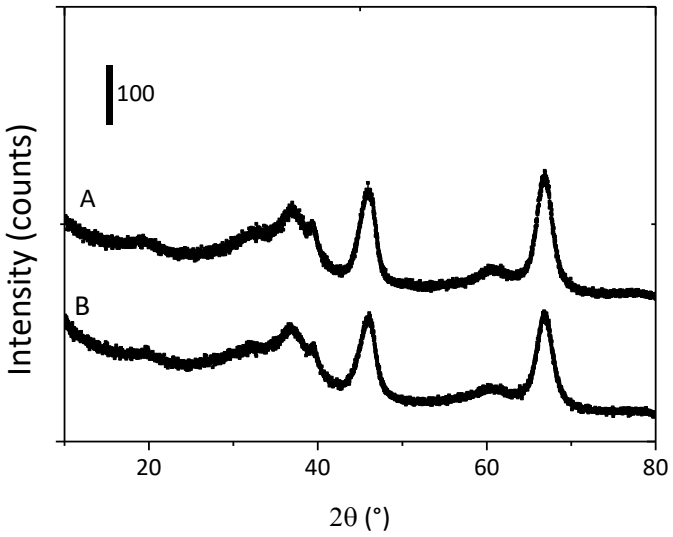

Figure 3. 2. XRD patterns of GAB (A) and GAB-M (B).

3.3.2.2. FTIR spectroscopy

The IR spectra of GAB powder before and after functionalization were reported in Figure 3.3. The presence of BBS is clearly visible in the GAB-BBS spectrum. In fact, as for pure BBS sample, it

shows the presence of OH groups and atmospheric moisture interacting with the surface and producing a signal at around 3500 cm^{-1} (ν_{OH} vibrations), a large signal at 1600 cm^{-1} due to both carbonylic stretching ($\nu_{C=O}$) and vibration of water molecules adsorbed at the surface (δ_{HOH} signal), and other two signals at 1400 and 1000 cm^{-1} due to carboxylic acid/ C–H bending and OCO vibrations, respectively. Another weak signals due to ν_{CH} stretching vibrations is visible at around 3000 cm^{-1}. In addition to these bands, the alumina samples are characterized by a very intense absorption below 1000 cm^{-1} due to the bulk vibrations of the solid framework.

The IR spectra of GAB-M before and after functionalization were collected in the same figure. The spectrum of GAB-M before functionalization is dominated by a very large signal at about 3400 cm^{-1} and by a couple of bands at about 1650 and 1300 cm^{-1}. All of them derive from the interaction of the solid samples with the molecules present in the atmosphere, H_2O and CO_2. In fact, the burning off of BBS, in the process of monolith formation, leaves in the material some inorganic residues naturally present in the BBS (namely, cationic and anionic species such as Mg^{2+}, K^{+}, Ca^{2+}, NO^{3-}, Cl^{-}) and these species interact very easily with moisture and CO_2 leading to the formation of intense ν_{OH} signals at high frequency and to the formation of symmetric and antisymmetric vibrations of surface carbonate-like groups at low frequency, respectively. In addition to these absorptions, the BBS-functionalization causes the formation of BBS typical bands, as mentioned for GAB-BBS sample.

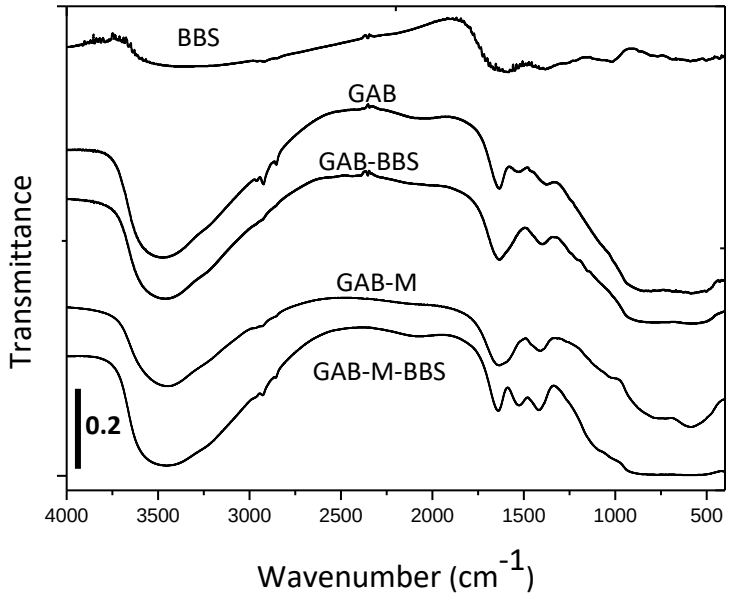

Figure 3. 3. FTIR spectra of sample powders and monoliths before and after functionalization with BBS. BBS IR spectrum was reported for the sake of comparison. The curves were shifted for the sake of clarity.

3.3.2.3. Gas-volumetric N_2 adsorption at 77K

Gas-volumetric analysis of N_2 adsorbed at 77K was carried out for all samples including reference powders. According to IUPAC classification, the adsorption/desorption isotherms of all samples, reported in Figure 3.4A, are of the IV type, with hysteresis loops at relative pressures higher than 0.4, confirming that all materials are meso or even macroporous. The formation of monolith from alumina powder does not affect significantly the specific surface area (198 vs 186 m^2/g), but changes significantly the porosity which appears higher and made up of larger mesopores and macropores of width up to 600 Å with respect to the pure powder (see Table 3.1 and Figure 3.4B). This effect was already evidenced in the previous work dealing with silica monolith formation

from powder(17) and it is due to the templating effect brought by BBS molecules during alumina particle aggregation.

In the case of monolith and reference powder, the functionalization process affects the specific surface area and the mesoporosity of all systems, as BBS occupy part of the pores (the largest ones) leading to a decrease of the total mesoporosity and consequently to the material surface area. This result confirms the BBS functionalization reaches also the core of the monolith pores, as also suggested by the visual examination of the internal part of the monoliths after functionalization.

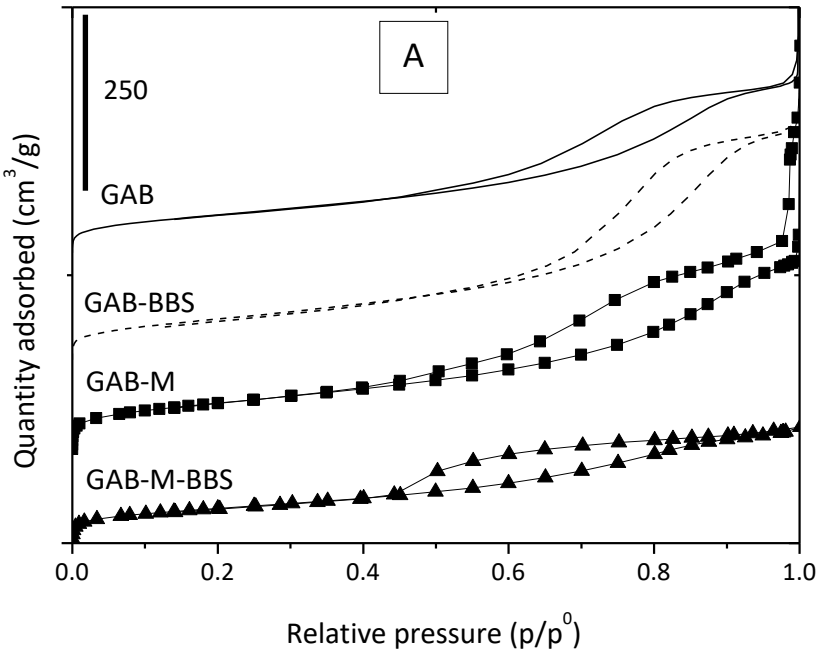

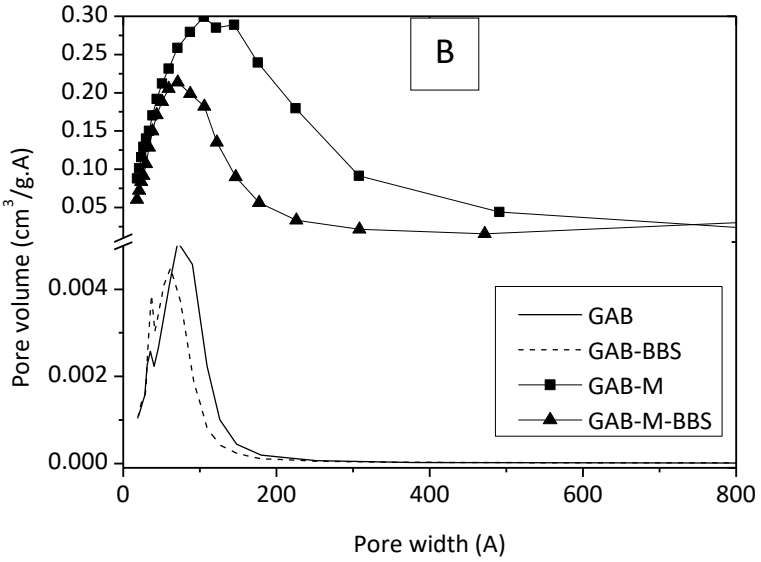

Figure 3. 4. Nitrogen adsorption/desorption isotherms (section A) and BJH adsorption pore size distribution (section B) of GAB (solid line), GAB-BBS (broken line), GAB-M (squares) and GAB-M-BBS (triangles). In the figure the curves were shifted for the sake of clarity.

Table 3. 1. Textural features of the samples.

Materials	BET Specific surface area (m^2/g)	BJH Pore volume (cm^3/g)
GAB	186	0.42
GAB-BBS	165	0.29
GAB-M	198	0.32
GAB-M-BBS	141	0.19

3.3.2.4. TGA

The results of TGA analysis on GAB and GAB-M before and after immobilization of BBS are shown in Figure 3.5, upper section. Figure 3.5, lower section, shows the curve due to BBS weight loss measured in the same conditions and reports two main regions of weight loss for pure BBS materials, the first one in the range of 40-200 °C due to water molecules elimination, and the second one is in the range of 200-650 °C due to the oxidation of BBS. In order to interpret the TGA curve of GAB-BBS and GAB-M-BBS we do need the BBS, GAB and GAB-M curves as references. As it can be seen in Figure 3.5 upper section, all the curves report the two important weight losses described in the case of BBS sample, but while the foster occurs in the range of 40-200 °C and is related to the removal of physisorbed and chemisorbed water molecules, the latter one, falling in the range of 200-650°C, is due to a couple of contributions, namely: i) loss of water obtained from OH groups condensation and ii) loss of organic matter by oxidation with formation of CO_2 and H_2O (1). To calculate the amount of organic matter present in the functionalized samples, it is needed to eliminate the contribution due to the condensation of OH groups. The results of this comparison are reported in Table 3.2. The amount of BBS loaded onto GAB-BBS is higher than that observed in the case of GAB-M-BBS, indicating that a small amount of BBS molecules can be hosted in the mesoporous structure of the monoliths with respect to the parent powder.

The amount of water physisorbed and chemisorbed present on the samples, and determined by the weight loss in the range 40-200°C, confirms that the presence of inorganic residues present

on the plain monoliths GAB-M, and the additional presence of BBS present in the functionalized monolith GAB-M-BBS, make the materials much more hydrophilic than the relative powdery ones.

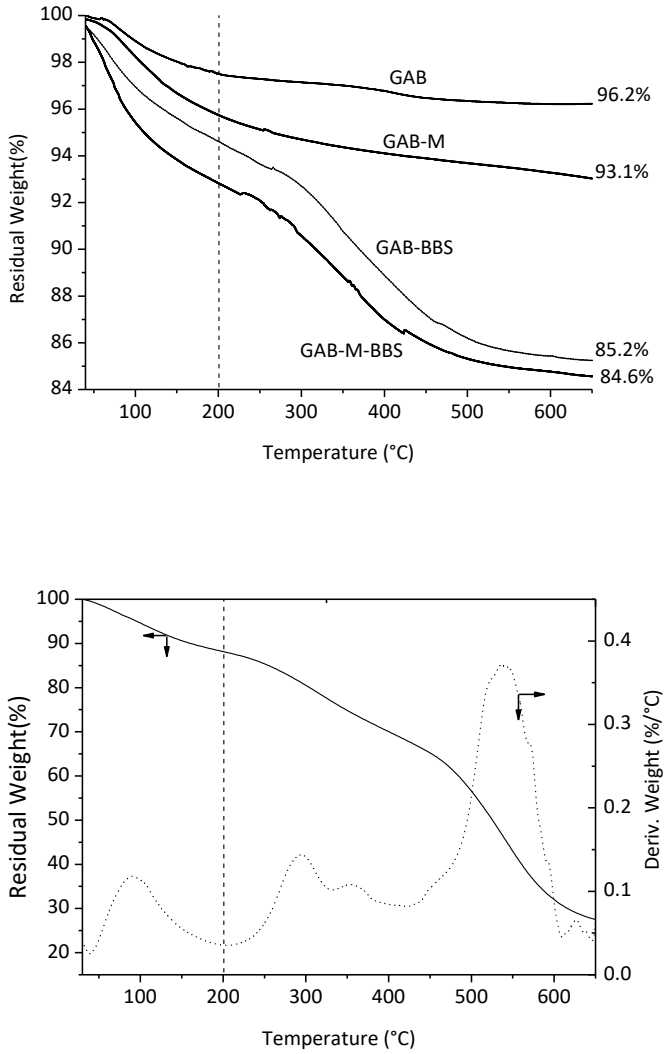

Figure 3. 5. TGA curves obtained in air for GAB, GAB-BBS, GAB-M and GAB-M-BBS in upper section; weight (solid line) and derivate weight (dotted line) curves of BBS in lower section. The values indicated in the figure indicate the residual weight measured for the materials at 650°C, the vertical broken lines indicate the temperature of 200°C used for the quantification of water and organics loss.

Table 3. 2. Weight losses observed for references and hybrid materials.

Materials	40-200°C Adsorbed water %	200-650°C Organic content and OH groups %	OH groups %	Measured organic content % ± 0.1
GAB	2.5	1.3	1.3	-
GAB-BBS	5.4	9.4	1.3	8.1
GAB-M	4.3	2.6	2.6	-
GAB-M-BBS	7.2	8.2	2.6	5.6

3.3.2.5. Zeta potential

Zeta potential (ZP) measurements were obtained in order to evaluate the surface charge of the materials before and after immobilization of BBS, as this is a very useful indication dealing with adsorption process in order to predict the type of substrate suitable for an efficient interaction with the adsorbent. The variations of the ZP values of the samples in the range of pH 3.0-11.0 are reported in Figure 3.6. GAB possesses a positive surface charge in the range of pH 4-7.9, then it becomes negative. Water soluble BBS molecules bring a negative charge at circumneutral pH caused by the presence of dissociated COOH and OH groups (21), therefore they can interact

quite easily with GAB support. After functionalization, the point of zero charge (PZC) of GAB-BBS shifts from 7.9 to 5.2 leading to a hybrid material with negatively charged surface at circumneutral pH, prone to the interaction with positive or even partially positive (i.e. polar) substrates (1). On the contrary, GAB-M and GAB-M-BBS show a negative charge in the entire pH range examined, with no substantial modifications brought by BBS functionalization. This feature suggests that only positively charged substrates should interact with these materials.

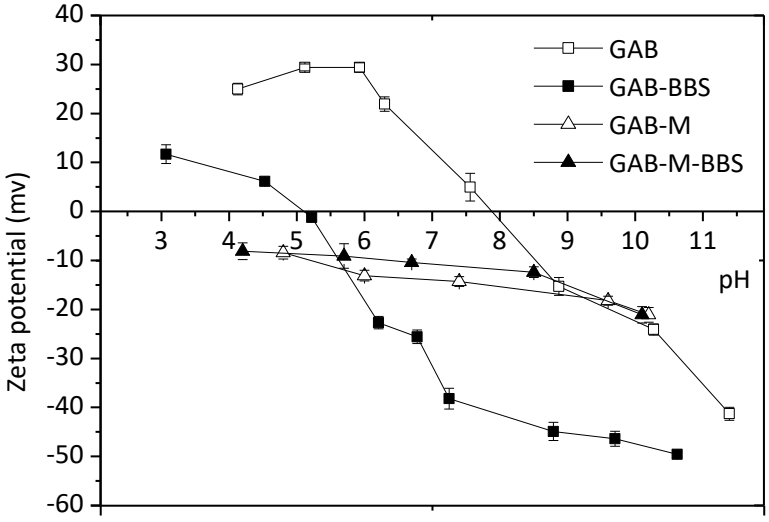

Figure 3. 6. ZP values of GAB, GAB-BBS, GAB-M and GAB-M-BBS as a function of pH.

3.3.3 Application of materials in contaminant removal.

3.3.3.1. Removal of dyes

Positively charged CV and negatively charged AO (whose molecular structures are shown in Scheme 3.2) were selected as model adsorptives to evaluate the mechanism at the base of the

interaction substrate-monoliths. For the sake of comparison, CV adsorption on the reference powdery materials GAB and GAB-BBS was taken into consideration.

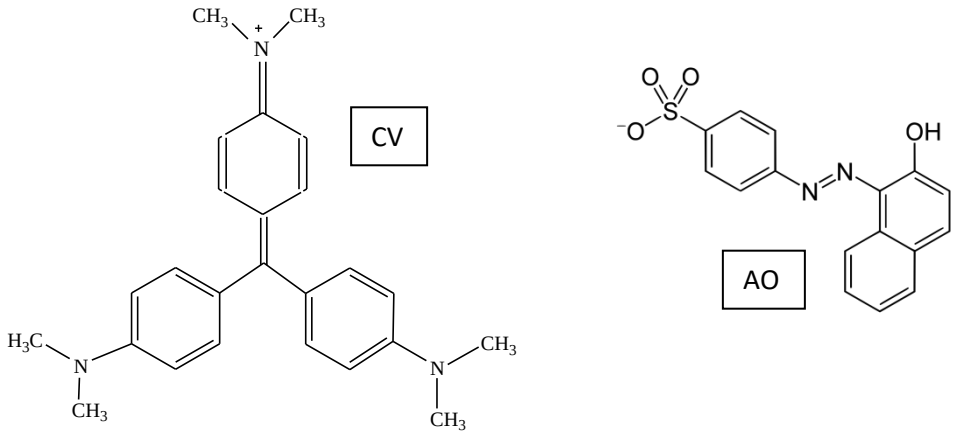

Scheme 3. 2. Molecular structure of Crystal Violet (CV) and Acid Orange 7 (AO).

Figure 3.7 shows the adsorption kinetics of CV on the monoliths GAB-M and GAB-M-BBS (section A) and on the reference powdery GAB and GAB-BBS (section B). No adsorption was evidenced contacting the negatively charged AO with the monolith systems.

As reported in (1), the adsorption of CV on the powdery GAB-BBS occurs very quickly and to a large extent, favored by the opposite charges carried by material and substrate. As already evidenced in (1) and as expected considering the positive charge carried by both material and substrate, the plain GAB powder does not give a good interaction.

The adsorption kinetic curves of CV on GAB-M and GAB-M-BBS are reported in Fig. 3.7B. In these cases the interaction occurs in longer time (the experiments took up to 8 days), as the large but flexible CV molecules need to diffuse into the mesopores of monoliths to be adsorbed. Indeed, no significant differences are evidenced for the plain and the functionalized systems in terms of maximum removal, as expected considering the ZP curves discussed in the previous paragraph: both systems are slightly negative, therefore they can interact almost the same way with the positive substrate.

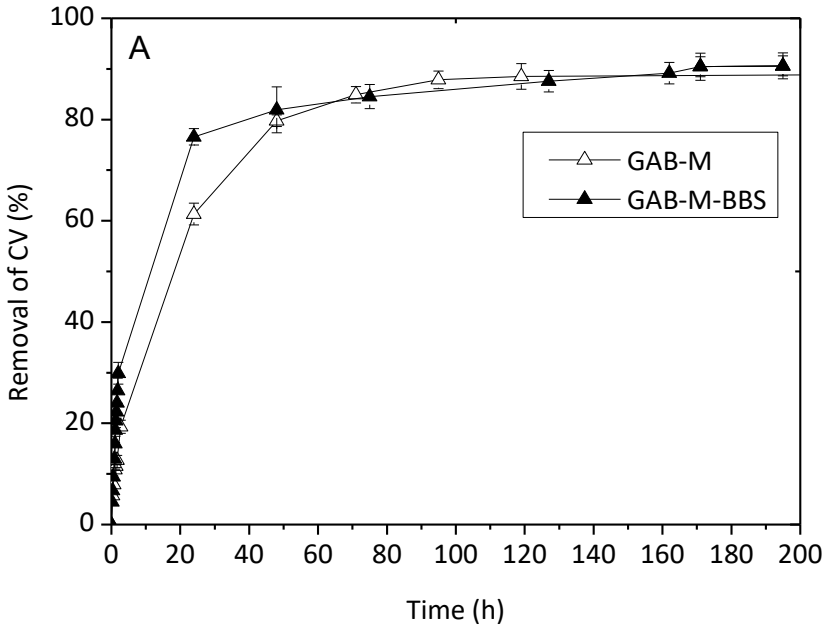

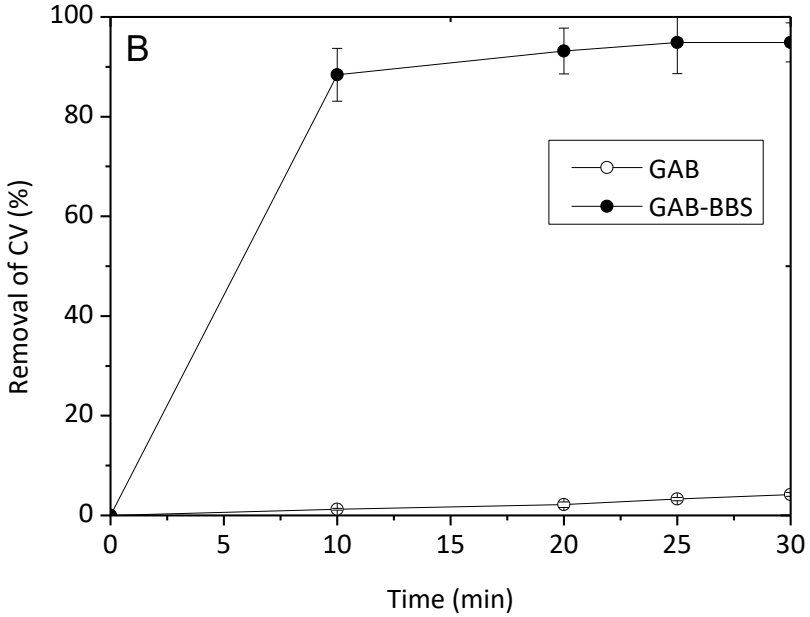

Figure 3. 7. Removal of CV by GAB-M and GAB-M-BBS (section A) and by GAB and GAB-BBS (section B)

No AO adsorption was revealed by GAB-M and GAB-M-BBS, neither for prolonged time of contact, as expected given the negative charge of the dye.

3.3.3.2. Removal of Contaminants of Emerging Concern

The molecular structure of the contaminants analyzed is reported in Scheme 3.3.

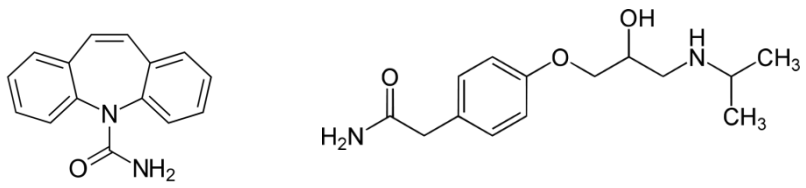

Scheme 3. 3. Molecular structure of Carbamazepine (left side) and Atenolol (right side).

Contrary to what happened with reference powders and reported in (1), Atenolol (polar non-charged substrate) and Carbamazepine (essentially apolar substrate) did not give valuable adsorption on monoliths, even if the large pores of these systems should favor the diffusion and consequent adsorption of the substrates. Probably the simple Van der Waals forces that could establish between the poorly charged monoliths and the non-charged substrates are not enough to produce a stable interaction.

3.4. Conclusions

Gamma-Alumina-based monoliths were prepared following a previously developed procedure (17). It results that they can be prepared in a reproducible way, with good mechanical property, large meso/macroporosity and a surface area similar to the parent powdery system. With respect to the pure powder, the monoliths contain some inorganic residues deriving from the BBS used as template/binder that remain in the alumina framework after the calcination performed to remove the organic matter and obtain the monoliths. The inorganic residues are responsible of the interaction with atmospheric moisture and CO_2, the last forming carbonate-like species on the monolith surface, and of the slightly negative surface charge of the material.

BBS molecules were also used to functionalize the alumina monolith in order to reproduce the results obtained with parent alumina powder and obtain a good adsorbent for polar pollutants, handleable and therefore useful for upscaling the material to real application. The interaction of the functionalized monoliths with positive, negative, polar non-charged and apolar molecules (chosen in the family of dyes and Contaminants of Emerging Concern) evidenced a good

interaction with positively charged species, opening the way to the use of the BBS-containing monoliths for the selective capture of pollutants based on their charge.

3.5. Acknowledgements

This project has received funding from the European Union's Horizon 2020 research and innovative programme under the Marie Sklodowska-Curie grant agreement no. 645551. The authors also thanks the contribution of Compagnia di San Paolo supplied under the pluriannual Convention (2016−2018) between the University of Turin and Compagnia di San Paolo.

3.6. References

1. Sadraei R, Paganini MC, Calza P, Magnacca G. An Easy Synthesis for Preparing Bio-Based Hybrid Adsorbent Useful for Fast Adsorption of Polar Pollutants. Nanomaterials. 2019;9(5):731.

2. Jaramillo M, O'Shea KE. Analytical methods for assessment of cyanotoxin contamination in drinking water sources. Curr Opin Environ Sci Heal. 2018;7:45–51. Available from: https://doi.org/10.1016/j.coesh.2018.10.003

3. Ren A, Zahid A, Fan D, Yang X, Imran MA, Alomainy A, et al. State-of-the-art in terahertz sensing for food and water security – A comprehensive review. Trends Food Sci Technol. 2019;85(January):241–51. Available from: https://doi.org/10.1016/j.tifs.2019.01.019

4. de Paul Obade V, Moore R. Synthesizing water quality indicators from standardized geospatial information to remedy water security challenges: A review. Environ Int. 2018;119(June):220–31. Available from: https://doi.org/10.1016/j.envint.2018.06.026

5. Vega M, Nerenberg R, Vargas IT. Perchlorate contamination in Chile: Legacy, challenges, and potential solutions. Environ Res. 2018;164(February):316–26. Available from: https://doi.org/10.1016/j.envres.2018.02.034

6. Julcour-Lebigue C, Krou NJ, Andriantsiferana C, Wilhelm AM, Delmas H. Assessment and modeling of a sequential process for water treatment-adsorption and batch CWAO regeneration of activated carbon. Ind Eng Chem Res. 2012;51(26):8867–74.

7. Fan HT, Fan X, Li J, Guo M, Zhang D, Yan F, et al. Selective removal of arsenic(V) from aqueous solution using a surface-ion-imprinted amine-functionalized silica gel sorbent. Ind Eng Chem Res. 2012;51(14):5216–23.

8. Unuabonah EI, Günter C, Weber J, Lubahn S, Taubert A. Hybrid clay: A new highly efficient adsorbent for water treatment. ACS Sustain Chem Eng. 2013;1(8):966–73.

9. Serbezov A, Moore JD, Wu Y. Adsorption equilibrium of water vapor on selexsorb-CDX commercial activated alumina adsorbent. J Chem Eng Data. 2011;56(5):1762–9.

10. Tang H, Hao L, Chen J, Wang F, Zhang H, Guo Y. Surface Modification to Fabricate Superhydrophobic and Superoleophilic Alumina Membranes for Oil/Water Separation. Energy and Fuels. 2018;32(3):3627–36.

11. Zeng H, Yin C, Qiao T, Yu Y, Zhang J, Li D. As(V) Removal from Water Using a Novel Magnetic Particle Adsorbent Prepared with Iron-Containing Water Treatment Residuals. ACS Sustain Chem Eng. 2018;6(11):14734–42.

12. Yu Z, Zhang X, Huang Y. Magnetic chitosan-iron(III) hydrogel as a fast and reusable

adsorbent for chromium(VI) removal. Ind Eng Chem Res. 2013;52(34):11956–66.

13. Ko YG, Lee HJ, Kim JY, Choi US. Hierarchically porous aminosilica monolith as a CO2 adsorbent. ACS Appl Mater Interfaces. 2014;6(15):12988–96.

14. Ye S, Liu Y, Feng J. Low-Density, Mechanical Compressible, Water-Induced Self-Recoverable Graphene Aerogels for Water Treatment. ACS Appl Mater Interfaces. 2017;9(27):22456–64.

15. Alauzun JG, Ungureanu S, Brun N, Bernard S, Miele P, Backov R, et al. Novel monolith-type boron nitride hierarchical foams obtained through integrative chemistry. J Mater Chem. 2011;21(36):14025–30.

16. Masika E, Mokaya R. Mesoporous aluminosilicates from a zeolite BEA recipe. Chem Mater. 2011;23(9):2491–8.

17. Magnacca G, Laurenti E, Vigna E, Franzoso F, Tomasso L, Montoneri E, et al. Refuse derived bio-organics and immobilized soybean peroxidase for green chemical technology. Process Biochem. 2012;47:2025–31.

18. Shanaghi A, Souri AR, Rafie M, Chu PK. Nano-mechanical properties of zirconia-alumina-benzotriazole nano-composite coating deposited on Al2024 by the sol-gel method. Thin Solid Films. 2019;689(July):137417.

19. Nayak N, Huertas R, Crespo JG, Portugal CAM. Surface modification of alumina monolithic columns with 3-aminopropyltetraethoxysilane (APTES) for protein attachment. Sep Purif Technol. 2019;229(December 2018):115674.

20. Sadraei R, Murphy RS, Laurenti E, Magnacca G, Accepted J. Characterization methodology to evaluate the activity of supported Soybean Peroxidase. Mater interfaces. 2019;

21. Montoneri E, Boffa V, Savarino P, Perrone DG, Musso G, Mendichi R, et al. Biosurfactants from urban green waste. ChemSusChem. 2009;2(3):239–47.

22. Montoneri E, Boffa V, Quagliotto PL, Mendichi R, Chierotti MR, Gobetto R, et al. Humic acid-like matter isolated from green urban wastes. Part I: Structur and surfactant properties. BioResources. 2008;3(1):123–41.

23. Montoneri E, Boffa V, Savarino P, Perrone D, Ghezzo M, Montoneri C, et al. Acid soluble bio-organic substances isolated from urban bio-waste. Chemical composition and properties of products. Waste Manag. 2011;31(1):10–7. Available from: http://dx.doi.org/10.1016/j.wasman.2010.08.029

24. Thommes M, Kaneko K, Neimark A V., Olivier JP, Rodriguez-Reinoso F, Rouquerol J, et al. Physisorption of gases, with special reference to the evaluation of surface area and pore size distribution (IUPAC Technical Report). Pure Appl Chem. 2015;87(9–10):1051–69.

Chapter Four

Characterization methodology to evaluate the activity of supported Soybean Peroxidase

Abstract

In this work the facile preparation of alumina-based hybrid systems supporting Soybean Peroxidase (SBP) for biocatalytic applications was tested and the resulting materials were compared with a previously examined heterogeneous biocatalyst containing SBP covalently immobilized on silica monoliths. The hybrid systems were investigated to obtain structural information regarding their activity. The amount of SBP immobilized, the stability and activity of the hybrid systems were tested. The joint use of infrared and fluorescence spectroscopy, using the adsorption of NO as a probe molecule, provided insights into the structure-activity relationship of free and supported SBP and to define a general strategy to predict the activity of supported enzymes.

Keywords: biocatalysis, Fe-heme accessibility, fluorescence spectroscopy, IR spectroscopy, Soybean Peroxidase

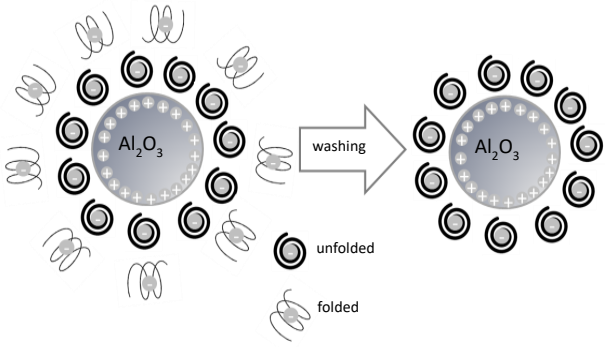

4.1. Introduction

Nowadays, the development of stable and efficient immobilized biocatalysts has become a major research avenue as the interest in enzymatic technology is increasing.

In fact, enzymes have been commonly used as versatile tools in different scientific and technical areas. For instance, they have wide applications in the fields of chemistry, biochemistry, biodiesel production (1),(2),(3),(4),(5), medicine (6), pharmaceutical science (7), water treatment and degumming of oil (8), food and textile. The main reason of this wide application is due to their high catalytic activity, high selectivity, low toxicity and water-solubility.

On the other hand, the issues underlying the practical applicability of enzymes in many processes are derived especially from economic burdens due to high production costs, storage and difficulty in recycling (9). For these reasons, the immobilization of enzymes on solid supports has become a very important challenge for overcoming these difficulties. As compared with the solubilized free form, immobilized enzymes usually show a lower activity yet higher stability (10), easy handling, and easy recycling (11),(12),(13),(14),(15),(16). Conventional immobilization methods are generally divided into four main categories: adsorption (17), covalent binding (11),

entrapment (18) and cross-linking (19), and different kinds of polymers and inorganic materials were used as support. Among them, porous materials like alumina and silica have been extensively explored for both physical entrapment and covalent immobilization due to their stable and rigid structures protecting the immobilized enzyme, accessible porosity, large surface area and presence of reactive surface sites useful for conjugation.

Unfortunately, occasionally the immobilization process is not innocuous for enzymes that can experience misfolding, or in general the lack of their active conformations, upon support interaction. As a result, it is important to test the supported enzyme activity studying its relation with enzyme features in order to design active heterogeneous biocatalysts.

In this study, two different precursors of alumina, ammonium aluminum carbonate hydroxide ($NH_4Al(OH)_2CO_3$) and aluminium oxyhydroxide or boehmite (AlOOH) were calcined to obtain defective alumina supports characterized by similar crystallographic structures and very different morphologic features. Ammonium dawsonite (AACH in the following) is a material isostructural with the mineral dawsonite ($NaAl(OH)_2CO_3$), it can be prepared via hydrothermal method and leads to finely dispersed and high-surface area Al_2O_3 with orthorhombic‑dipyramidal structure (space group Imam)(20),(21),(22). Aluminium monohydroxide (AlOOH in the following) crystallizes into microcrystals of various shapes. Both precursors were transformed into defective aluminas after a thermal treatment in air in the range 500-1000°C, to produce crystalline materials with specific surface areas ranging from 300 to 100 m^2/g. The surface functionalization of these materials with organic molecules (as well as polymers and surfactants) can be carried out following several methods (23),(24),(25). The present work describes a very straightforward

method for immobilizing Soybean Peroxidase (SBP) enzyme on alumina, capitalizing on the strong electrostatic interactions between the positively charged surface of alumina and the negatively charged enzyme. However, the presence of these strong electrostatic interactions can affect the SBP conformation and consequently its activity, necessitating this investigation.

Thus, the present study aims to characterize the properties of different phases of alumina (obtained from dawsonite and boehmite) used as supports by means of X-ray diffraction (XRD), N_2 adsorption at 77K, scanning and transmission electron microscopies (SEM and TEM) and Zeta potential measurements, and to investigate the features of SBP immobilized onto alumina particles by means of UV-visible (UV-Vis), fluorescence and Fourier transform infrared (FTIR) spectroscopies. Further, the adsorption test of NO gas onto the solid samples was performed in order to clarify the accessibility of the enzyme active site (Fe-heme group). Moreover, these results were compared with those obtained in a previously studied silica-based heterogeneous biocatalyst (HBC) where the same enzyme was covalently bound to the support (26).

4.2. Materials and methods

Commercial boehmite (AlOOH) was kindly supplied by Centro Ricerche FIAT (Torino, Italy); SBP was purchased from Bio-Research Products Inc. (USA), hydrogen peroxide (30% aqueous solution), 3-(dimethylamino)benzoic acid (DMAB), 3-methyl-2-benzothiazolinone hydrazone (MBTH), aluminum nitrate and urea were purchased from Sigma-Aldrich (Italy).

FK320 from Evonik and Bio-Based Substances (BBS) extracted from compost were used for the production of the monolith support, whereas 3-aminopropyltriethoxysilane and glutaraldehyde were used for the enzyme immobilization as described in (26).

4.2.1. Supports preparation

Ammonium dawsonite (AACH) was synthesized optimizing the hydrothermal method reported in (27). Aluminum nitrate and urea were mixed with 45 mL of deionized water. The mixture was stirred for 1 h, and then poured into a 250-mL PTFE autoclave. The autoclave has kept at 120°C for 24h. The product was washed with distilled water and then dried at room temperature for 24h. The dried sample was then calcined in air at 500°C and 1000°C for 1h in order to obtain the decomposition of the precursor and the formation of alumina, as reported in (28). Herein, these samples will be denoted AACH500 and AACH1000, respectively.

The AlOOH precursor was calcined at 500 °C and 1000°C for 1h to obtain two different alumina phases as reported in (28). These samples will be denoted AlOOH500 and AlOOH1000, respectively.

For the sake of comparison, a monolith siliceous support was used to covalently immobilize SBP. The procedure for producing this support is reported in (26).

4.2.2. Immobilization of SBP on aluminas

2 mg of SBP was dissolved in 7 mL of distilled water/acetate buffer (pH=5.5) and stirred for 1 h. Then 3.5 mL of solution was withdrawn and mixed with 30 mg of alumina supports at room temperature (22°C). The suspensions were stirred at room temperature and the immobilization of SBP onto alumina supports was measured by means of UV-Vis spectroscopy measuring the absorbance of the supernatant at 403 nm (for SBP, ε_{403} = 96400 M^{-1} cm^{-1}) (9) in order to follow the support coverage and observe the completion of the process. The amount of SBP immobilized was calculated as the difference between the initial amount of enzyme (3×10^{-6} M) and that recovered in the solution after interaction with the powders.

After SBP immobilization, all the samples were then washed sequentially with several water solutions for different times as reported in Table 4.1 to check the stability of the prepared hybrid materials. To do so, the activity test described in section 2.4 was carried out separately on the supernatant and on the powder (separated by centrifugation) after each washing step.

Table 4. 1. Washing process of hybrid materials

Washing solvents	Time of washing (h)
Distilled Water pH 7	1
Distilled Water pH 7	3
Distilled Water pH 7	20

Distilled Water pH 9	2
Distilled Water pH 11	96
Acetate Buffer pH 5.5	1
Acetate Buffer pH 5.5	15
0.5 M NaCl and 50 °C	3
2 M NaCl and 50 °C	22

After the stability test, the solids were dried at room temperature for 24h and stored at 4°C before characterization.

4.2.3. Sample characterization

X-ray diffraction (XRD) pattern of materials were obtained with a X'Pert PRO MPD diffractometer from PANalytical, equipped with Cu anode (at 45 kV and 40 mA) by using a Bragg-Brentano geometry in flat sample-holder configuration.

N_2 gas volumetric adsorption at 77K were carried out by means of ASAP 2010 Micromeritics in order to determine the specific surface area (SSA) by BET method and the pore volume and the pore size distribution by BJH method (29). The samples were activated at 60 °C under vacuum (residual pressure 10^{-2} mbar) prior to the analysis.

Zeta potential measurements were undertaken with the instrument Zetasizer by Malvern. The particle suspensions of aluminas were prepared prior to the experiments by mixing 20 mg of sample in 20 mL of milliQ water under constant stirring at 400 rpm for 15 min. The pH of alumina suspensions was adjusted in the range of 3-11 by addition of 0.1 M HCl and 0.1 M NaOH solutions. A digital pH-meter (Metrohm, model 827 pH lab, swiss mode) was employed to measure the pH of the suspensions. The suspensions were then incubated at 22 °C for 15 min until the pH stabilized. In all batch experiments the refractive index value of alumina was chosen. The experiments were performed in duplicate.

To determine the structure of the SBP enzyme after its adsorption onto alumina, fluorescence and FTIR spectroscopies were applied. Fluorescence spectra were obtained at constant temperature (i.e., 21.0 ± 0.1 °C) with a PTI QuantaMaster spectrofluorometer, and the excitation and emission slits were set such that the bandwidths were 2. The data interval and integration time were 0.5 nm and 0.5 s, respectively. For the protein studies, emission scans were recorded between 340 and 670 nm with the excitation wavelength of 330 nm. For this purpose, the solid samples were suspended in the same quantity of water (4 mL) and stirred for about 10 min prior the measurements.

The SiO_2/SBP sample used for the sake of comparison was characterized in (26).

FTIR measurements were carried out in transmission mode with a Bruker Vector 22 spectrophotometer equipped with Global source, DTGS detector in the range of 4000-400 cm^{-1} (4 cm^{-1} resolution). Thin pellets (approximate density 10 mg cm^{-2}) were prepared using a press and protected in a holed gold envelop for adsorption and spectroscopic studies. The samples

were placed in a home-made quartz cell allowing to outgas the samples under vacuum (residual pressure 10^{-4} mbar) at various temperatures (up to 800°C). The spectrum of SBP was obtained dispersing a small amount of SBP powder in KBr and analyzing the pressed powdery mixture.

4.2.4. Kinetic measurements

The kinetic measurements were carried out in a quartz cuvette by using a UNICAM UV300 Thermospectronic double beam UV-Visible spectrometer equipped with magnetic stirrer at constant temperature.

The stability test on the prepared alumina-based hybrid materials was carried out evaluating the release of SBP from the solid after washing directly with the washing solution using UV-Vis spectroscopy (supernatant test). Namely, 1.5 mL of the washing solution, 1.5 mL of DMAB (5×10^{-4} M), 30 µL of MBTH (2.1×10^{-5} M) and 15 µL of H_2O_2 (6.4×10^{-5} M; prepared daily from a concentrated stock solution of 1.3×10^{-2} M) were stirred for 5 minutes. The absorption at λ_{max}=590 nm with an extinction coefficient of ε_{590}=47600 M^{-1} cm^{-1} was used to determine the concentration of SBP (30),(9). These experiments were carried out in duplicate.

Similarly, the efficiency of the hybrid materials was investigated using the same reagents directly in contact with the solid (3 mg, separated by centrifugation from the washing solutions) for 5 min and then measuring the absorption at λ_{max}=590 nm (biocatalytic activity test). These experiments were performed in duplicate. The specific activity was obtained from the slope of the regression equation obtained between initial rates and time, dividing the result by the weight of the analyzed samples.

After the reaction, the powder was briefly washed to remove the reagents, centrifuged and dried for testing the activity in another cycle.

4.3. Results and discussions

4.3.1. Characterization of the supports

4.3.1.1. XRD measurements

X-ray powder diffraction analysis was carried out to determine the crystal structure of the materials after decomposition of AACH and AlOOH precursors (Figure 4.1). In all cases the crystallographic patterns of the precursors are not visible anymore, whereas the typical reflections of low-temperature transition alumina gamma (after calcination at 500°C) and delta (after calcination at 1000°C) phases of alumina are clearly visible for AlOOH500, AlOOH1000 and AACH1000, respectively. The only exception is related to AACH500 which shows the principal reflections of the gamma phase of alumina with a short-range order, probably due to a crystal habit not completely formed.

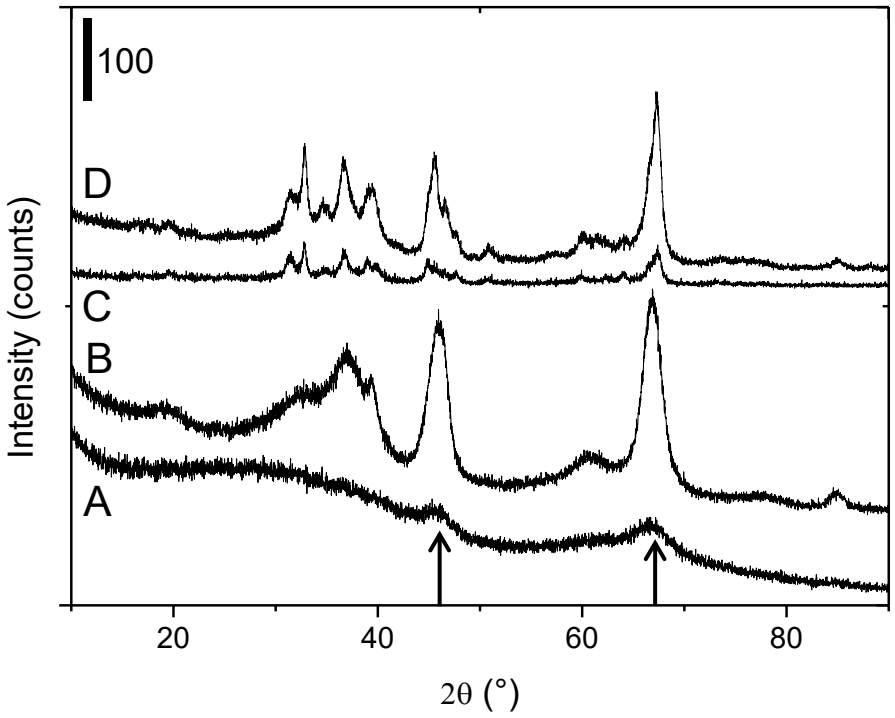

Figure 4. 1. Powder X-ray diffractograms of AACH500 (A) AlOOH500 (B), AACH1000 (C) and AlOOH1000 (D). The curves were shifted for the sake of clarity. The arrows indicate the principal reflections of the γ-Al_2O_3 phase.

4.3.1.2. Gas-volumetric N_2 adsorption at 77K

The adsorption-desorption isotherms and BJH distribution of pores are presented in Figure 4. 2A and 2B respectively, whereas Table 4.2 reports the values observed for BET specific surface areas and BJH total porosity as derived from the adsorption branch of the isotherms. All materials exhibited a type IV isotherm (IUPAC classification) indicating the presence of mesopores whose size distribution curve covers different dimension: smaller for samples calcined at 500°C, and larger for samples calcined at 1000°C. Increasing the calcination temperature, the area of

materials decreases and the mesopore size increases. The largest area and porosity (both volume and pore size) was exhibited by AACH500 sample.

It is worth noting that the TEM images of AlOOH samples (reported in the next section) provide support for particle sizes on the order of tens of nm, very similar to the pore size evidenced by BJH model, suggesting that the porosity shown by AlOOH samples forms between aggregated particles. The images of AACH samples, on the other hand, indicate much larger particle sizes whose porosity are due to void spaces in the particles. The high porosity observed should also be responsible of the high surface area shown by the AACH500 support.

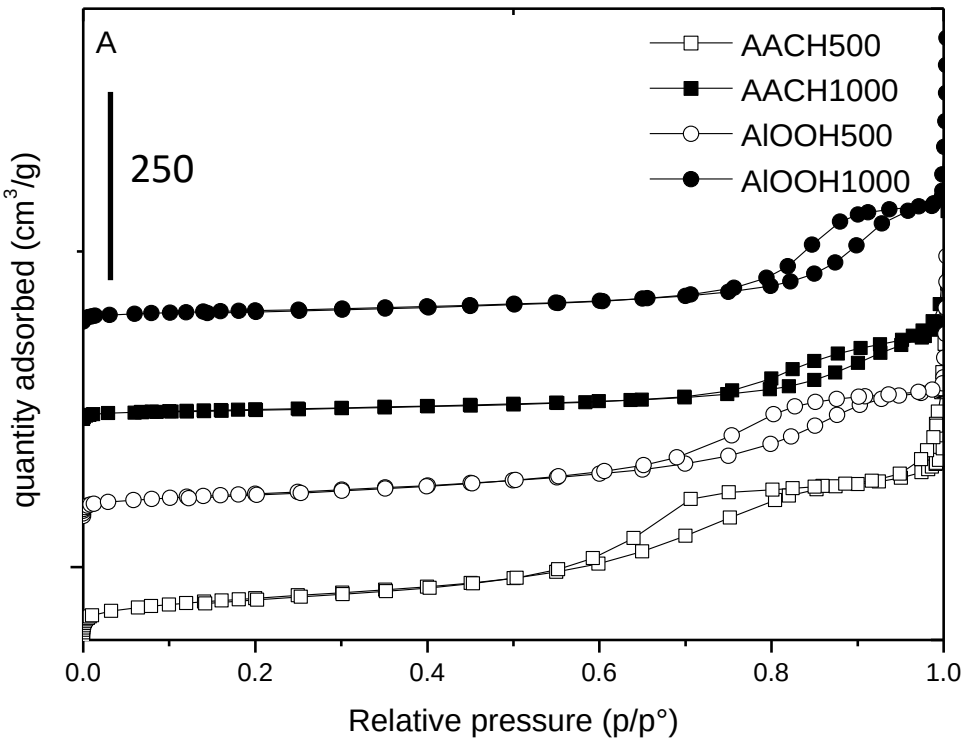

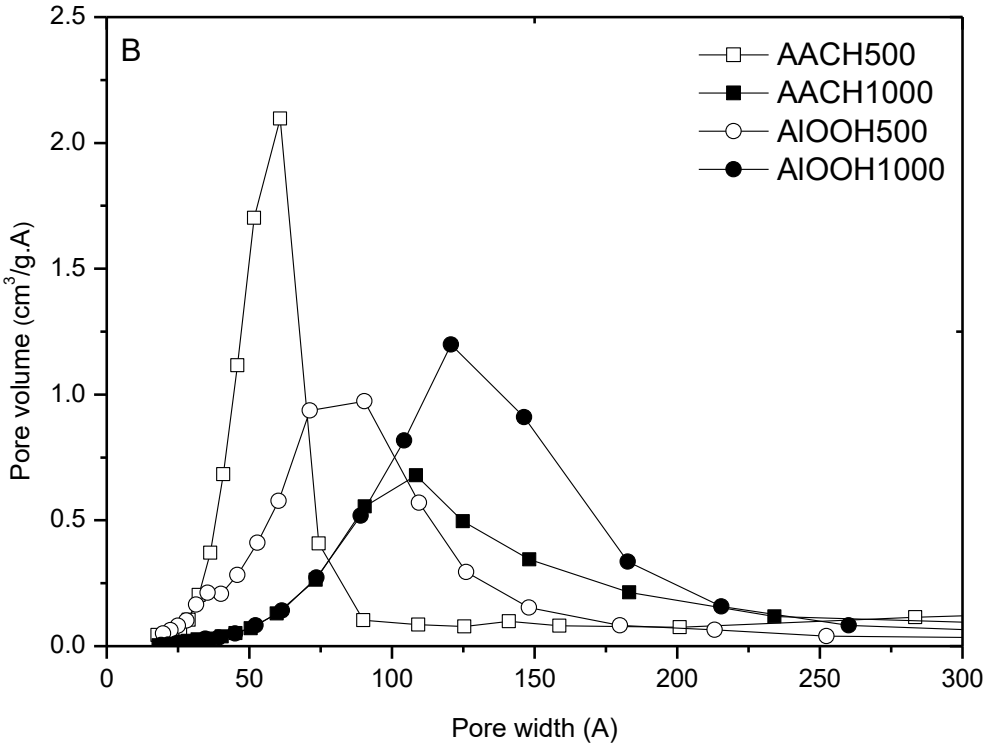

Figure 4. 2. Nitrogen adsorption-desorption isotherms (section A) and BJH pore size distribution (section B) of AACH500 (white squares), AACH1000 (black squares), AlOOH500 (white circles) and AlOOH1000 (black circles). In section A the curves were shifted for the sake of clarity.

Table 4. 2. Texture features of the different supports.

Supports	Crystalline Phase	BET Specific surface area (m2/g)	BJH Pore volume (cm3/g)
AACH500	Incipient γ-Al_2O_3	311	0.73
AACH1000	δ- Al_2O_3	88	0.37

AlOOH500	γ - Al_2O_3	186	0.43
AlOOH1000	δ- Al_2O_3	102	0.40

4.3.1.3. Electron microscopies

The morphology of the materials was studied using electron microscopy. SEM and TEM images of the samples are presented in Figure 4.3 and show evidence for completely different particle shapes for AlOOH and AACH precursors: acicular particles of several hundreds of nm in length and of about 50 nm in thickness derives from the decomposition of AACH, whereas more roundish particles, of tens of nm of diameter, presenting high aggregation, derives from AlOOH precursor.

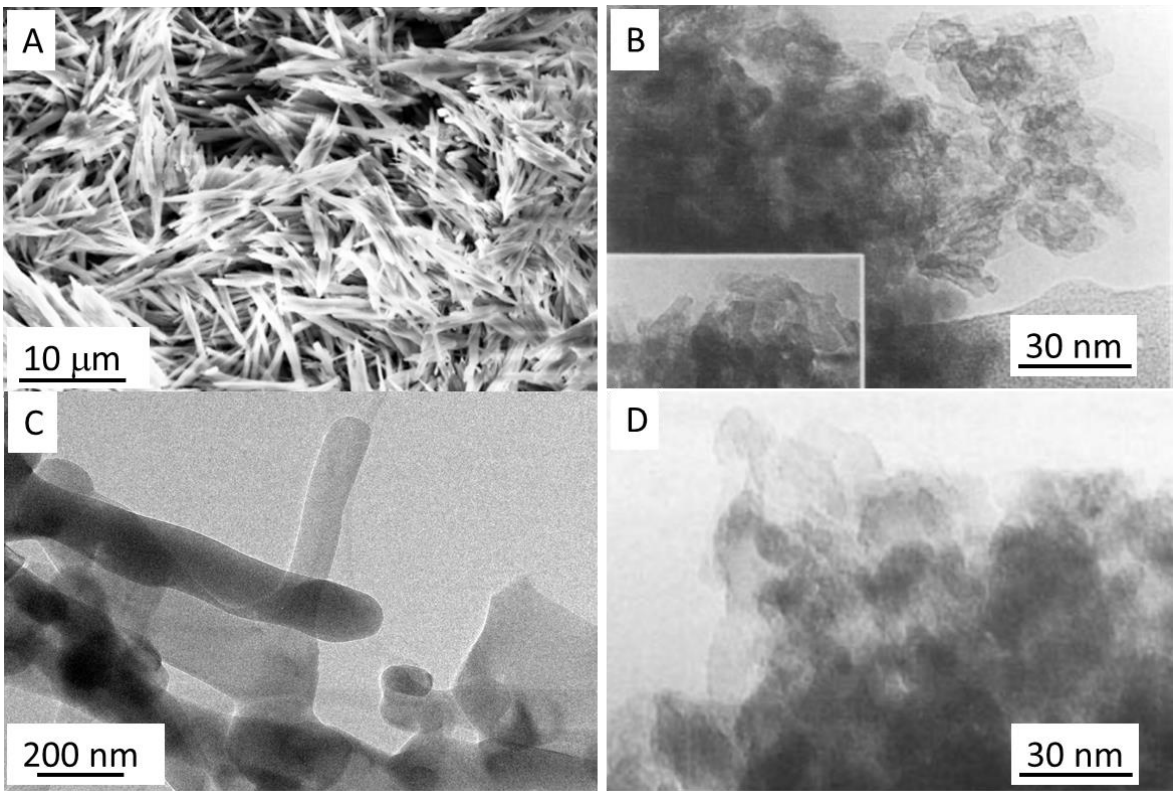

Figure 4. 3. SEM images of AACH500 (A), TEM images of AlOOH500 (B), AACH1000 (C) and AlOOH1000 (D).

4.3.1.4. Zeta potential measurements

Figure 4.4 shows the surface charge of the materials over a pH range of 3-11. All alumina samples exhibit positive zeta potential values at low pH and negative values at high pH with an isoelectric point at a pH values higher than 7. Given the isoelectric point of SBP is about 4.1(31), and in order to facilitate the interactions between the enzyme and the supports, all the functionalization procedures were performed at pH 5.5 in acetate buffer in order to have the enzyme in its negative form and a positive charge at the supports surface.

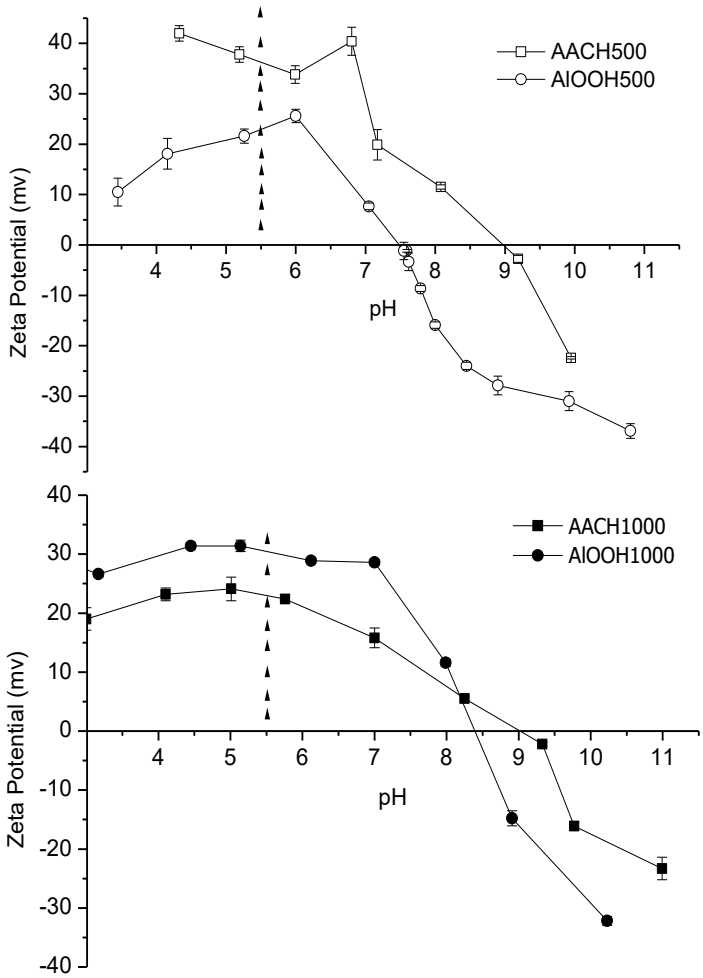

Figure 4. 4. Zeta potential measurement results in the pH range 3-11 for AACH500 and AlOOH500 (upper session), AACH1000 and AlOOH1000 (bottom session). The broken vertical lines represent the pH used for the functionalization procedures.

4.3.2 Immobilization and stability studies

As reported in Figure 4.5 the immobilization of SBP onto alumina from AACH occurred with high efficiency, reaching 100% of removal from the solution in less than 30 minutes. Otherwise, the interaction with alumina from AlOOH occurred more slowly and to a more limited extent (only 90% of SBP results blocked at the AlOOH surface after 13 h of contact).

Actually, none of the physico-chemical features observed for the plain supports could explain a similar behavior, as the crystalline structure, even still in formation for AACH500 sample, the specific surface area and porosity and the surface charge change in all samples with no correlation with the observed SBP immobilization trend. The only aspect we can consider explaining the different behaviors is the morphology of the particles, such as a larger extension of the particle surface (like in the case of AACH precursor) may favor the interaction with large enzymatic molecules.

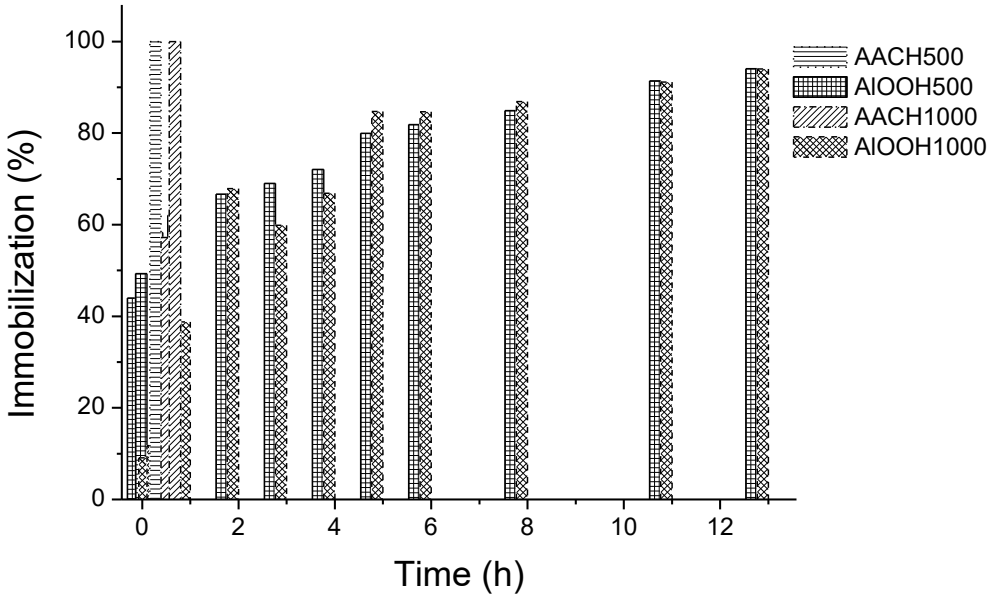

Figure 4. 5. Immobilization % of SBP onto AlOOH500, AlOOH1000, AACH500 and AACH1000.

To verify this hypothesis, and to test the stability of the HBC prepared on the different supports, several washing procedures were carried out, starting from water at different pH values (namely from 7 to 11), with acetate buffer at pH=5.5, and NaCl (0.5-2 M), as reported in Table 4.1. The release of SBP was evaluated testing the enzymatic activity in the washing solution (supernatant test) and in the presence of the powders (biocatalytic activity test).

Considering the supernatant test, only the washing procedure carried out with water at pH = 7 for up to 20 h (Figure 4.6) reveals a SBP release, and in particular the highest amount of SBP released belongs to AlOOH samples, i.e. the materials showing the slower and more limited interaction with the enzyme. On the other hand, activity tests seem to indicate a presence of a limited amount of SBP in the supernatant. If compared with the initial concentration of SBP solution used for the immobilization of the enzyme on the supports, corresponding to 3×10^{-6} M, the release never overcomes the value of 4×10^{-8} and therefore it results almost negligible.

These data suggest that the enzyme is stably immobilized on the supports and consequently, at least in principle, the hybrid materials prepared could be used for biocatalytic applications.

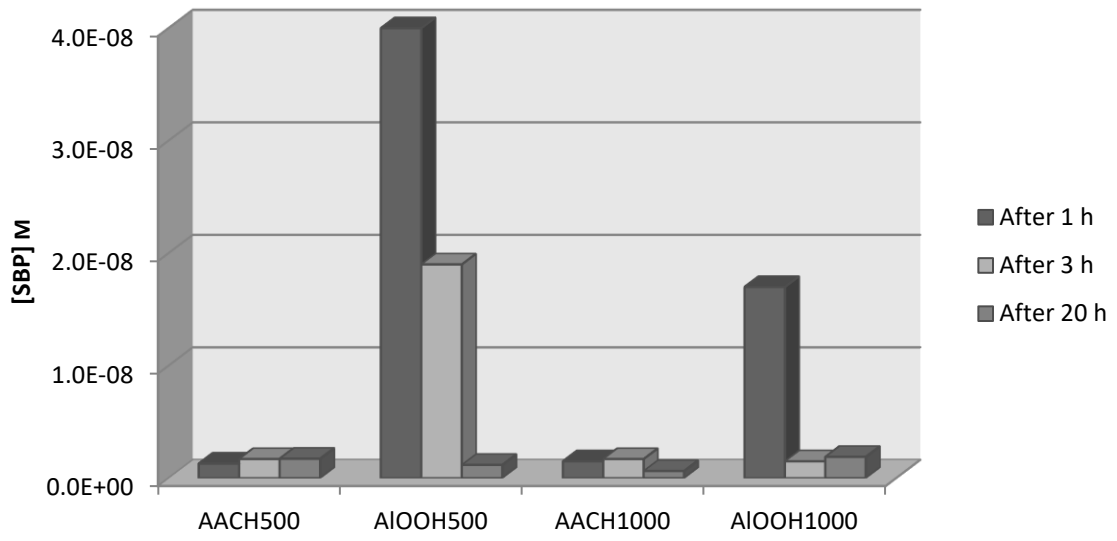

Figure 4. 6. Supernatant tests. Release of SBP by washing process in water at pH=7 from AACH500, AlOOH500, AACH1000 and AlOOH1000.

To confirm the goodness of the alumina-based hybrid materials as HBC, the powders were tested in three reaction cycles. Specifically, the hybrid systems were dispersed in a reaction mixture, allowed to react for 5 min, recovered by filtration, briefly washed with water to remove the residues of reagents and products and used again for another reaction cycle in the presence of fresh reagents. Unexpectedly, the activity decreases very fast and becomes negligible after only three reaction cycles (Figure 4.7).

As a conclusion of these tests, and as the presence of the enzyme on the supports was proven, given the limited release, the structure of the enzyme immobilized on the supports needs to be studied carefully in order to explain the observed lack of activity. The phenomenon could be probably explained considering two aspects: i) the Fe-heme active sites of SBP are not available anymore for catalyzing the H_2O_2-based reaction, or ii) the strong interaction of the enzyme with

Al_2O_3 supports causes the unfolding of the protein secondary structure which causes, in turn, the lack of activity. In order to explain the results observed, a characterization study based on FTIR and fluorescence spectroscopies was performed on SBP supported on AlOOH500 and, for the sake of comparison, on the active silica-based HBC.

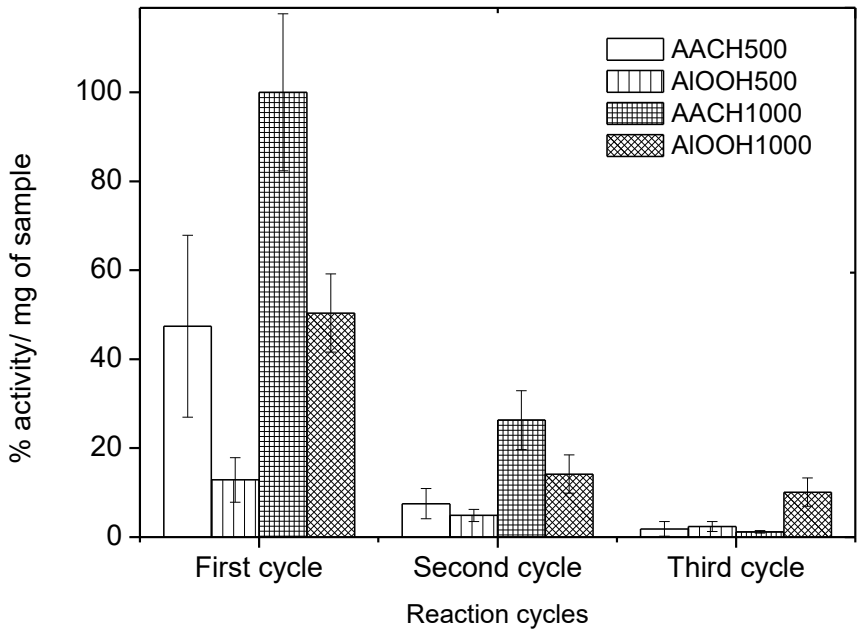

Figure 4. 7. Biocatalytic activity test. Specific activity of SBP immobilized on alumina powders in three reaction cycles.

4.3.3 Characterization of supported SBP

4.3.3.1 Accessibility of SBP active sites – FTIR spectroscopy using NO as probe molecule

SBP activity is based on the presence of accessible Fe-heme groups that can form intermediates useful for H_2O_2 activation (32). Fe-heme availability can be easily checked taking advantage of the high affinity between iron and NO molecules, therefore gaseous NO has been put in contact with dried SBP-containing systems in form of thin pellet, in order to check the NO adsorption via FTIR spectroscopy.

FTIR spectroscopy of NO adsorbed onto solid samples has been studied by many authors in order to explore iron availability at the surface of oxides, catalysts and so on. Based on the literature data, the Fe-NO bond is highly specific, can be monitored looking at the stretching signal of NO molecule (around 1800 cm^{-1}) and the consequent observable absorption in the IR range is highly sensitive, guaranteeing that also a low amount of Fe can be detected by this method (33),(34),(35).

To carry out this experiment, thin pellets of the powdery AlOOH500-based hybrid system and of the crushed silica-based biocatalyst were outgassed in vacuum at room temperature and put in contact with 40 mbar of NO using a home-made cell useful for studying the adsorption of the molecule and for allowing the contemporary registration of IR spectra in transmission mode. Figure 4.8 shows the infrared spectra obtained subtracting the spectrum of the bare adsorbent (AlOOH500 and silica, respectively) to that obtained after NO contact and removing the contribution of NO gas. A complex signal related to the adsorbed NO is present in both samples in the range 1950-1800 cm^{-1}, with the most important signal at 1905 cm^{-1}. As reported in the

literature, iron in heme group is typically six-coordinated and presents a band due to NO interaction at 1917 cm^{-1} (36). In addition, it is also possible to observe the interaction of NO with a five-coordinated Fe center at around 1850 cm^{-1}.

Based on these results, the Fe-heme groups are accessible to reactants in both samples supporting SBP, the active SiO_2-based HBC and AlOOH500.

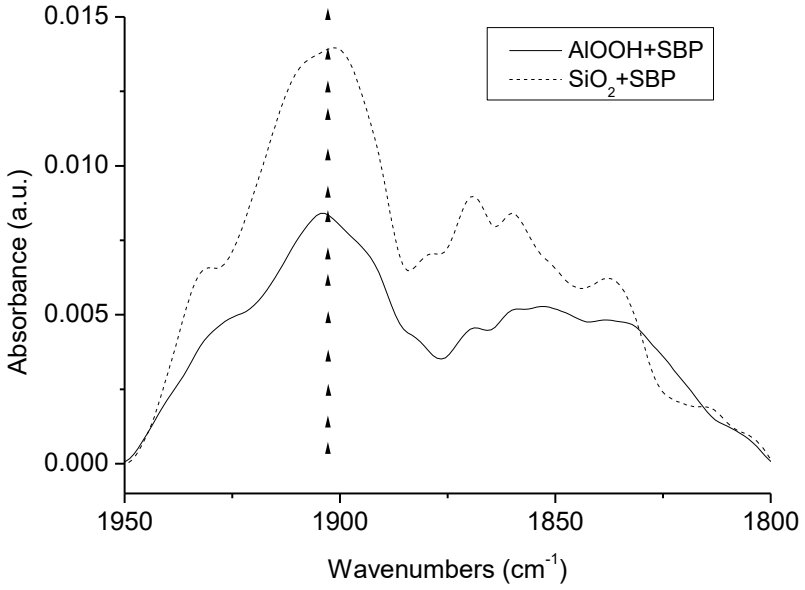

Figure 4. 8. Differential FT-IR spectra of NO adsorbed at room temperature onto AlOOH500+SBP and SiO2+SBP. The spectra were obtained after subtraction of the contribution of the bare support and NO gas. The broken line indicates the main contribution from Fe(III)-heme groups.

4.3.3.2 Protein backbone structure - FTIR spectroscopy

4.3.3.2.a – Amide vibrational signals

FTIR spectroscopy can also be very useful to monitor the structure of a protein based on the characteristic signals of the amide group. Amide I and amide II produce two main bands visible in the infrared spectra of proteins. The amide I band (IR signal present in the range 1600-1700 cm^{-1}) is mainly associated with the C=O stretching vibration (70-85%) and is directly related to the backbone conformation. The amide II band is in the range 1500-1580 cm^{-1} and results from the N-H bending vibration (40-60%) and from the C-N stretching vibration (18-40%). All these bands are sensitive to the protein conformation (37).

Figure 4.9 reports the differential FTIR spectra, calculated with respect to the bare supports, relative to AlOOH500+SBP before and after washing and after thermal treatment at 300 °C (used to denature the protein). In addition, the spectra of silica monolith supporting SBP after a simple outgassing at 30°C and after a thermal treatment at 120 and 210 °C (sufficient to obtain the deactivation of the enzyme) are reported. All the samples were prepared as thin pellets, analyzed in transmission mode and treated in vacuum before spectroscopic analysis in order to remove water physisorbed at the support surface and its spectral contributions. For the sake of comparison, also the spectrum of free SBP in its native conformation dispersed in KBr pellet was reported.

FTIR spectrum of native SBP is characterized by two bands at 1650 and 1535 cm^{-1} (section c). This pattern changes as a result of interaction with the solid support, both in the AlOOH500+SBP and SiO_2+SBP samples. In the case of AlOOH500+SBP, the amide I band is visible both before and, in

minor extent, after washing (black and grey curves in section b, respectively). This is not surprising, as we already determined that SBP is partially released from the alumina support during the washing procedure. On the other hand, when the alumina-based material is treated at 300°C, evident modifications of the spectrum occur: both the signals decrease in intensity, a new band at about 1580 cm^{-1} and a shoulder at about 1735 cm^{-1} appear (dotted line curve in section b). Similar modifications are also observed as a consequence of thermal treatment of the SiO^{2-} based materials, but, in this case, shift, intensity and shape of the amide I band are less affected by the treatment at high temperatures (grey and dotted line curves in section a), indicating a lower perturbation of the native protein conformation.

The presence of the signal at about 1650 cm^{-1} in the washed AlOOH500+SBP (grey curve in section b) seems to indicate that the enzyme immobilized at the Al_2O_3 surface shows a conformation similar to the native one, in apparent contrast with the results of enzymatic activity, therefore further studies are needed and the use of a more sensitive technique is necessary. In the next section the results obtained by using fluorescence spectroscopy will be discussed.

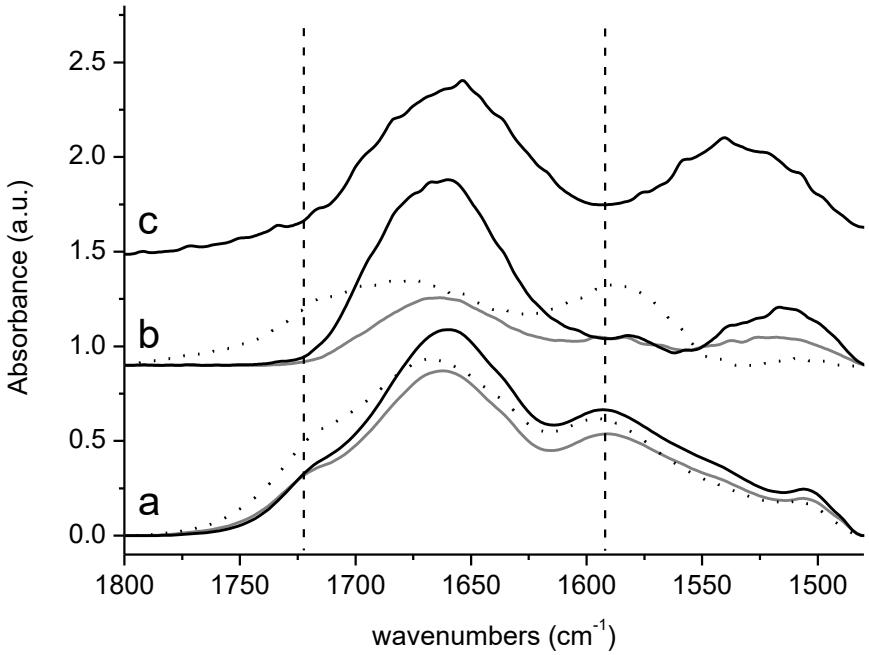

Figure 4. 9. Differential FTIR spectra, calculated with respect to the bare supports, relative to silica-based HBC (section a) and AlOOH500-based sample (section b). The spectrum of free SBP dispersed in KBr is reported in section c. Section a: SiO2+SBP outgassed at 30°C (black line), heated at 120°C (grey line) and 210°C (dotted line); section b: AlOOH500+SBP non-washed (black line), washed (grey line) and heated at 300°C (dotted line). The broken vertical lines indicate the signals expected for the unfolded enzyme.

4.3.3.3 Fluorescence spectroscopy study

Fluorescence spectroscopy is one of the most common methods used to determine the presence and the conformation of an enzyme in a sample. In particular, the observed fluorescence in the case of SBP is due to an electron transfer from the heme group (a typical active site of peroxidases) to tryptophan (Trp) residues, which have an emission band at around 350 nm(38). Further, fluorescence spectroscopy can be used to reveal the secondary structure of proteins as

fluorescence quenching is greater when the alpha-helix of a protein unfolds into a beta-sheet or random coil conformation (39).

Figure 4.10. illustrates the fluorescence spectra of SBP before and after immobilization on silica and AlOOH500 supports. As described earlier, both materials and relative supports were suspended in water and analyzed. The supports do not fluoresce resulting in a relatively flat spectrum, whereas the two hybrid systems based on non-washed AlOOH500 and silica show signals very similar to those of the free enzyme. Specifically, in the presence of silica support (Figure 4.10A), for which the enzyme was covalently bonded to the silica surface, the broad emission band of the supported enzyme is blue-shifted with respect to the free enzyme and no modification of the spectrum is observed after washing (data not shown). This indicates that a stable and strong interaction, due to the covalent immobilization of the enzyme on silica, has been established. The situation is completely different in the AlOOH500+SBP samples (Figure 4.10B). The main bands observed for the non-washed AlOOH500+SBP system are very similar to those of the free enzyme, whereas no emission is observed for the washed AlOOH500. As the quantitative tests based on SBP release described above indicate, a significant amount of SBP is still present at the surface of the AlOOH500 support after washing. Thus, we can conclude that some regions of SBP interact with the Al_2O_3 support through a very weak (physical) interaction while other regions of SBP interact strongly. The weakly bound SBP appears to have been released from the support during the analysis of the aqueous suspension as its emission spectrum is similar to free SBP, while the strongly bound SBP remains on the alumina support. Notably, it interacts so strongly with the support that its secondary structure is modified and its emission is quenched.

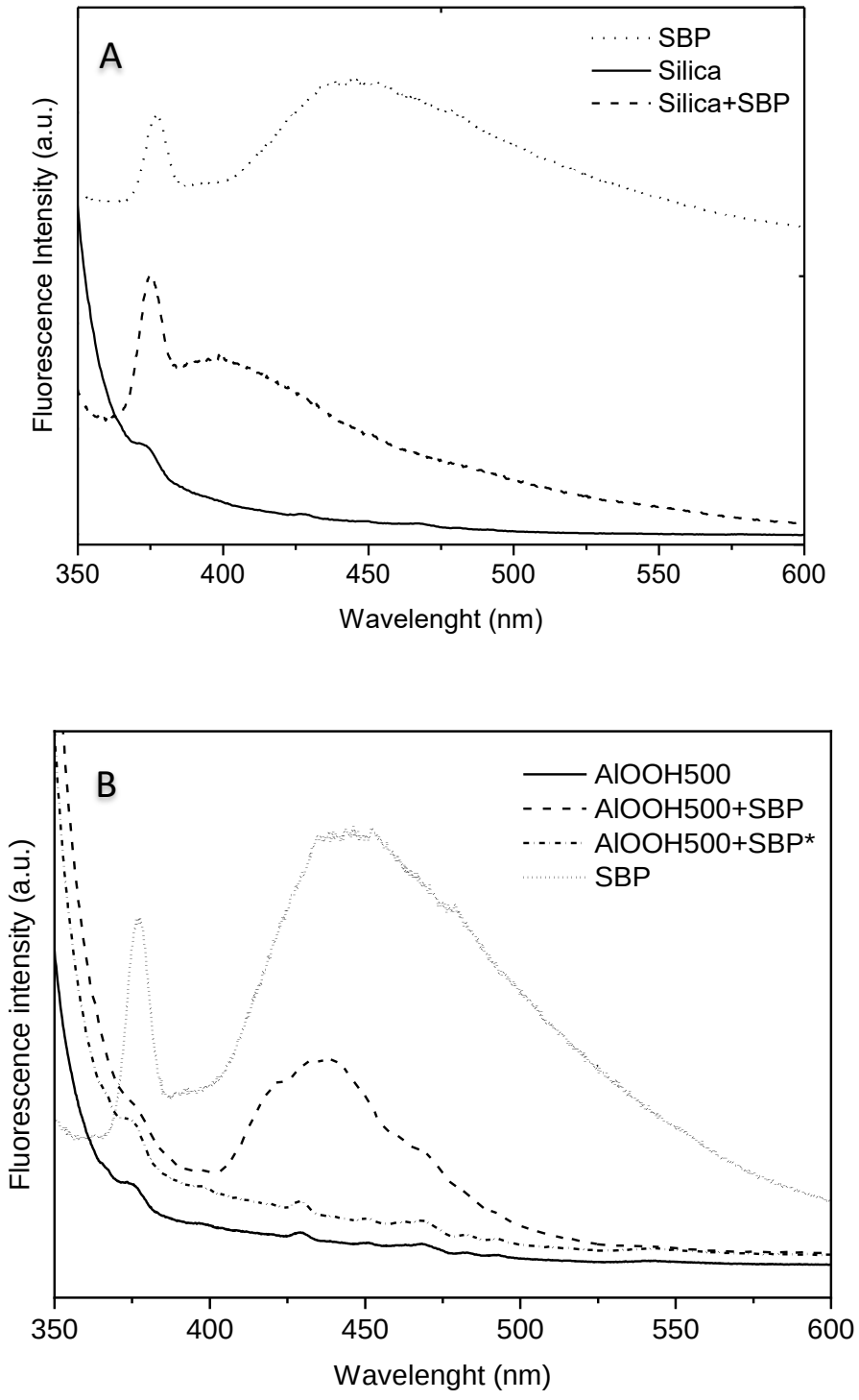

Figure 4. 10. Normalized fluorescence intensity of immobilized SBP. Section A: SiO2 support, SiO2+SBP and free SBP; section B: AlOOH500, AlOOH500+SBP and AlOOH500+SBP after washing process (indicated by *).

4.4. Conclusions

The electrostatic interaction at the base of the functionalization procedure used to obtain the hybrid alumina-based systems produces very stable materials where SBP is strongly bonded to the surface of the aluminas. Unfortunately, the interaction is so strong that it causes the unfolding of the enzyme and the consequent lack of activity, as suggested by fluorescence data. A partial loss of catalytic activity attributable to the same phenomenon was previously observed for SBP in the presence of a poorly shielded magnetic field in magnetic hybrid magnetite-based heterogeneous biocatalysts (40), but in our case the effect of enzyme-support interactions seems to be so strong as to completely remove the catalytic potential. In conclusion, a methodological approach has been developed to understand the underlying mechanism of the biocatalytic action of a heterogeneous biocatalyst. Notably, strong interactions with supports can affect the activity of supported enzymes.

4.5. Acknowledgments

This project has received funding from the European Union's Horizon 2020 research and innovative programme under the Marie Sklodowska-Curie grant agreement No 645551. The authors also thank the contribution of Compagnia di San Paolo supplied under the pluriannual Convention (2016-2018) between the University of Turin and Compagnia di San Paolo.

4.6. References

1. Sivaramakrishnan R, Incharoensakdi A. Direct transesterification of Botryococcus sp . catalysed by immobilized lipase : Ultrasound treatment can reduce reaction time with high yield of methyl ester. Fuel. 2017;191:363–70. Available from: http://dx.doi.org/10.1016/j.fuel.2016.11.085

2. Tran D, Chen C, Chang J. Continuous biodiesel conversion via enzymatic transesterification catalyzed by immobilized Burkholderia lipase in a packed-bed bioreactor. Appl Energy. 2016;168:340–50. Available from: http://dx.doi.org/10.1016/j.apenergy.2016.01.082

3. Peñarrubia Fernandez IA, Liu DH, Zhao J. LCA studies comparing alkaline and immobilized enzyme catalyst processes for biodiesel production under Brazilian conditions. Resour Conserv Recycl. 2017;119:117–27.

4. Singh J, Singh MK, Kumar M, Thakur IS. Bioresource Technology Immobilized lipase from Schizophyllum commune ISTL04 for the production of fatty acids methyl esters from cyanobacterial oil. Bioresour Technol. 2015;188:214–8. Available from: http://dx.doi.org/10.1016/j.biortech.2015.01.086

5. Dikshit PK, Moholkar VS. Bioresource Technology Kinetic analysis of dihydroxyacetone production from crude glycerol by immobilized cells of Gluconobacter oxydans MTCC 904. Bioresour Technol. 2016;216:948–57. Available from: http://dx.doi.org/10.1016/j.biortech.2016.06.042

6. Altinkaynak C, Tavlasoglu S, Özdemir N, Ocsoy I. Enzyme and Microbial Technology A new generation approach in enzyme immobilization : Organic-inorganic hybrid nanoflowers with enhanced catalytic activity and stability. Enzyme Microb Technol. 2016;93–94:105–12. Available from: http://dx.doi.org/10.1016/j.enzmictec.2016.06.011

7. Marchis T, Cerrato G, Magnacca G, Crocellà V, Laurenti E. Immobilization of soybean peroxidase on aminopropyl glass beads : Structural and kinetic studies. Biochem Eng J. 2012;67:28–34. Available from: http://dx.doi.org/10.1016/j.bej.2012.05.002

8. Qu Y, Sun L, Li X, Zhou S, Zhang Q, Sun L. LWT - Food Science and Technology Enzymatic degumming of soybean oil with magnetic immobilized phospholipase A 2. LWT - Food Sci Technol. 2016;73:290–5. Available from: http://dx.doi.org/10.1016/j.lwt.2016.06.026

9. Marchis T, Cerrato G, Magnacca G, Crocellà V, Laurenti E. Immobilization of soybean peroxidase on aminopropyl glass beads: Structural and kinetic studies. Biochem Eng J. 2012;67:28–34.

10. Ungcharoenwiwat P, Canyuk B, H-kittikun A. Synthesis of jatropha oil based wax esters using an immobilized lipase from Burkholderia sp . EQ3 and Lipozyme RM IM. Process Biochem. 2016;51(3):392–8. Available from: http://dx.doi.org/10.1016/j.procbio.2015.12.019

11. Luo H, Zhu L, Chang Y, Liu X, Liu Z, Sun H, et al. Microenvironmental pH changes in immobilized cephalosporin C acylase during a proton-producing reaction and regulation by a two-stage catalytic process. Bioresour Technol. 2017;223:157–65.

12. Mehta J, Bhardwaj N, Bhardwaj SK, Kim K. Recent advances in enzyme immobilization

techniques : Metal-organic frameworks as novel substrates. Coord Chem Rev. 2016;322:30–40. Available from: http://dx.doi.org/10.1016/j.ccr.2016.05.007

13. Maria P, Chagas B, Arriel J, Cristina M, Duarte A. International Journal of Biological Macromolecules Immobilized soybean hull peroxidase for the oxidation of phenolic compounds in coffee processing wastewater. Int J Biol Macromol. 2015;81:568–75. Available from: http://dx.doi.org/10.1016/j.ijbiomac.2015.08.061

14. Raquel L, Merten M, Jose A, Dillon P, Claudete R, Augusto C, et al. Fermentation kinetics of acid – enzymatic soybean hull hydrolysate in immobilized-cell bioreactors of Saccharomyces cerevisiae , Candida shehatae , Spathaspora arborariae , and their co-cultivations. Biochem Eng J. 2014;88:61–7. Available from: http://dx.doi.org/10.1016/j.bej.2014.04.004

15. Bolivar JM, Eisl I, Nidetzky B. Advanced characterization of immobilized enzymes as heterogeneous biocatalysts. Catal Today. 2016;259:66–80. Available from: http://dx.doi.org/10.1016/j.cattod.2015.05.004

16. Wang B, Shangguan L, Wang S, Zhang L, Zhang W, Liu F. Preparation and application of immobilized enzymatic reactors for consecutive digestion with two enzymes. J Chromatogr A. 2016;1477:22–9. Available from: http://dx.doi.org/10.1016/j.chroma.2016.11.027

17. Guzik U, Hupert-Kocurek K, Wojcieszynska D. Immobilization as a strategy for improving enzyme properties- Application to oxidoreductases. Vol. 19, Molecules. 2014. p. 8995–9018.

18. Cazaban D, Wilson L, Betancor L. Lipase Immobilization on Siliceous Supports: Application to Synthetic Reactions. Curr Org Chem. 2016;21(2):96–103.

19. Xie W, Wang J. Immobilized lipase on magnetic chitosan microspheres for transesterification of soybean oil. Biomass and Bioenergy. 2011;36:373–80. Available from: http://dx.doi.org/10.1016/j.biombioe.2011.11.006

20. Stoica G, Pérez-Ramírez J. Reforming dawsonite by memory effect of AACH-derived aluminas. Chem Mater. 2007;19(19):4783–90.

21. Bénézeth P, Palmer DA, Anovitz LM, Horita J. Dawsonite synthesis and reevaluation of its thermodynamic properties from solubility measurements: Implications for mineral trapping of CO2. Geochim Cosmochim Acta. 2007;71(18):4438–55.

22. Yalfani MS, Contreras S, Llorca J, Medina F. Enhanced Cu activity in catalytic ozonation of clofibric acid by incorporation into ammonium dawsonite. Appl Catal B Environ. 2011;107(1–2):9–17.

23. Solis C, Rivera J, Rosa D, Lucio-ortiz CJ, Valente JS, Castaldi MJ. Synthesis and characterization of functionalized alumina catalysts with thiol and sulfonic groups and their performance in producing 5-hydroxymethylfurfural from fructose. Fuel. 2017;198:134–44. Available from: http://dx.doi.org/10.1016/j.fuel.2016.10.004

24. Wiśniewska M, Chibowski S, Urban T. Modification of the alumina surface properties by adsorbed anionic polyacrylamide-Impact of polymer hydrolysis. J Ind Eng Chem. 2015;21:925–31.

25. Shivaprasad P, Singh PK, Saharan VK, George S. Nano-Structures & Nano-Objects Synthesis of nano alumina for defluoridation of drinking water. Nano-Structures & Nano-

Objects. 2018;13:109–20. Available from: https://doi.org/10.1016/j.nanoso.2018.01.001

26. Magnacca G, Laurenti E, Vigna E, Franzoso F, Tomasso L, Montoneri E, et al. Refuse derived bio-organics and immobilized soybean peroxidase for green chemical technology. Process Biochem. 2012;47(12):2025–31. Available from: http://dx.doi.org/10.1016/j.procbio.2012.07.021

27. Li J, Li W, Nai X, Bian S, Liu X, Wei M. Synthesis and formation of alumina whiskers from hydrothermal solution. J Mater Sci. 2010;45(1):177–81.

28. Lafficher R, Digne M, Salvatori F, Boualleg M, Colson D, Puel F. Ammonium aluminium carbonate hydroxide NH4Al(OH)2CO3 as an alternative route for alumina preparation: Comparison with the classical boehmite precursor. Powder Technol. 2017;320:565–73.

29. Thommes M, Kaneko K, Neimark A V., Olivier JP, Rodriguez-Reinoso F, Rouquerol J, et al. Physisorption of gases, with special reference to the evaluation of surface area and pore size distribution (IUPAC Technical Report). Pure Appl Chem. 2015;87(9–10):1051–69.

30. Magnacca G, Laurenti E, Vigna E, Franzoso F, Tomasso L, Montoneri E, et al. Refuse derived bio-organics and immobilized soybean peroxidase for green chemical technology. Process Biochem. 2012;47(12):2025–31.

31. Gillikin JW, Graham JS. Purification and Developmental Analysis of the Major Anionic Peroxidase from the Seed Coat of Glycine max. Plant Physiol. 2008;96(1):214–20.

32. Kamal JKA, Behere D V. Activity, stability and conformational flexibility of seed coat soybean peroxidase. J Inorg Biochem. 2003;94(3):236–42.

33. Zecchina A, Rivallan M, Berlier G, Lamberti C, Ricchiardi G. Structure and nuclearity of active sites in Fe-zeolites: Comparison with iron sites in enzymes and homogeneous catalysts. Vol. 9, Physical Chemistry Chemical Physics. 2007. p. 3483–99.

34. Jiang M. Adsorption properties of iron and iron-manganese catalysts investigated by in-situ diffuse reflectance FTIR spectroscopy. J Phys Chem B. 2000;104(32):7636–43.

35. Wang Y, Lei Z, Zhang R, Chen B. Journal of Molecular Structure : THEOCHEM Adsorption of NO and N 2 O on Cu-BEA zeolite. J Mol Struct THEOCHEM. 2010;957(1–3):41–6. Available from: http://dx.doi.org/10.1016/j.theochem.2010.07.004

36. Mcquarters AB, Kampf JW, Alp EE, Hu M, Zhao J, Lehnert N. Ferric Heme-Nitrosyl Complexes : Kinetically Robust or Unstable. Inorg Chem. 2017;56(17):10513–28. Available from: https://pubs.acs.org/doi/10.1021/acs.inorgchem.7b01493

37. Lin Z, Hu R, Zhou J, Ye Y, Xu Z, Lin C. A further insight into the adsorption mechanism of protein on hydroxyapatite by FTIR-ATR spectrometry. Spectrochim Acta - Part A Mol Biomol Spectrosc. 2017;173:527–31.

38. Zhang W, Dai X, Zhao Y, Lu X, Gao P. Comparison of the different types of surfactants for the effect on activity and structure of soybean peroxidase. Langmuir. 2009;25(4):2363–8.

39. Tsaprailis G, Sze Chan DW, English AM. Conformational states in denaturants of cytochrome c and horseradish peroxidases examined by fluorescence and circular dichroism. Biochemistry. 1998;37(7):2004–16.

40. Donadelli JA, García Einschlag FS, Laurenti E, Magnacca G, Carlos L. Soybean peroxidase

immobilized onto silica-coated superparamagnetic iron oxide nanoparticles: Effect of silica layer on the enzymatic activity. Colloids Surfaces B Biointerfaces. 2018;161:654–61. Available from: http://dx.doi.org/10.1016/j.colsurfb.2017.11.043

Chapter Five

Removal of pyrene, as model of crude oil, from produced-water by lipophilic hybrid materials

Abstract

Inorganic-lipid hybrid particles, whereby arachidic acid is immobilized on alumina and silica particle surface by electrostatic interaction between a negative polar head group of lipid and positively charged support, were prepared. The apolar tails of lipid are available to establish strong interactions with apolar substrates in order to apply the materials to purify the oilfield-produced water.

Fourier transform infrared spectroscopy (FTIR) and thermogravimetric analysis (TGA) were used to characterize the hybrid materials and evaluate the hydrophilicity/hydrophobicity of their surface. Pyrene solution in water was chosen as a model for simulating the presence of oil in produced water and fluorescence spectroscopy was chosen to demonstrate the efficiency of the materials towards pyrene removal from aqueous media.

The hydrophobic adsorbents prepared in a very easy and reproducible way, result rapid, low-cost and efficient towards the removal of apolar substrates as demonstrated by the tests carried out in the presence of pyrene.

Keywords: removal of oil; pyrene adsorption; produced water treatment; surface-functionalized oxides; hydrophobic interaction; lipid hydrophobic monolayer; hydrophobic surface.

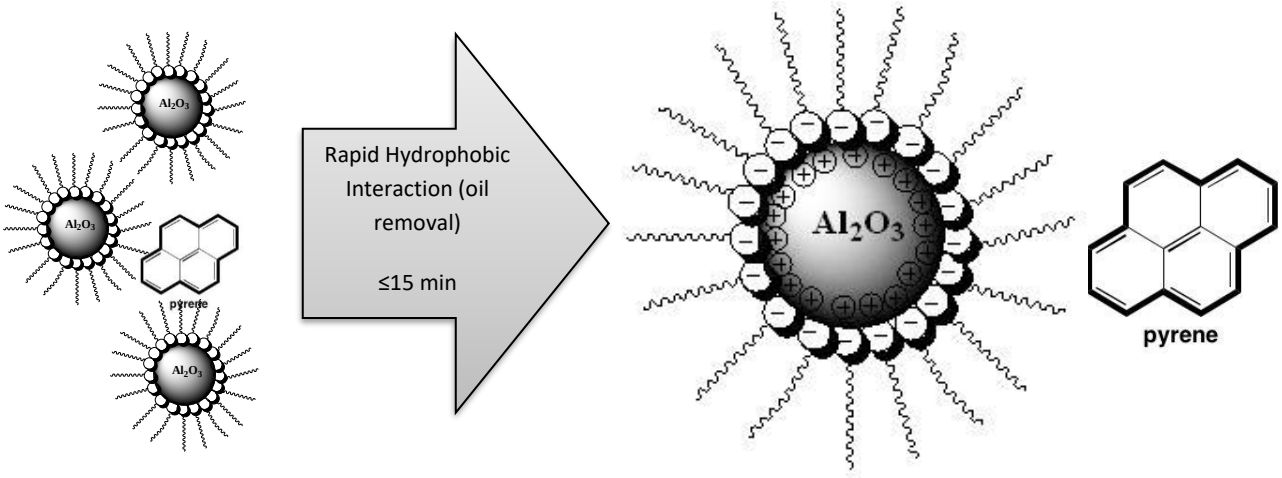

5.1. Introduction

Water preservation and treatment have been widely considered in last decades because the increase of the population and the human consumption make urgent an appropriate water management, in particular considering the large amount of wastewater produced in industrial processes.

Water co-produced with oil and gas is commonly indicated as “produced water” (PW) (1). PW is the water returned from the bitumen or heavy oil reservoir which regularly generates when saline water and hydrocarbons are mixed during the extraction of natural gas and crude oil (2). The normal operation related to this extraction involves huge quantity of injected water to facilitate the petroleum recovery. This water is then pumped to the surface with hydrocarbons, salts and other solutes (3),(4),(5) and needs to be purified before reintroduction in the environment. PW is generated with a global estimation three times larger than the production of oil and gas (6),(7),(8), consequently, PW treatment is a topic of extreme interest especially for oil-producing-countries with water scarcity (9), as they must develop more efficient methods for its treatment, recycle, and reuse.

Conventionally PW is treated by a combination of different physical, chemical and biological processes (7) such as flocculation (9), electro-chemical coagulation (4), flotation (10), photocatalytic processes (2), hydrocyclones, Fenton and ozonation (11), membrane and Mixed Matrix Membrane (MMMs) processes (3),(6),(12) as well as biological method (1). There are some drawbacks related to the chemical and biological methods as they can produce hazardous sludge and the cost of chemicals is typically high (1), whereas physical methods have no impact on the environment and are reasonably economical. According to S. Jimenez (7), adsorption is one of the possible treatments to achieve higher water quality. Adsorption can be actualized through electrostatic interaction (13), hydrophobic interaction (14) or by means of encapsulation method (15) on inorganic or polymer support (16).

On the other hand, oxides typically possess very good behaviors to act as adsorbing materials, as they usually possess high specific surface area and open porosity. Unfortunately, they also show a typical hydrophilic character, as a result of the presence of hydroxyl groups on the surface. Nevertheless, the hydroxyl groups can be exploited to functionalize the surface with chosen hydrophobic molecules, for instance molecules carrying hydrophobic chains well interacting with apolar substrates (17),(12),(18).

Here, we investigate the possibility to establish electrostatic interactions between polar head groups of amphiphilic molecules and oxide surfaces with opposite charge, namely using gamma and delta-theta transition aluminas from boehmite (AlOOH) and ammonium dawsonite (AACH) precursors, which were proved to efficiently interact with negatively charged substrates in a wide range of pHs (19),(20),(21). Together with alumina supports, we consider the possibility to produce a material with enhanced hydrophobic behaviors exploiting the surface functionalization of commercial Aerosil 200 fumed silica [produced by Evonik, Essen Germany], which is known to be a material hydrophobic in nature for the high temperature method used for its synthesis. Also silica, similarly to alumina, possesses surface hydroxyl groups, but the more covalent character of the Si-O bonds makes this system much more hydrophobic than aluminas, so prone to interact with hydrophobic functionalizing molecules via dispersion forces.

The amphiphilic molecule chosen to functionalize the above mentioned oxide supports is the arachidic (or icosanoic) acid. It is a saturated fatty acid almost insoluble in water. The polarity of the carboxylic head groups makes possible the interaction with hydrophilic surfaces, while the alkyl chain tail causes the hydrophilicity decrease (22) and in principle it confers to the material

the hydrophobicity necessary to interact with apolar substrates (23). The hydrophilicity/hydrophobicity behavior, predicting in general the efficiency of material in interacting prevalently with water or oil (18), can be determine by means of: Dynamic Contact Angle measurements (24), infrared spectroscopy (25),(26),(27), microcalorimetric (28) and microgravimetric (29) procedures.

Despite many studies reported the immobilization of lipid onto support to prepare a useful component for many applications (30), almost no studies in the field of water purification have been reported in the literature. In this study, pyrene has been applied as a model contaminant due to its specific volatility and water miscibility behaviors. Pyrene is a well-known polyaromatic hydrocarbon (PAH) (31), considered harmful to human health, leading to cancer and acting as a mutagen belonging, whose limit concentration in water is 2 ppb (31) and belonging to a group of persistent hydrophobic contaminants which can be monitored spectroscopically by fluorescence measurements. It is the primary organic contaminants in oilfield-produced water (9).

5.2. Experimental

5.2.1. Materials

Commercial boehmite (AlOOH) was kindly supplied by Centro Ricerche FIAT. Aluminum nitrate, urea and silica Aerosil 200 were purchased from Aldrich. Arachidic acid (≥99.9%) and chloroform (≥99.9%) were purchased from Avanti polar lipids and Sigma-Aldrich respectively. All chemicals were used without further purification.

Pyrene was supplied by the University of Regina (Canada) recrystallized from ethanol (95%) five times and sublimed once (32) prior adsorption experiments (9).

All aqueous solutions were obtained using ultrapure water Millipore Milli-QTM.

5.2.2. Sample preparation

Ammonium dawsonite (AACH) was synthesized as reported in previous chapter.

Gamma and delta-theta phases of Al2O3 from AlOOH and AACH were prepared by calcination in an oven at 500°C and 1000°C, respectively, for 3 hours (20),(21).

Aluminas and Silica Aerosil 200 (paper alumina monolith under review) were used as supports for immobilization of lipid molecules. They are indicated in the text as A (gamma from AlOOH), B (gamma from AACH), D (delta-theta from AlOOH), E (delta-theta from AACH) and C (silica).

A thin lipid film was prepared by dissolving 10, 20 and 40 mg of lipid separately in a certain volume (5 ml) of chloroform solution in three 50 ml round-bottomed flasks (23). The solvent was removed by rotary evaporation at 40 °C for about 1 h to leave a thin lipid film in the bottom of glass flasks. Then 10 ml of milliQ water (MQ) was poured in each flask and sonicated for about 30 min in order to make a lipid film hydrated. The other 10 ml of MQ was poured to each suspension and then shacked to afford a clear colorless solution. Several batches with different quantities of lipid were prepared. In all cases the lipid concentration was kept below the critical micellar concentration (CMC=$3.7*10^{-5}$ M) (33) in order to avoid formation of polar micelles or bilayer lipid structures onto the support surface. The hybrid materials with different support/lipid

weight ratios (5, 10 and 20) were prepared by mixing 0.2 g of supports at room temperature and pH=7 with the proper amount of hydrated lipid film in 4 ml of MQ. The solution was then incubated overnight at room temperature. To remove the lipid excess, the solution after incubation was centrifuged for 20 min at 2000 rpm, the supernatant was removed and the slurry was dried in oven at 40 °C. The obtained hybrid materials were indicated in the text by a letter indicating the support, F indicating the film-based preparation procedure and a number indicating the support/lipid ratio, therefore AF5 indicates a gamma-Al_2O_3 from AlOOH in ratio 5:1 with the lipid film.

In order to avoid the use of chloroform, other hybrid materials were prepared using arachidic acid in powder keeping the same support/lipid ratio previously considered (5, 10 and 20) starting from 0.1 g of support **A**, **B** and **C** (34). 4 ml of MQ was poured in each batch containing the mixture of powdery lipid and support, then the solution was incubated overnight at room temperature in water at pH=7. To remove the excess lipid, the solution after incubation was centrifuged for 20 min at 2000 rpm, the supernatant was removed and the slurry was dried in oven at 40 °C. These hybrid materials were indicated by a letter indicating the support and a number indicating the support/lipid ratio, therefore A5 indicates a gamma-Al_2O_3 from AlOOH in ratio 5:1 with the lipid powder.

5.2.3. Stability test

In order to check the stability, 10 mg of each hybrid material was put in a glass test tube contacted with 4 ml of MQ at 21.0 ± 0.5°C, kept under shaking overnight and then placed in a centrifuge (at 2000 rpm for 20 min). After centrifugation, some samples presented a cloudy and fatty phase in

the supernatant phase, indicating a release of lipid from hybrid materials. These materials were considered non-stable and not used in the subsequent tests.

5.2.4. Adsorption experiments

A methanolic pyrene solution with a concentration 1.6 mM was prepared as stock solution and used every day to prepare a 2 µM aqueous pyrene solution. The solution was stirred for about 30 min prior adsorption experiments.

The adsorption experiments were carried out in glass bottles inert towards pyrene adsorption. 10 mg of adsorbent were dispersed in 2 ml of MQ in the presence of 2 ml of pyrene solution at pH 7. The bottles were sealed using Teflon caps and horizontally shaken on a vortex shaker (200 rpm) at room temperature (21.0 ± 0.5°C). The pyrene adsorption was evaluated by means of a fluorescence spectrophotometer measuring every 5 minutes the residual amount of pyrene in the supernatant after centrifugation at 2000 rpm for 20 min. All the adsorption tests were carried out in duplicate. In all the experiments the adsorption equilibrium was achieved within less than 15 min.

5.2.5. Adsorbed amount evaluation

The amount of pyrene adsorbed onto hybrid adsorbents at equilibrium q_t was determined as follows:

$$q_t = (C_0 - C_t)V/m$$

Where C_0 and C_t are respectively the initial and equilibrium concentrations of pyrene (µg/L) in the aqueous phase at time t, V is the volume of solution (L) and m is the mass of solid phase (g). The capacity of adsorption was followed after 5 and 15 minutes of pyrene contact.

5.2.6. Instrumentation

Fourier transform infrared (FTIR) spectra were carried out in transmission mode by means of a Bruker Vector 22 spectrophotometer equipped with Global source, DTGS detector in the range of 4000-400 cm^{-1} (4 cm^{-1} resolution), at room temperature and using OPUS software. All the samples were dispersed in KBr (approximately sample: KBr weight ratio was 0.01).

Thermo-gravimetric analysis (TGA) was performed using a TQ600 by TA. TGA measurements were carried out with a heating ramp of 10 ◦C/min from 30 to 750 ◦C under air. This analysis allowed quantifying the amount of lipid functionalizing alumina and silica surface.

Study state fluorescence spectra were obtained by PTI QuantaMaster spectrofluorometer made in USA, Birmingham, NJ in the University of Regina, Canada. The temperature during all measurements was adjusted at 21.0 ± 0.5°C and the excitation and emission slits were set such that the bandwidths were 2nm.The data interval and integration time were 0.5 nm and 0.5 s, respectively (9). For this study excitation scans were recorded between 200-360 nm and the emission wavelength was set at 380 nm. All fluorescence spectra were normalized by subtracting the baseline fluorescence spectrum.

5.3. Results and discussion

5.3.1. Stability results

The results of stability test showed that most of the hybrid materials were stable in water, as the electrostatic interaction established between the support surfaces and the polar head groups of lipid was strong. Only in a few cases the interactions were not strong enough and the lipid was partially released. According to Scheme 5.1, B5, BF5, EF10, and EF20 were completely unstable in water, whereas B10 and BF10 were partially stable. These samples were not characterized or tested in pyrene removal.

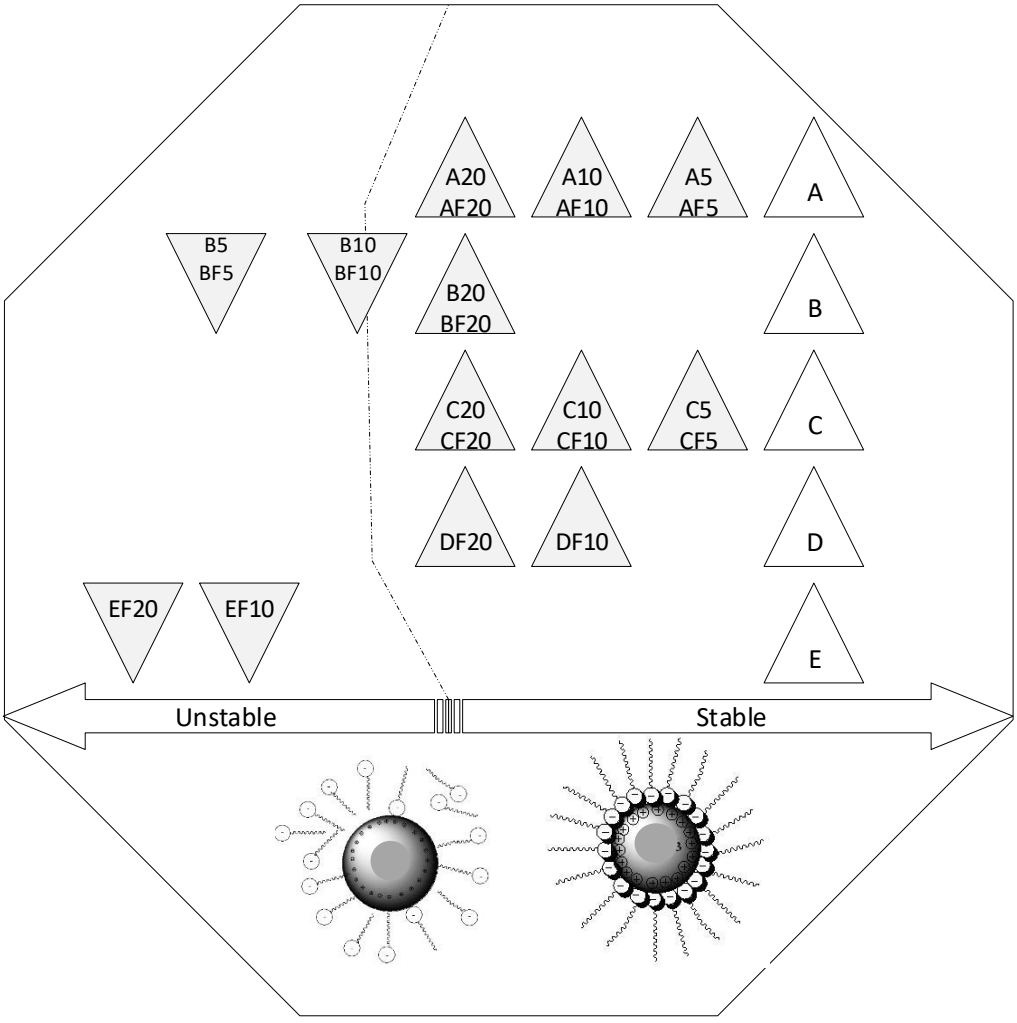

Scheme 5. 1. Stability of hybrid materials in water at 21.0 ± 0.5°C.

5.3.2. FTIR spectroscopy.

FTIR spectra for bare and functionalized supports, as well as pure lipid, are reported in Figure 5.1a and b, as representative of all the examined samples. Excluding the main absorptions of the support, as indicated in Table 5.1, illustrating the principal signals due to lipids, it is possible to recognize the contribution of C-H stretching vibrations (3000–2800 cm^{-1}) originated by the hydrocarbon chains. In the low wavenumber region of the spectrum it is visible the C=O stretching vibration for carboxylic acids at 1700 cm^{-1}. Also weak signals at 1220 and 1150 cm^{-1}, assignable to lipid presence, are visible. In the presented spectra, all the lipid bands are more evident on the sample gamma-Al_2O_3 from AlOOH functionalized with the lipid film, suggesting a higher functionalization efficiency, but the quantitative extent of the lipid interaction will be assessed more precisely using TGA measurements.

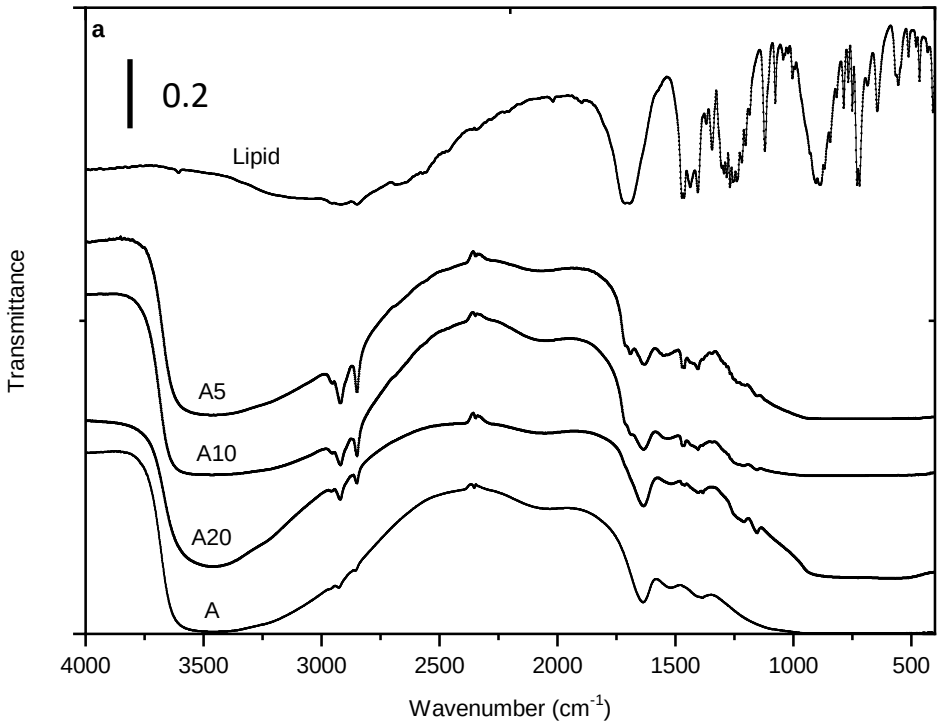
a
0.2
Lipid
A5
A10
A20
A
Transmittance
4000
3500
3000
2500
2000
1500
1000
500
Wavenumber (cm-1)

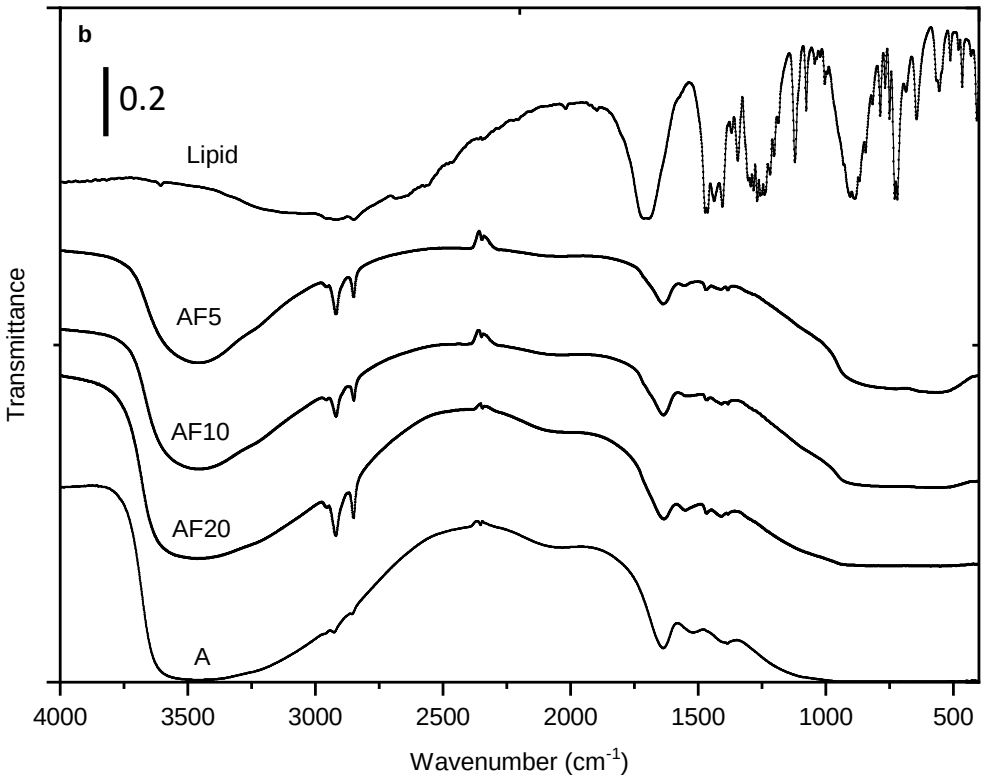
b
0.2
Lipid
AF5
AF10
AF20
A
Transmittance
4000
3500
3000
2500
2000
1500
1000
500
Wavenumber (cm-1)

Figure 5. 1. FTIR spectra of support A before and after functionalization with lipid powder (a section) and lipid film (b section). All the spectra are shifted for the sake of clarity.

Table 5. 1. Typical lipid IR signals.

Peaks (cm^{-1})	Assignment
3100–2800	C-H stretching vibrations (35)
2960	CH3 asymmetric stretching vibration
2919	CH2 asymmetric stretching vibration
2850	CH2 symmetric stretching vibration
1700	C=O stretching vibration for carboxylic acids (26)
1580	CO2- symmetric stretching vibration for carboxylate
1468, 1411, 1382	CO2- asymmetric stretching vibration for carboxylate

5.3.3. Thermal properties and lipid quantification

Figure 5.2a illustrate the results of TGA analysis on pure reference lipid powder in the temperature range 40-750°C under air. The lipid weight change curve indicates clearly the presence of two steps of decomposition, one major in the range 40 to 180 °C attributed to physisorbed and chemisorbed water elimination, and the second in the range 180 to 750°C associated with the oxidation of lipid and transformation into CO_2 and H_2O. The curves obtained for all the materials before and after functionalization by lipid film are similar, those related to DF20 and D support are reported as representatives in Figure 5.2b. The support shows a first weight loss in the range 40-180 °C due to elimination of physisorbed and chemisorbed water molecules and a second step in the range 180-750 °C due to the condensation of OH groups and consequent elimination of water molecules. At the same time, the hybrid system shows the first weight loss due to water elimination (as expected, less pronounced for the hydrophobic hybrid material with respect to the hydrophilic non-functionalized support), and a second step due to the condensation of OH groups and the oxidation of lipid. The amount of lipid immobilized on the supports is therefore quantified as the difference of the weight loss of the hybrid material in the range 180-750 °C and the weight loss observed in the same range for the pure support (assuming the amount of OH groups does not change significantly during the functionalization procedure). The results are reported in Table 5.2.

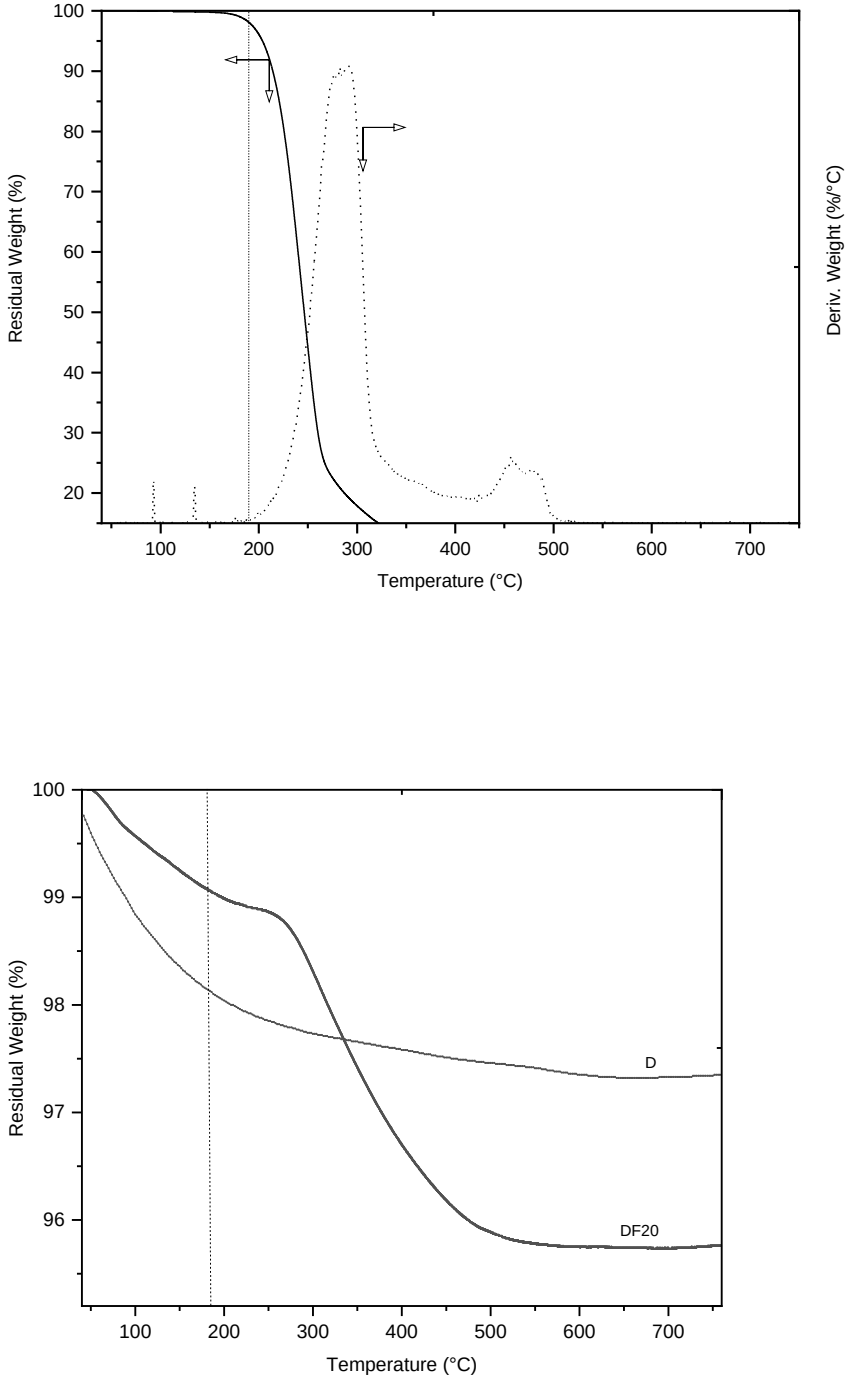

Figure 5. 2. TGA curves obtained in air for lipid (upper section) and for D and DF20 materials (lower section). The vertical dotted line indicates the temperature of 180°C used for the quantification of water and organics loss.

Table 5. 2. BET surface area and amount of water, OH groups and organics for references and hybrid materials. The affinity values were calculated considering the amount of organic immobilized by 1 m2 of support.

Materials	BET surface area (m2/g)	40-180°C (Adsorbed water %)	180-750°C (Organic content and OH groups eliminated %)	OH groups eliminated (%)	Measured organic content (%)	Affinity g(organic)/m2
A	186	4.88	-	3.53	-	
AF5		2.59	7.53	3.53	4.00	0.21
AF10		3.47	7.48	3.53	3.90	0.21
AF20		3.83	7.32	3.53	3.79	0.20
B	311	10.68	-	5.67	-	
BF20		13.16	20.77	5.67	15.10	0.48
D	102	1.85	-	0.85	-	
DF10		0.93	3.66	0.85	2.81	0.27
DF20		0.97	3.28	0.85	2.43	0.24
C	200	0.6	-	1.03	-	
CF5		0.67	13.87	1.03	12.84	0.64
CF10		0.47	9.63	1.03	8.60	0.43

CF20		0.51	3.50	1.03	2.47	0.12

The extent of lipid functionalization for each support increases as expected decreasing the ratio support/lipid from 20 to 5 and increases increasing the specific surface area of the supports. Therefore, BF20 sample (specific surface area of the support 311 m^2/g) shows the most efficient functionalization process, with an amount of organic content of 15.10%. Also CF5 and CF10 samples (specific surface area of 200 m^2/g) show a large functionalization extent with respect to the other materials, whereas A and D samples seem to be not so prone to establish a strong interaction with lipid giving the most limited functionalization extent. In order to assess the real affinity lipid/support, the amount of lipid immobilized was related to the specific surface area of the support giving an affinity evaluation reported in the last column of Table 5.2. Considering equal the amount of lipid used in the functionalization procedure (support/lipid=20), the largest affinity is shown by BF20 sample, whereas, unexpectedly, the lowest affinity is shown by C support. Nevertheless, CF5 shows in absolute terms the largest amount of lipid immobilized on an unitary surface of support, suggesting this could be the best pyrene adsorbing system.

5.4. Pyrene removal: adsorption kinetic

Figure 5.3 and 5.4 show the percentage and the total amount of pyrene removal from aqueous solutions, respectively, by different supports before and after lipid-functionalization from powder (section a) and film (section b) and after 5 and 15 minutes of pyrene contact. Almost all the hybrid materials indicate a significant removal comparing to their bare supports. In general,

the extent of functionalization affects the removal, i.e. the highest the amount of lipid functionalizing the material (as resulting from TGA measurements), the highest the pyrene removal. Unexpectedly, the C-based hybrid samples from powdery lipid show a different behavior, as the nominal decrease of lipid amount in the materials causes a slight increase of pyrene adsorption, even if the error bars indicate the change is not relevant in absolute terms. The best material in terms of performance is CF5 that was the material showing the highest affinity in Table 6.3. It is able in removing almost the 100% of pyrene corresponding to an absolute amount of about 0.35 mg/g. Similar results can be achieved with AF5 sample, and in general the materials prepared from lipid film are more efficient in pyrene removal than powdery lipid-based ones, showing in almost all cases an adsorption of more than 80%. This result suggests the films functionalize the surface of supports in a more efficient way with respect to powder dispersions, even if the green functionalization method without chloroform allows to achieve a removal always higher than 50% in 15 minutes.

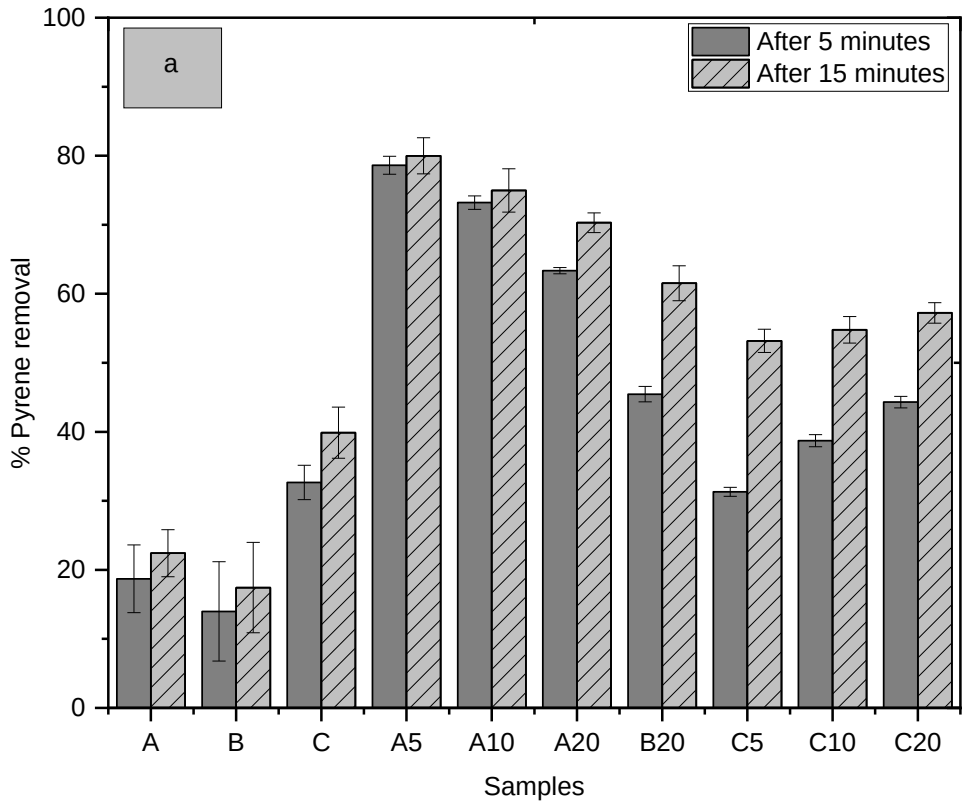
a
After 5 minutes
After 15 minutes
% Pyrene removal
100
80
60
40
20
0
A
B
C
A5
A10
A20
B20
C5
C10
C20
Samples

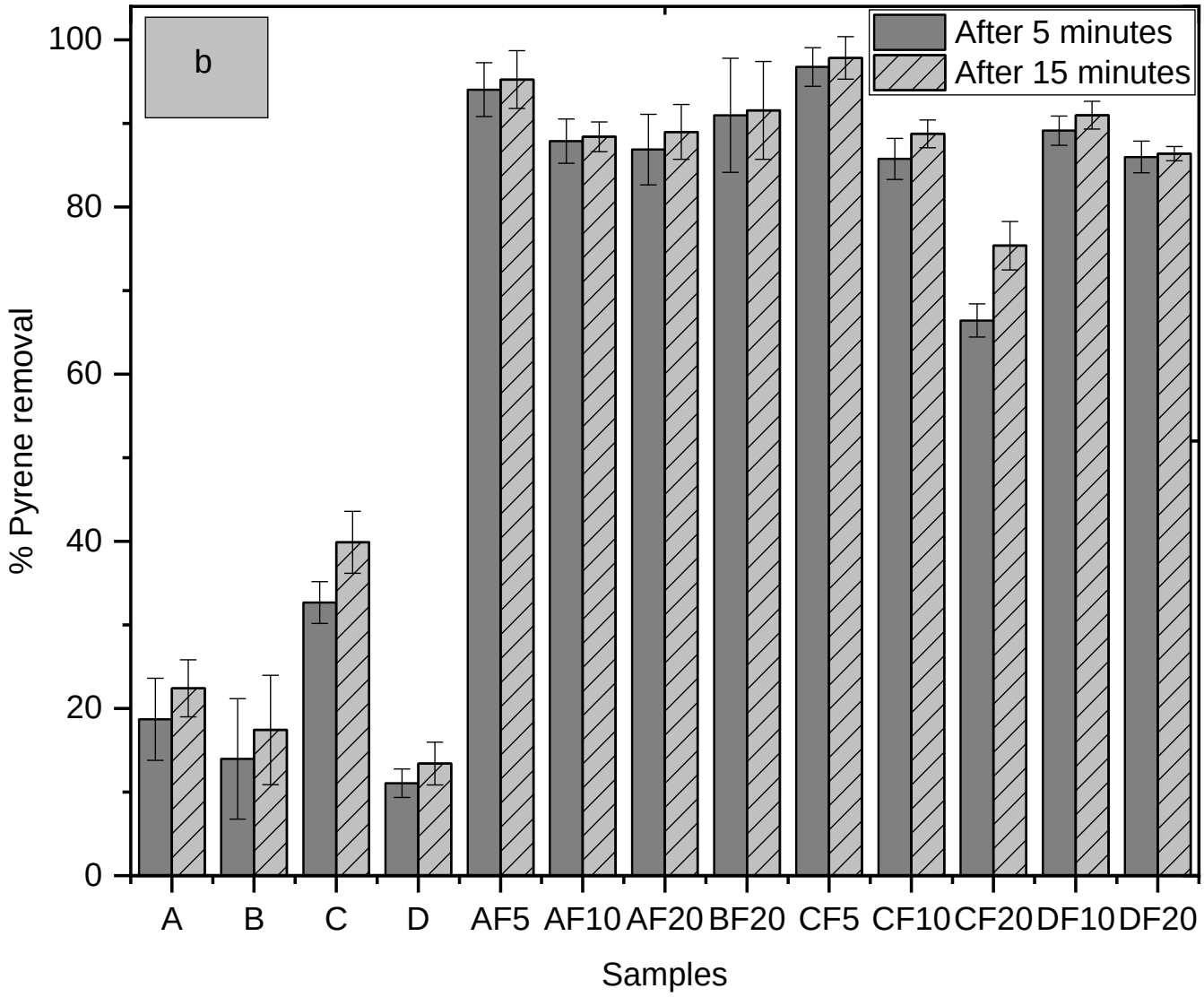

Figure 5. 3. Percentage of pyrene removal by supports and hybrid materials from powdery lipid (section a) and lipid film (section b) at pH 7 and temperature 21.0 ± 0.5°C after 5 and 15 minutes of pyrene contact.

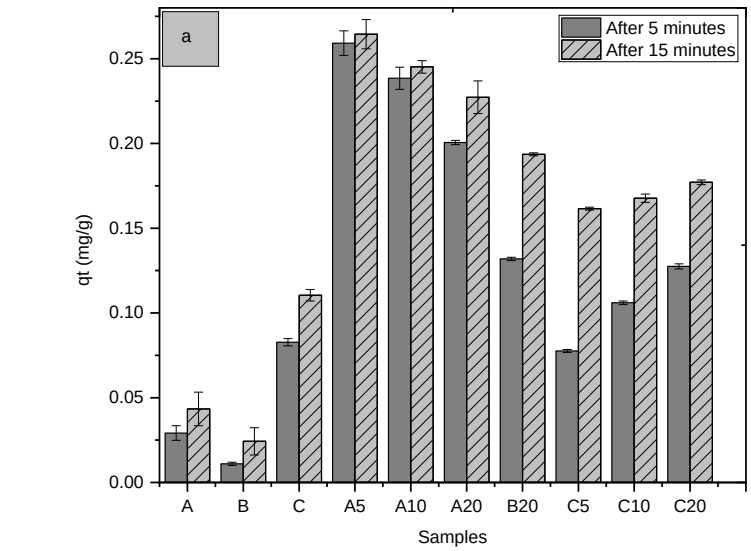

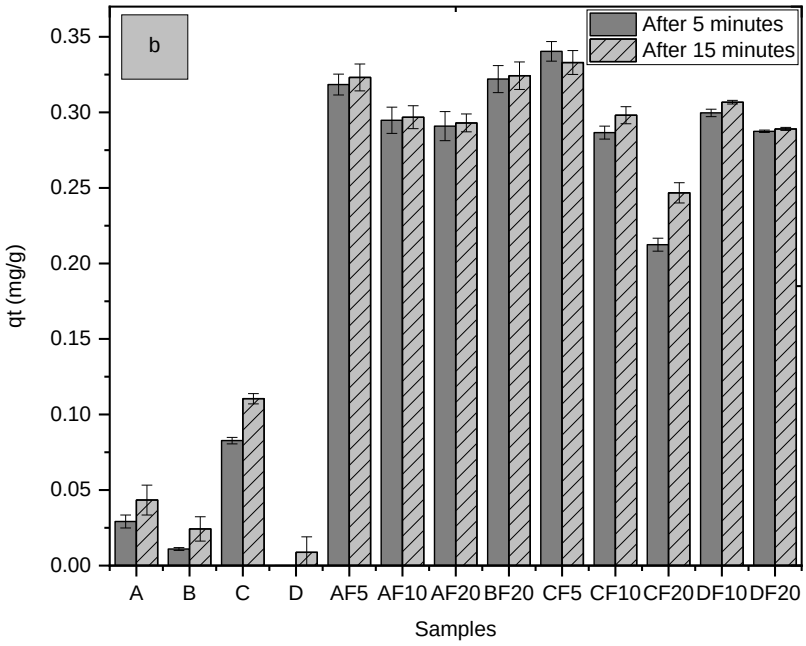

Figure 5. 4. Capacity adsorption of supports and hybrid adsorbents after 5 and 15 min of pyrene contact at 21.0 ± 0.5°C and pH 7.

5.5. Conclusions

Lipid immobilization on the surface of alumina and silica allows to decrease their intrinsic hydrophilicity producing hydrophobic materials able in capturing hydrophobic pyrene molecules and, at least in principle, similar apolar substrates. The preparation methods considered were very simple to apply, as they base on the formation of electrostatic interactions between the oxide surface and the polar head of the functionalizing agent allowing to expose the hydrophobic tails able in establishing dispersive interactions with apolar molecules. The lipid was prepared in form of film using chloroform but also simply dispersed as powder avoiding the use of organic solvents in order to test a green preparation method. The pyrene adsorption occurs very fast on all the samples, in particular in the presence of the highest amount of lipid (support/lipid ratio 5), giving a removal of about 0.30 mg/g in several cases and almost never minor than 0.20 mg/g in 15 minutes. In conclusion, the promising results obtained in the trials carried out with pyrene in water indicate the hybrid materials could conveniently apply to real PW samples.

5.6. Reference

1. Sudmalis D, Da Silva P, Temmink H, Bijmans MM, Pereira MA. Biological treatment of produced water coupled with recovery of neutral lipids. Water Res. 2018;147:33–42. Available from: https://doi.org/10.1016/j.watres.2018.09.050

2. Andreozzi M, Álvarez MG, Contreras S, Medina F, Clarizia L, Vitiello G, et al. Treatment of saline produced water through photocatalysis using rGO-TiO2 nanocomposites. Catal Today. 2018;315(October 2017):194–204.

3. Xu J, Srivatsa Bettahalli NM, Chisca S, Khalid MK, Ghaffour N, Vilagines R, et al. Polyoxadiazole hollow fibers for produced water treatment by direct contact membrane distillation. Desalination. 2018;432(August 2017):32–9.

4. Shamaei L, Khorshidi B, Perdicakis B, Sadrzadeh M. Treatment of oil sands produced water using combined electrocoagulation and chemical coagulation techniques. Sci Total Environ. 2018;645:560–72. Available from: https://doi.org/10.1016/j.scitotenv.2018.06.387

5. Li X, Lu H, Liu D, Wang B. Preparation of composite switchable water with hydrophobic tertiary amine for washing oil sands. J CO2 Util. 2019;29(December 2018):254–61. Available from: https://doi.org/10.1016/j.jcou.2018.12.012

6. Kusworo TD, Aryanti N, Qudratun, Utomo DP. Oilfield produced water treatment to clean water using integrated activated carbon-bentonite adsorbent and double stages membrane process. Chem Eng J. 2018;347(February):462–71. Available from: https://doi.org/10.1016/j.cej.2018.04.136

7. Jiménez S, Micó MM, Arnaldos M, Medina F, Contreras S. State of the art of produced water treatment. Chemosphere. 2018;192:186–208.

8. Sadraei R, Sadeghi VJ, Sadraei M. Biotechnology revolution from academic entrepreneurship to industrial: chemo-entrepreneurship. Biometrics Biostat Int J. 2018 Nov 28;7(6):546–50. Available from: http://medcraveonline.com/BBIJ/biotechnology-revolution-from-academic-entrepreneurship-to-industrial-chemo-entrepreneurship.html

9. Ottaviano JG, Cai J, Murphy RS. Assessing the decontamination efficiency of a three-component flocculating system in the treatment of oilfield-produced water. Water Res. 2014;52:122–30. Available from: http://dx.doi.org/10.1016/j.watres.2014.01.004

10. Nielsen EK, Jespersen S, Zhang X, Ravn O, Lind M. On-line Fault Diagnosis of Produced Water Treatment with Multilevel Flow Modeling. IFAC-PapersOnLine. 2018;51(8):225–32. Available from: https://doi.org/10.1016/j.ifacol.2018.06.381

11. Hong PKA, Xiao T. Treatment of oil spill water by ozonation and sand filtration. Chemosphere. 2013;91(5):641–7. Available from: http://dx.doi.org/10.1016/j.chemosphere.2013.01.010

12. Ali A, Quist-Jensen CA, Drioli E, Macedonio F. Evaluation of integrated microfiltration and membrane distillation/crystallization processes for produced water treatment. Desalination. 2018;434(December 2017):161–8. Available from: https://doi.org/10.1016/j.desal.2017.11.035

13. Duan X, Zhang R, Ding M, Huang Q, Xu WS, Shi T, et al. Adsorption of a hydrophobic cationic polypeptide onto acidic lipid membrane. Polymer (Guildf). 2017;122:125–38. Available from: http://dx.doi.org/10.1016/j.polymer.2017.06.058

14. Guzmán E, Liggieri L, Santini E, Ferrari M, Ravera F. DPPC-DOPC Langmuir monolayers modified by hydrophilic silica nanoparticles: Phase behaviour, structure and rheology. Colloids Surfaces A Physicochem Eng Asp. 2012;413:174–83. Available from: http://dx.doi.org/10.1016/j.colsurfa.2011.12.059

15. Dening TJ, Joyce P, Webber JL, Beattie DA, Prestidge CA. Inorganic surface chemistry and nanostructure controls lipolytic product speciation and partitioning during the digestion of inorganic-lipid hybrid particles. J Colloid Interface Sci. 2018;532:666–79. Available from: https://doi.org/10.1016/j.jcis.2018.08.015

16. Wong JY, Majewski J, Seitz M, Park CK, Israelachvili JN, Smith GS. Polymer-cushioned bilayers. I. A structural study of various preparation methods using neutron reflectometry. Biophys J. 1999;77(3):1445–57. Available from: http://dx.doi.org/10.1016/S0006-3495(99)76992-4

17. Sadraei R. A Simple Method for Preparation of Nano-sized ZnO. Res Rev J Chem. 2016;5(1):8–10.

18. Anuzyte E, Vaisis V. Natural oil sorbents modification methods for hydrophobicity improvement. Energy Procedia. 2018;147:295–300. Available from: https://doi.org/10.1016/j.egypro.2018.07.095

19. Sadraei R, Paganini MC, Calza P, Magnacca G. An Easy Synthesis for Preparing Bio-Based Hybrid Adsorbent Useful for Fast Adsorption of Polar Pollutants. Nanomaterials. 2019;9(5):731.

20. Sadraei R, Murphy RS, Laurenti E, Magnacca G, Accepted J. Characterization methodology to evaluate the activity of supported Soybean Peroxidase. Mater interfaces. 2019;

21. Razieh S. Protein Adsorption from Aqueous Solution by Supports. Bioinforma Proteomics Open Access J. 2017;1(2):1–2.

22. Turov V V., Gun'ko VM, Pakhlov EM, Krupska T V., Tsapko MD, Charmas B, et al. Influence of hydrophobic nanosilica and hydrophobic medium on water bound in hydrophilic components of complex systems. Colloids Surfaces A Physicochem Eng Asp. 2018;552(May):39–47. Available from: https://doi.org/10.1016/j.colsurfa.2018.05.017

23. Yang JA, Murphy CJ. Evidence for patchy lipid layers on gold nanoparticle surfaces. Langmuir. 2012;28(12):5404–16.

24. Salay LC, Carmona-Ribeiro AM. Synthetic bilayer wetting on SiO2 surfaces. J Phys Chem B. 1998;102(20):4011–5.

25. Sherazi STH, Mahesar SA, Bhanger MI, Van De Voort FR, Sedman J. Rapid determination of free fatty acids in poultry feed lipid extracts by SB-ATR FTIR spectroscopy. J Agric Food Chem. 2007;55(13):4928–32.

26. Derenne A, Vandersleyen O, Goormaghtigh E. Lipid quantification method using FTIR spectroscopy applied on cancer cell extracts. Biochim Biophys Acta - Mol Cell Biol Lipids. 2014;1841(8):1200–9. Available from: http://dx.doi.org/10.1016/j.bbalip.2013.10.010

27. Lam HS, Proctor A, Nyalala J, Morris MD, Smith WG. Quantitative determination of low density lipoprotein oxidation by FTIR and chemometric analysis. Lipids. 2004;39(7):687–92.

28. Boffa V, Parmeggiani L, Nielsen AH, Magnacca G. Hydrophilicity and surface heterogeneity of TiO2-doped silica materials for membrane applications. Microporous Mesoporous Mater. 2016;221:81–90. Available from: http://dx.doi.org/10.1016/j.micromeso.2015.09.017

29. Molinari A, Magnacca G, Papazzoni G, Maldotti A. HydrophobicW10O324-/silica photocatalyst for toluene oxidation in water system. Appl Catal B Environ. 2013;138–139(4):446–52. Available from: http://dx.doi.org/10.1016/j.apcatb.2013.03.025

30. Müller S, Totsche KU, Kögel-Knabner I. Sorption of polycyclic aromatic hydrocarbons to mineral surfaces. Eur J Soil Sci. 2007;58(4):918–31.

31. Radian A, Mishael Y. Effect of humic acid on pyrene removal from water by polycation-clay mineral composites and activated carbon. Environ Sci Technol. 2012;46(11):6228–35.

32. Mangold N. Ice sublimation as a geomorphic process: A planetary perspective. Geomorphology. 2011;126(1–2):1–17. Available from: http://dx.doi.org/10.1016/j.geomorph.2010.11.009

33. Sun YE, Xia W, Tang X, He Z, Chen J. Effects of fatty acid chain length and degree of unsaturation on the surface activities of monoacyl trehaloses. Front Chem Eng China. 2009;3(4):407–12.

34. Liu Z, Yao L, Pan X, Liu Q, Huang H. A green and facile approach to the efficient surface modification of alumina nanoparticles with fatty acids. Appl Surf Sci. 2018;447:664–72. Available from: https://doi.org/10.1016/j.apsusc.2018.04.035

35. Wang W, Wang J. Comparative evaluation of sorption kinetics and isotherms of pyrene onto microplastics. Chemosphere. 2018;193:567–73. Available from: https://doi.org/10.1016/j.chemosphere.2017.11.078

Chapter Six

6.1 General conclusions

The principal aim of my work was applying fast, green and easy methods for surface functionalizing different phases of aluminas. Although alumina per se shows numerous advantages like high surface area, open porosity, presence of defective active surface sites and positive surface charge, a surface modification can produce more active systems for capturing different types of pollutant from wastewater.

In this thesis the surface of aluminas has been functionalized with different molecules like BBS, a protein and a lipid in order to prepare several hybrid materials. Electrostatic forces, establishing between positively charged alumina surface and functional groups of organic molecules, were exploited to prepare the hybrid materials. The physico-chemical characterization was perfomed by means of X-Ray Diffraction (XRD) to evidence the crystal structure of different phases of alumina, Fourier Transform Infrared spectroscopy (FT-IR) for evaluating the presence of organic molecules immobilized onto alumina surface, thermogravimetric analysis (TGA) to measure the thermal stability of the hybrid materials and quantify of the organic molecules amount immobilized on them, N_2 adsorption at 77K for the investigation on the surface area and porosity of the systems, zeta potential measurements to determine the surface charge of aluminas before and after the immobilization process.

Most part of the studied applications deals with the removal of pollutants from water by means of adsorption process. Firstly, the hybrid materials were used for capturing polar molecules: organic dyes such as crystal violet (CV) and methylene blue (MB) with different surface charge, but also contaminants of emerging concern like carbamazepine and atenolol

with different polarity and structure. Also non-polar substrate removal was considered functionalizing the alumina surface with hydrophobic molecules (arachidic acid) in order to investigate the treatment of oil field produced-water. The behavior of the materials was tested with proper substrates in order to assess the adsorption capacity and the reversibility of the adsorption.

Finally, alumina was chosen as support for a biocatalytic system allowing interesting insights into the enzyme-support interaction.

Chapter Seven

7.1 Future work

The work accomplished in this thesis has opened up several avenues for further investigations. Outlined below are some experimental questions generated from my thesis that would be of interest to follow up on.

1. The studies described in Chapter 2 and 3 allowed to establish that BBS-functionalized aluminas are interesting systems to eliminate polar contaminants from wastewater by adsorption. The use of handleable supports (monoliths), which do not require a filtration step in the water treatment procedure, surely opens the way to an upscaling of the process, but the possibility of recycling, regenerating and reusing the materials still needs to be investigated.

2. In Chapter 4, different phases of alumina were applied as supports for immobilization of Soybean Peroxidase (SBP) for biocatalytic applications. The amount of SBP immobilized and the stability of the hybrid systems were tested. Moreover, the hybrid systems were investigated to obtain information regarding structure/activity relationship revealing interesting features. In future study, the immobilization of other enzymes on alumina surface could be investigated.

3. Chapter 5 describes the functionalization of alumina and silica surface by arachidic acid. The lipid immobilization allows decreasing the intrinsic hydrophilicity of alumina producing hydrophobic materials able in capturing apolar pyrene molecules and, in principle, similar apolar substrates. As we assumed an electrostatic

interaction between the oxide surface and the polar head of the functionalizing agent and alumina surface, it would be interesting to investigate the immobilization of other types of lipids, for instance with more than one polar head group or with longer hydrophobic chains, also investigating the effect of the same functionalization onto monolith supports.

Chapter Eight

8.1 My published papers

Sadraei, Razieh, R Scott Murphy, Enzo Laurenti, Giuliana Magnacca, and Just Accepted. 2019. "Characterization Methodology to Evaluate the Activity of Supported Soybean Peroxidase." *Materials and Interfaces*. https://doi.org/10.1021/acs.iecr.9b03495.

Sadraei, Razieh, Maria Cristina Paganini, Paola Calza, and Giuliana Magnacca. 2019. "An Easy Synthesis for Preparing Bio-Based Hybrid Adsorbent Useful for Fast Adsorption of Polar Pollutants." *Nanomaterials* 9 (5): 731. https://doi.org/10.3390/nano9050731.

Razieh, S. 2017. "Protein Adsorption from Aqueous Solution by Supports." *Bioinformatics & Proteomics Open Access Journal* 1 (2): 1–2.

Sadraei, Razieh, Vahid Jafari Sadeghi, and Maryam Sadraei. 2018. "Biotechnology Revolution from Academic Entrepreneurship to Industrial : Chemo- Entrepreneurship." *Biometrics & Biostatistics International Journal* 7 (6): 546–50. https://doi.org/10.15406/bbij.2018.07.00257.

Sadraei, R. 2016. "A Simple Method for Preparation of Nano-Sized ZnO." *Research & Reviews: Journal of Chemistry* 5 (1): 8–10. https://doi.org/10.1207/S15327647JCD0302_3.